Quasi-Oscillatory Motion of Single Cells on Micropatterns

Fang Zhou

München 2019

Quasi-Oscillatory Motion of Single Cells on Micropatterns

Fang Zhou

Dissertation

an der Fakultät für Physik

der Ludwig-Maximilians-Universität

München

vorgelegt von

Fang Zhou

aus Shandong, China

München, 15th Oktober 2019

Erstgutachter: Prof. Dr. Joachim Rädler

Zweitgutachter: Prof. Dr. Erwin Frey

Tag der mündlichen Prüfung: 28th November, 2019

Zusammenfassung

Zellmigration spielt eine grundlegende Rolle bei Prozessen wie Embryogenese, der Immunantwort, Wundheilung und bei der Metastasierung von Krebs. Daher ist der Mechanismus der Zellmigration, insbesondere die Dynamik des Zytoskeletts, Aktinpolymerisierung und Reaktionsdiffusionsprozesse, von großem Interesse für die Lebenswissenschaften. Zellen sind hochkomplexe dynamische Systeme, die ihren Zustand ständig verändern, wodurch sich bestimmte Morphologien und Migrationsmodi ausprägen. Die resultierenden Migrationsmuster werden durch externe Faktoren beeinflusst, die unter klassischen Kulturbedingungen nicht kontrolliert sind. Eine zentrale Herausforderung bei der Untersuchung der Zellmigration ist daher die Entwicklung spezifischer Methoden, um die Wirkung einzelner Parameter, die das Zellverhalten regulieren, untersuchen zu können.

Ein möglicher Weg, die Komplexität der Umgebung zu reduzieren, besteht darin, Mikrostrukturierungstechniken zu verwenden um Zellen auf eine definierte Mikroumgebung zu beschränken. Mit solchen Strukturen kann der Freiheitsgrad der Zellbewegung reduziert werden, was es ermöglicht gezielt spezifische Eigenschaften der Zellmigration zu studieren. Darüber hinaus kann man mit Mikrostrukturierungstechnologie Felder von einer großen Anzahl identischer funktioneller Oberflächenstrukturen herstellen und so Hochdurchsatzmessungen durchführen.

Im ersten Teil dieser Arbeit werden Studien zu einem neu entdeckten quasi-oszillatorischen Migrationsmodus von Einzelzellen auf kreisförmigen Mikrostrukturen vorgestellt. Wir beobachten persistente polarisierte Zellen und gerichtete Pol-zu-Pol-Bewegungen innerhalb der Strukturen. Die Zellen depolarisieren auf einer Seite der Mikrostuktur, gefolgt von einer verzögerten Repolarisierung in entgegengesetzter Richtung. Weiter wird gezeigt, dass mehrere Zelllinien (z.B. MDCK-, Huh7-, MDA-MB-231-Zellen) diesen oszillierenden

Migrationsmodus auf kreis-, ellipsen- und streifenförmigen Mikrostrukturen zeigen. Im Vergleich zu kreisförmigen und elliptischen Strukturen ist das Auftreten von Oszillationen auf Streifen gehäuft feststellbar.

Streifen bieten eine ideale und einfache Plattform um neue Migrationsmuster von Zellen und um den molekularen Mechanismus, der der Dynamik des Zytoskeletts zugrunde liegt, zu studieren. Im zweiten Teil dieser Arbeit analysieren wir das Zellverhalten mit Hilfe der räumlichen Geschwindigkeitsverteilung und dem Frequenzspektrum der Bewegung. Die experimentellen Daten werden mit einem zellulären Potts-Modell verglichen, das ein minimales mechanistisches Modell des dynamischen Zytoskeletts enthält. Insbesondere betrachten wir die Dauer des Umkehrprozesses als Maß für die Dauer spontaner Repolarisierung von Zellen und für die Zeit, die das führende Lamellipodium benötigt um sich am Ende des Streifens zurück zu bilden. Mit LifeAct-GFP transfizierten Zellen und Streifen mit unterschiedlich geformten Enden lassen sich Veränderungen im Verhalten an den Enden beobachten. Dies zeigt, dass die Form der Streifenenden und damit die lokale Krümmung der Zellfront Einfluss auf die Aktinpolymerisation hat. Diese Arbeit zeigt, dass Streifen für die quantitative Untersuchung von Zellmigration nützlich sind und dass erweiterte zelluläre Potts-Modelle mit einfachen mechanistischen Regeln die unterschiedlichen Migrationsphänotypen von Zellen in einer beengten Umgebung erfassen können.

Abstract

Cell migration plays a fundamental role in processes such as embryogenesis, immune response, wound healing and cancer metastasis. Hence the mechanisms of cell migration in particularly cytoskeleton dynamics, actin assembly, and reaction diffusion processes have received great interest in life science. Cells are highly complex dynamic systems that constantly alter their states, which leads to emerging morphologies and migratory modes. The resulting migration patterns are influenced by external cues, which are uncontrolled under classic culture conditions. Thus, a key challenge of studying cell migration is the design of specific methods to disentangle the effect of separate parameter regulating cellular behavior.

A possible way to reduce the complexity of the environment is to confine cells to a defined external microenvironment by applying micropatterning techniques. Using these geometries, the degree of freedom of the cell motion can be reduced, which allows selectively studying specific characteristics of cell migration. Moreover, micropatterning technology can realize large-scale arrays of functional surface coatings, so that high throughput measurements can be obtained. In the first part of this work, studies on a newly discovered quasi-oscillatory migration mode of single cells on isotropic circular-micropatterns are presented. We observe persistent polarized cell shapes and directed pole-to-pole motion within the patterns. Cells depolarize at one side of the given micropattern, followed by delayed repolarization progressing towards the opposite side. We then show that several cell lines (e.g. MDCK, Huh7, MDA-MB-231 cells) exhibit the oscillatory migration mode on circular-shaped, ellipse-shaped, and stripe-shaped micropatterns respectively. Compared to circular and ellipse patterns, stripe-shaped microlanes enhance the occurrence of oscillations.

Microlanes provide an ideal and simple platform for the exploration of emerging migration patterns of cells and the molecular mechanisms underlying cell cytoskeleton dynamics. In the second part of this work, we analyze cell motility by

the spatial velocity distribution and frequency spectrum. The experimental data are compared to a Cellular Potts model that includes a minimal mechanistic model of the dynamical cytoskeleton. In particular, we evaluate the “reversal time” as a measure for spontaneous repolarization of cells as well as the time required to quench the leading lamellipodium at the microlane ends. Using LifeAct-GFP transfected cells and microlanes with differently shaped geometric ends, we found distinct scenarios at the leading edge showing that the tip geometry and hence the local deformation of the leading edge has an effect on actin polymerization. This work shows that microlanes are useful for quantitative assessment of cell migration and that extended Cellular Potts models with simple mechanistic rules capture the distinct migration phenotypes in confinement.

Contents

Chapter 1 Introduction

Cell migration is a highly integrated process, which orchestrates embryonic morphogenesis [1], drives to tissue repair and regeneration [2] and is involved in the development of the nervous system [3]. Cell migration contributes to lots of important pathological progressions, such as mental retardation, vascular disease, osteoporosis and cancer, or chronic inflammatory diseases including multiple sclerosis [4]. Hence, understanding of the mechanism as well as the phenomenological features of cell migration are not only central to our understanding of the function of all organisms, but also holds the promise of effective diagnostics and pharmaceutical approaches for treating diseases and emphasizing, innovations of artificial tissues and cellular transplantation [5-8]. Our current understanding of cell migration comes from the study of different cell lines and the contributions of different parameters governing cellular behavior. In general, cell migration can be conceptualized as a highly regulated processes of the cell cytoskeleton, in which the intracellular network enables cells to undergo morphological changes and to navigate in complex environments [9]. In 2D cell culture large-scale measurable phenotypic behavior, such as cell morphology, cell motility, and chemotactic migration has been investigated for long and the observed protrusion-retraction type motion has been related to polymerization and flow dynamics of actin.

Actin is the central component in the cytoskeleton of eukaryotic cells that endows cells with the ability to migrate and modulate cell shape. Actin polymerization and crosslinking prevails in the formation of filaments, protrusions and lamellipodia [10, 11]. The dynamics of the actin networks in cells show many peculiarities including traveling wave patterns [12-15], retrograde actin flow at the leading edge [11, 16-18] which leads to protrusion-retraction cycles and persistent polarity [19, 20]. Understanding the underlying actin transport and polymerization dynamics and its regulation is a key challenge in cell migration. The spontaneous front-rear

polarization of cells and the formation and persistence of protrusions underlies the macroscopic scale, spontaneous and persistent polarization leads to persistent random walk [11]. Theory predicts the emergence of cell polarization to result from a bi-stable reaction-diffusion system [21]. Detailed spatiotemporal models of the signaling biochemistry of cytoskeleton regulating Rho family GTPases with the cell membrane and actin binding proteins reproduce front-rear polarization and cell shape [22-24]. Apart from polarization, in general, such bi-stable mass-conserving reaction-diffusion equations can also exhibit oscillations [25]. Here, related observations are the occurrence of actin waves or oscillatory cell shape dynamics. For example in dictyostelium Discoideum, PIP signal polarization, and the PI3K and PTEN regulation show spontaneous waves and oscillations relevant for chemotaxis [26-28]. However, even though these oscillations share general features, spontaneous large-scale oscillations in the eukaryotic cytoskeleton remains a rare phenomenon.

In recent years artificial micro-pattern have been used to confine cell migration to defined geometries [29], in particular micro-lanes [30-33]. In micro-lanes cell motion is described by a one-dimensional persistent random walk, which reveals a universal relation of persistence and cell velocity [16]. Other micro-patterns with non-trivial geometries give rise to novel migratory behavior. Circular adhesion islands lead to rotational migration of small cohorts of cells [34], ratchet geometries induce directed migration [35], in dumbbell-shaped micropatterns cells undergo repeated stochastic transitions characterized by intricate nonlinear migratory dynamics [36], and micro-lanes with gaps show emergence of stochastic cell reversal and transits [37]. In addition, migration pattern may change by inducing changes in the cytoskeleton. For example depolymerization of microtubules turns cells from persistent to oscillatory migration on linear micro-lanes [38]. Also zyxin depleted cells perform oscillatory migration in 1D linear micro-patterns [39]. Hence, micro-patterns are well suited to verify computational models of cytoskeleton dynamics and to advance our understanding of the regulatory network. In particular, computer simulations predict periodic migration of cells on 1D micro-patterns [40]. Similar findings were reported in reaction-

diffusion modeling of actin waves in flexible boundaries [12]. These theoretical studies suggest that confining geometries might reinforce oscillatory cell migration. However， systematically experimental studies of oscillatory cell migration on micro-pattern have not been carried out yet.

Here, the aim of this thesis is threefold: On the one hand, we investigate how our easily to handle micropatterning approach can be used to systematically study the emergence of quasi-oscillatory motion of single cells. On the other hand, we concentrate on microlanes perform a detailed analysis of the cell motion. Thirdly, we study how the geometries at the tips affect the repolarization progress.

This thesis starts with the theoretical background that is related to this work. Chapter 2 introduces fundamental concepts of cell migration and the relevant micro-patterning techniques. In particular, the cytoskeleton and the major components involved in cell migration are presented, and the underlying mechanism is described. Different theoretical models are briefly introduced, such as reaction-diffusion and the lattice-free models.

Chapter 3 introduces the experimental setups, materials and methods. The working principles of the phase-contrast microscopy, time-lapse microscopy and fluorescence microscopy that were used in this research are described. Afterwards micropatterning approaches are introduced, which are capable of producing homogeneous patterns of controlled protein density and which can confine cells on substrates. Furthermore, the protocols for cell culture, seeding and cell transfection as well as the image processing are given.

The main results of this thesis are presented in Chapter 4 and Chapter 5. Chapter 4 describes that using micro plasma-induced protein patterning (μPIPP) and micro contact printing (μCP) we create arrays of micropattern with different shapes such as circles and ellipses. In initial experiments, we observe the emergence of quasi-oscillatory cell motion for various cell types, among others the Madin Darby Canine Kidney (MDCK) cells, the human liver cells Huh7, and the breast cancer cells MDA-

MB-231. The quasi-oscillation motion exhibits phases of directed back and forth migration interrupted by phases of random motions. Next, we introduce stripe-shaped microlanes with different length or width for MDA-MB-231 cells to study the emerging of sustained oscillatory cell behavior. In Chapter 5, we investigated the probability density, velocity distribution and periodicity of single-cell motion as a function of microlane lengths. The trajectories show repeated cycles of directed migration with pronounced cell polarization, termination of the protrusion of the leading edge at the end of the pattern and spontaneous repolarization of cells in the opposite direction. We recapitulate these migratory features in a dynamic Potts-Model, which includes simulation of a polarizable actin density field. We evaluate the apparent repolarization time distribution both in experiment and computer simulation. While the simulation reproduces the over-all cell motion and time distribution and there are differences when the tips of the microlanes have different geometric shapes. We discuss how micropatterns will allow further investigate how emerging migration patterns are connected to excitable dynamics of the cytoskeleton and the influence of geometrical cues.

Chapter 2 Fundamental Concepts

This chapter gives an introduction of the fundamental theoretical background that is relevant to this thesis. Since living cells are the research targets of this work, a detailed description of elements of the cytoskeleton that are related to the cell motion are listed in this section, the actin filaments and the regulators of actin polymerization are highlighted. In particular, current research backgrounds on the visualization of F-actin are introduced in Section 2.1.3. The study of quasi-oscillatory migration behavior is based on the mechanism of cell migration, thus the general process and morphology of cell migration are described in Section 2.2. Understanding of cell migration as an integrated process requires studying the effect of the molecular switches, such as integrins and Rho family proteins, which are also listed in this part. Moreover, this section provides knowledge that some theoretical description and models of cell migration which are important for understanding the analysis of results in the following main text.

2.1 The Cytoskeleton and Actin

Cell motility is driven by the dynamic cycle of the cytoskeleton, a coordinated network of protein filaments extending throughout the cytoplasm of living cells. In this section we will focus on the major players and the molecular basis involved in this complex process.

2.1.1 Overview of the Cytoskeleton

The cytoskeleton is a dynamic equilibrium system formed by the interaction of macromolecules with mechanics, chemistry and biology. The cytoskeleton is composed of microtubules, the intermediate filaments and actin filaments, as illustrated in Figure 2.1. The three components of the cytoskeleton are linked to each other by means of specific linkage (cross-linking by connexins) and non-specific linkage (in a spatially intertwined connection) [41], which is an extremely complex polymorphic dynamic network structure with multi-scale characteristics. The cytoskeleton interacts with cell membranes, nuclei, cytosols, and dissolved protein molecules in cell fluids to form semidilute network structures that form a highly ordered living cell from a messy population of molecules on surface.

The cytoskeleton carries out a great variety of functions. It can be summarized as three functions: the cytoskeleton supports the entire cell structure; it helps the cells to complete the transportation of biological molecules [42] and response to external environment by physically and biochemistry connection; it determines cell shape and movement by generating coordinated forces [43]. Thus, the cytoskeleton plays a primary role in a series of physiological processes such as cell spreading, migration, growth, and differentiation [4, 44-46]. The most important differences between the three structures of the cytoskeleton are their stiffness, the assemble dynamics, the polarity and their associated molecular motors [43].

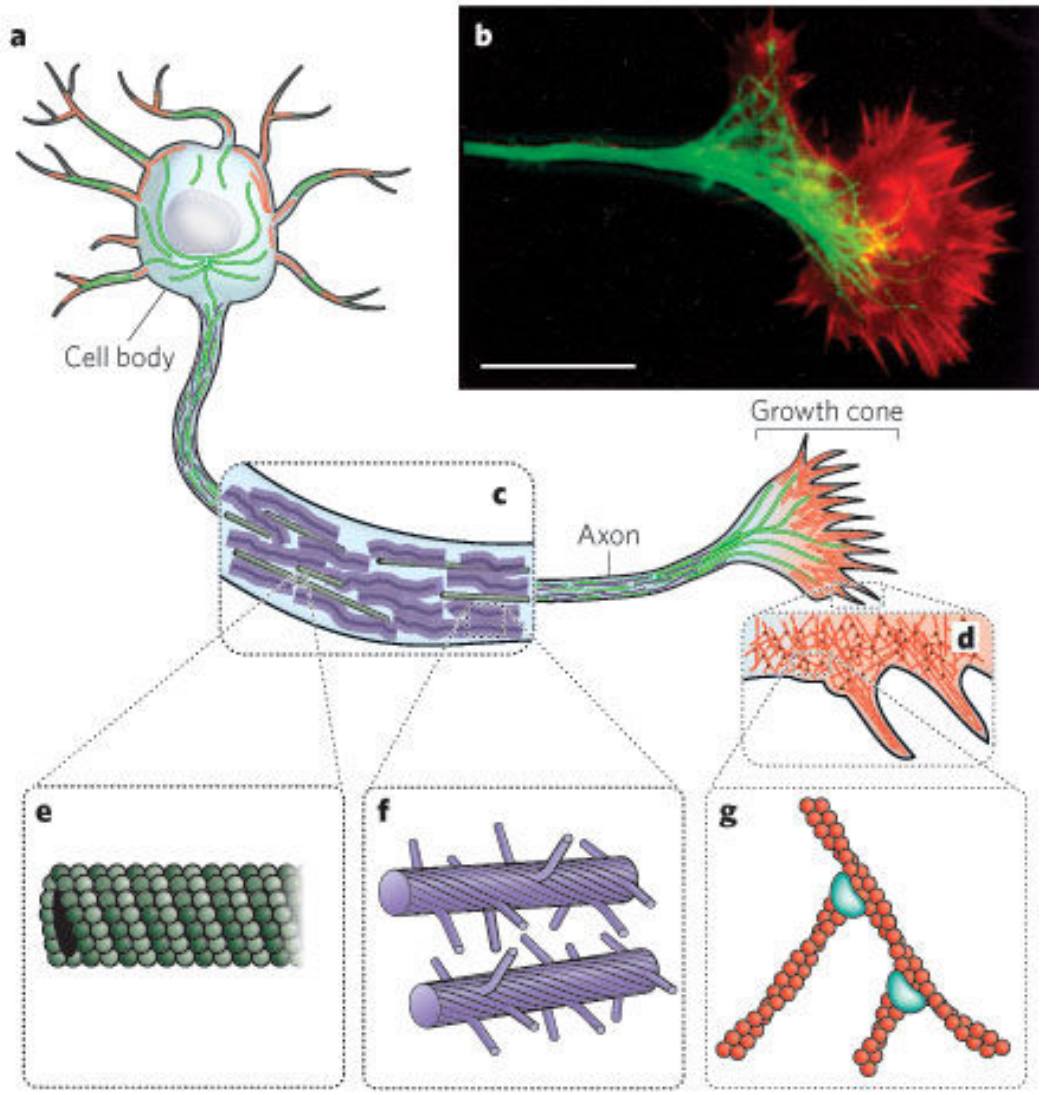

Figure 2.1 Elements of the cytoskeleton.

(a) The cytoskeleton of neurons, like other eukaryotic cells, consists of three main polymers: (e) microtubules (green), (f) intermediate filaments (purple) and (g) actin filaments (red). (b) A fluorescence micrograph of the neuronal growth cone. (c) The neuronal axon is a long membrane-bounded extension. (d) The growth cone contains dendritic actinfilament networks and parallel actin-filament filopodia. (e) Microtubules consist of 13 protofilaments of tubulin dimers arranged in a hollow tube. (f) Neurofilaments have flexible polymer arms that repel neighboring neurofilaments and determine the radius of the axon. (g) Actin filaments, which are formed by the Arp2/3 complex (blue), are arranged into networks. Adapted from [43].

Microtubules

Among the three components of the cytoskeleton, microtubules are the stiffest. In shape, microtubules have a large persistence length, typically between 1 μm and 20 μm, can form a pipeline across the whole cell scale, or much longer which can reach a maximum of millimeters in vitro, and can be flexed under certain external forces [47]. Microtubules are cylindrical polymers which are composed of a regular lattice of the tubulin dimer (α-tubulin and β–tubulin, of dimensions 4 nm × 5 nm × 8 nm and 100,000 daltons in mass), with extreme outer and inner diameters of ~30 nm and ~18 nm, respectively [42, 48]. The wall of a microtubule can be represented as a circular array of 13 protofilaments, each a linear sequence of tubulin dimmers (Figure 2.1e). [49] Microtubules have a complex assembly and disassembly dynamics. They can be converted between the state of polymerization (steady-state growth) and dissociation (rapid depolymerization and shrinking), the growing state of microtubules with a curved sheet of protofilaments at their ends is stabilized by a GTP cap, by contrast, the shrinking state has lost this cap with a knife end [50]. A phenomenon between the steady growth and the phase of disassembly called dynamic instability. The dynamic instability enables microtubules to search for chromosomes in the cytosol during the formation of mitotic spindle and to reorganize quickly [51]. Moreover, the dynamics of microtubules are essential for the directional migration of cells, since the microtubule-organizing center (MTOC) is oriented towards the migrating direction. Cell migration requires the reorganization of microtubules and the actin cytoskeleton [52].

Intermediate Filaments

The filaments were named *intermediate* because of their diameter (~ 10nm), which is between the thick microtubules and the thin actin filaments (~6 nm) [53]. Unlike microtubules, intermediate filaments (IFs) exhibit much diversity. Intermediate filaments display cell-type-specific and complex patterns of expression, but they share common structure: a rod-like dimer composed of two coiled-coil of two α helical chains oriented in parallel, with changeable head and tail domains at the

two ends [54]. The rod is usually about 46 nm [53]. The dimers associate in linear arrays, four of which assemble in an antiparallel fashion, forming protofilaments by half-staggered manner; the protofibrils intertwine to build into the actual intermediate filament [55], as shown in Figure 2.2.

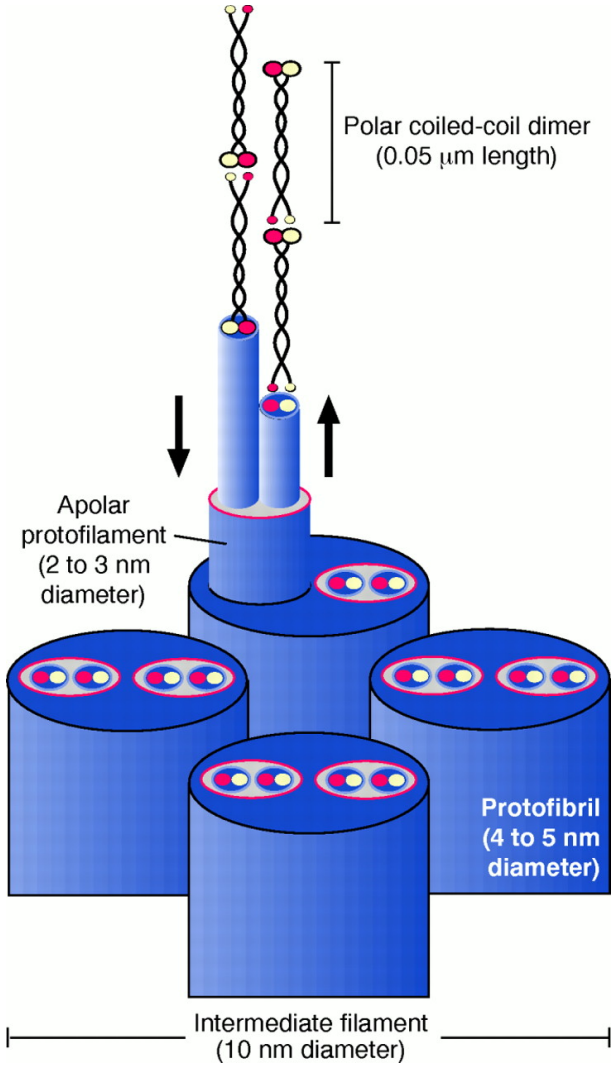

Figure 2.2 A structural model of intermediate filament.

The monomers assemble to a polar coiled-coil dimmers, which form antiparallel non-polar tetramers. The tetramers associate into apolar protofilaments. Two to four protofibrils assemble to intermediate filament. Adapted from[55].

The intermediate filaments are the least rigid among the main three cytoskeleton components. The intermediate filaments display in lots of forms. They can crosslink to each other and can be connected to the microtubules and actin filaments via a

kind of proteins called plectins [56], enable the cytoskeleton able to better withstand tensile or pressure forces. Intermediate filaments of some cell types can be assembled under the stimulation of mechanical forces [57]. One class IFS, a component of the nuclear lamina, contributes to the spindle assembly and trigger the breakdown of the nuclear-envelope in mitosis [58]. In contrast to microtubules and actin filaments, Ifs are non-polar and they are not directly involved in supporting directional motility of molecular motors [43].

Actin Filaments

As an important part of the cytoskeleton, actin is a central player in various biological progresses such as cell response to environmental forces, cell morphology, cell polarity, cell migration and cell division [59]. Actin is a 43 kDa polypeptide consisting of 375 amino acids crosses twice between two domains, which are stabilized by an adenine nucleotide, with N-termini and C-termini [60]. The gaps between the domains are the binding site of adenosine-triphosphate (ATP), where it can be hydrolyzed to adenosine-di-phosphate (ADP), as illustrated in Figure 2.3. Actin monomer is a globular protein, called G-actin. ATP-boud G-actins helically assemble together to build the F-actin filaments, with a diameter of ~7 nm. The polymerization of actin filaments divides into a nucleation phase and an elongation phase. In nucleation phase, unstable actin dimmers and trimers are formed, resulting in a rate-limited nucleation step of polymerization [61]. So this process requires some cofactors such as nucleation factors. Once stable tetramers interact, the polymerization runs into the second elongation phase, in which the rate is diffusion-limited by the concentration of available monomers [62]. Because of the asymmetry of G-actin, the elongation possess polarity with one slowly polymerizing “pointed end” and one much faster growing “barbed end” [63]. When the continuous growth at the barbed end is equal to the shrink at the pointed end, the filament remains an almost constant length, called treadmilling state [64].

The treadmilling is encouraged by the hydrolysis of ATP, and the energy contributes to cellular process. Although actin filaments are much less stiff than microtubules,

it provides a continuous driving force for cell migration, for example the highly ordered bundled actin filaments and the cross-linked networks can support the motion of protrusions and lamellipodia in migrating cells and generate protrusive forces to push the membrane at the cell front. Furthermore, all actin-driven cellular process depends on the relevant cofactors [65], thus, important cofactors will further introduced.

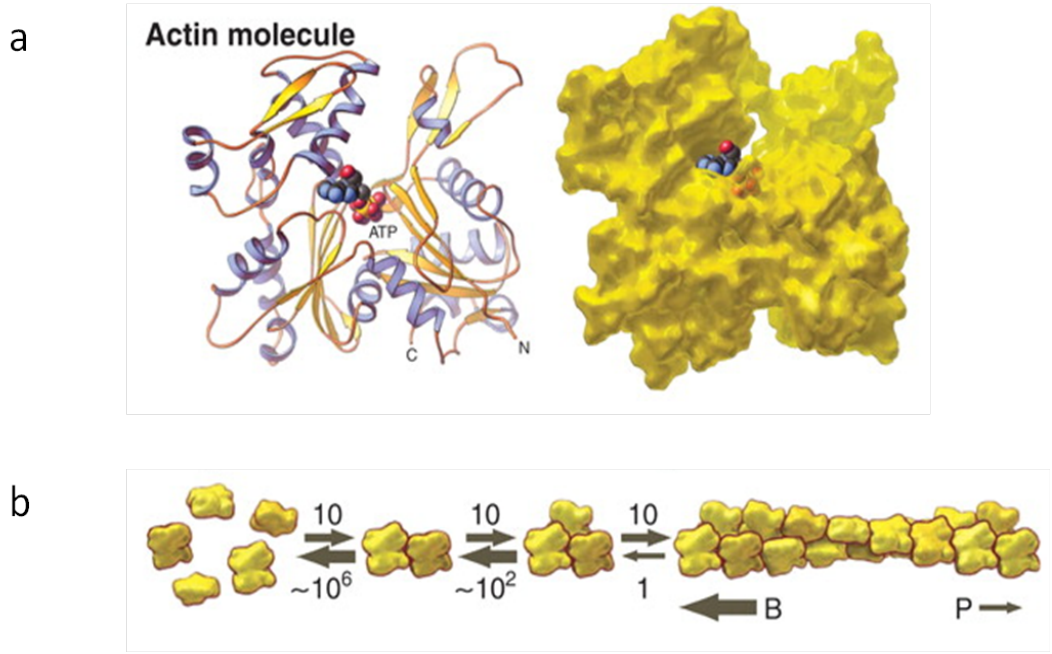

Figure 2.3 Schematic illustrations of actin structures.

(a) Ribbon (left) and space-filling (right) models of the actin molecule. (b) The spontaneous nucleation and elongation of actin. Dimers and trimers are unstable until form to longer polymer. It grows slowly at the pointed end (P) and rapidly at the barbed end (B). Adapted from [59].

2.1.2 Regulators of Actin Polymerization

A number of actin-binding proteins play regulatory roles in actin polymerization. These regulators can be grouped into sequesters, nucleators, severing proteins, capping proteins, crosslink proteins, motor proteins, and so on. Several types are briefly introduced in this section.

Sequesters

Sequesters (e.g. thymosin-β4, profilin and cofilin) can bind to actin monomers and control the pool of unpolymerized actin and exchange the nucleotide bound to actin, as depicted in Figure 2.4a. Thymosin-β4 has more affinity with ATP-actin monomer than with ADP-actin. It not only can inhibit actin's growth but nucleotide's exchange. Profilins have highest affinity with nucleotide-free actin monomer, they catalyze the exchange of ADP and ATP. Moreover, Profilins inhibit nucleation and elongation at the pointed end, but promote the actin polymerization by bringing the G actin –profilins to the barbed end. Like thymosin and profiling, cofilin forms a complex with G-actin, but have higher affinity with ADP-actin than ATP-actin. It inhibits nucleotide exchange but not polymerization. Cofilin as well as profiling have complementary roles in regulating actin assembly into filaments.[66, 67]

Nucleators

The rate-limited step of actin polymerization is usually nucleation, so nucleators such as Arp2/3 complex, WASP, formins are particularly essential for this process, as depicted in Figure 2.4b-c. The actin-related proteins (Arp) 2/3 complex consists of seven proteins, including Arp2 and Arp3, and bind to actin monomers. Arp2/3 nucleates the formation of the new branched filaments from the sides of pre-existing actin filaments where it serves as a nucleation site[68]. The C-terminal domains of Wiskott-Aldrich syndrome protein (WASP) and related proteins Scar initiate the Arp2/3 complex to nucleate daughter filament on the mother filament, other domains of WASP can also regulate this activity under the control of some proteins e.g. the small guanosine triphosphatase (GTPase) CDc42 [69]. Formin, which is a multidomain polypeptide, acts as a homodimer by activating the polymerization of free actin monomers and remains associated with the barbed end. Formins bound to Profilin-actins can transfer actins to the barbed end of the filament as well [70].

Capping proteins

Most of capping proteins (e.g. CapZ, tensin, tropomodulin) bind with high affinity to a filament end, either the barbed end or the pointed end of actin filament, as illustrated in Figure 2.4d. Capping proteins either prevent the addition of more actin monomer or promote actin disassemble. For example, CapZ regulates the actin polymerization by eliminating of annealing at the barbed end of actin filaments [71], in contrast, tropomodulins (Tmod) bind to the pointed end of F-actin, and inhibit the elongation at this end.[65]

Severing proteins

Cells also contain proteins that sever filaments into short fragments by severing proteins (e.g. gelsolin, fragmin, severin, cofilin), as illustrated in Figure 2.4d. For example, gelsolin competes with actin depolymerizing factor (ADF) cofilin for binding to actin filaments. Both of them can change the conformation of actin filaments and sever F-actin. They are able to capture ADP-G-actin with higher affinity than ATP-G-actin, thereby they facilitate its dissociation at the pointed end [65, 72]. The severing proteins promote the depolymerization of actin filaments, resulting in short filaments, which can be applied for further reorganization.

Crosslinking proteins

Crosslinking proteins (e.g. α-actin, fascin, filamin, fimbrin) also affect the organization of filaments. They possess two actin-binding sites which enable to link filaments to form higher-order structures, bundles or networks, as illustrated in Figure 2.4d. For example, the crosslinker fimbrin preferentially stabilize the regular bundles of filaments such as in microvilli or filopodia, in contrast, crosslinker α-actin which is broadly found in the cortical actin networks well as at the intervals along stress fibers, can stabilize the orthogonal gels and the parallel bundles. Interestingly, if the crosslinker dissociates from the actin filaments with a higher

rate, the filaments tend to form bundles with lower rate as well as act as a more disordered state [73].

Motor proteins

Motor proteins provide driving force in most active cellular processes. Motor proteins myosin family, for example, bind to actin filament and use it as motion tracks, as shown in Figure 2.4e. Myosin II is a familiar and conventional for studies of muscle contraction, actually myosins consist a large superfamily of other motor proteins with quite different tail domains., they share a common domain that interacts with actin, hydrolyzes ATP and generate force for the movement towards the barbed end of actin filaments (myosin VI shifts towards the pointed end) [74, 75].

Taken together, on one hand, these regulators of actin filaments lead to the formation of a complex actin networks and establish a functional cytoskeleton, which play essential role for cell motility; on the other hand, some of regulators disrupt the actin networks, enabling the recycle use of actin subunits.

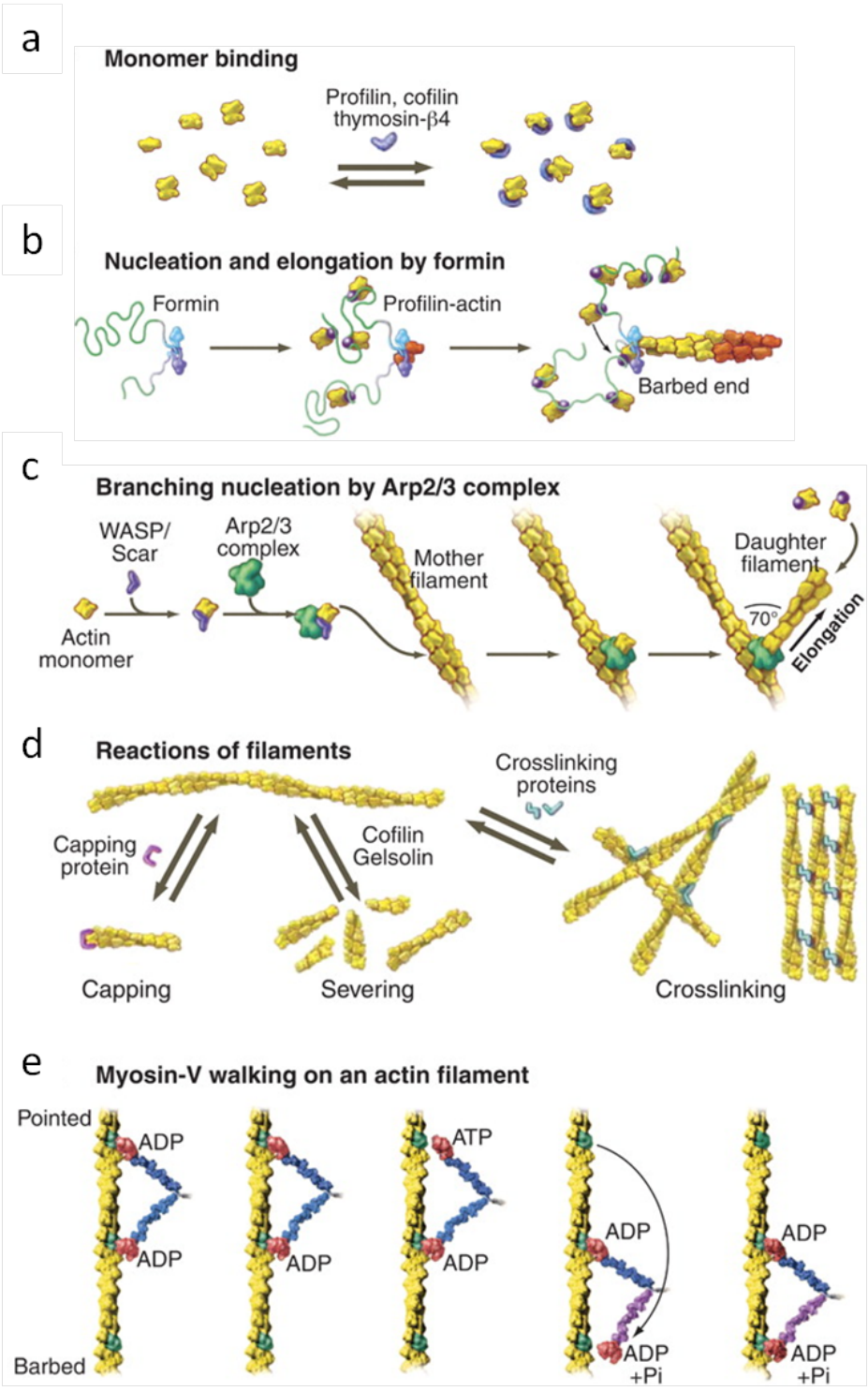

Figure 2.4 Schematic diagrams of actin regulators and fundamental reactions.

(a) Actin monomer binding sequesters thymosin-β4, profilin and cofilin. (b) The nucleation and elongation by formins. (c) The nucleation by Arp2/3 complex. (d) Reactions of the capping proteins, severing proteins and crosslinking proteins. (e) Motor protein myosins use cycles of ATP hydrolysis to walk along actin filaments. Adapted from [59].

2.1.3 Visualization of F-actin in Cells

As introduced, actin is involved in many cellular structures, Naturally, F-actin plays a central role in cell movement and other fundamental processes. Hence it is more important to visualize F-actin in living cells, so that actin dynamics can be easily observed. Furthermore, some cellular processes such as cell migration and cell polarization can be better studied.

The universal probe for F-actin in fixed cells and tissues is phalloidin or fluorescently labeled actin, which can stabilize actin filaments at the same time. Widely used probe in live cells is actin coupled to fluorophores, such as actin-GFP (GFP, the green fluorescent proteins) [76]. These probes exhibit good labelling function of the cytoskeleton. However, they also have some drawbacks: phalloidin or fluorescently labeled actin has the toxic side effects on cells and affects the actin distribution [77]. Actin-GFP fusions display a strong signal background and affect the actin dynamics. As well as those GFP of fusions to actin-binding domains, such as LimE in *Dictyostelium discoideum*, ABP120 in *D. disxoideum* and mammalian cells, consisting of large domains, competing with their endogenous counterparts and may adjust the stability of the actin [78] [79].

In this thesis, the peptide “Lifeact “, a C-terminal GFP fusion (Lifeact-GFP), as an adaptable marker was used to visualize F-actin. “Lifeact”, first identified in 2008, was the first 17 amino acids (aa) of actin-binding protein 140 (Abp140) [80], as shown in Figure 2.5. Abp140 in *Saccharomyces cerevisiae* consists 628 aa and is a 71kDa protein. Compared with other GFP-fusions, Abp140-GFP with its localization to F-actin structures in budding yeast, is the best live marker for visualization of actin cables at that time, until its first 17aa (Lifeact) were found, which were sufficient to support actin localization comparable to the full-length protein in 2008. The short peptide Lifeact with its small size make it an excellent actin marker for living imaging of cells, test results shown in Figure 2.5c-f. In addition, the key advantage of Lifeact is reduction of unwanted perturbations due to its low affinity with F-actin, as well as has no interference with cellular process.[80]

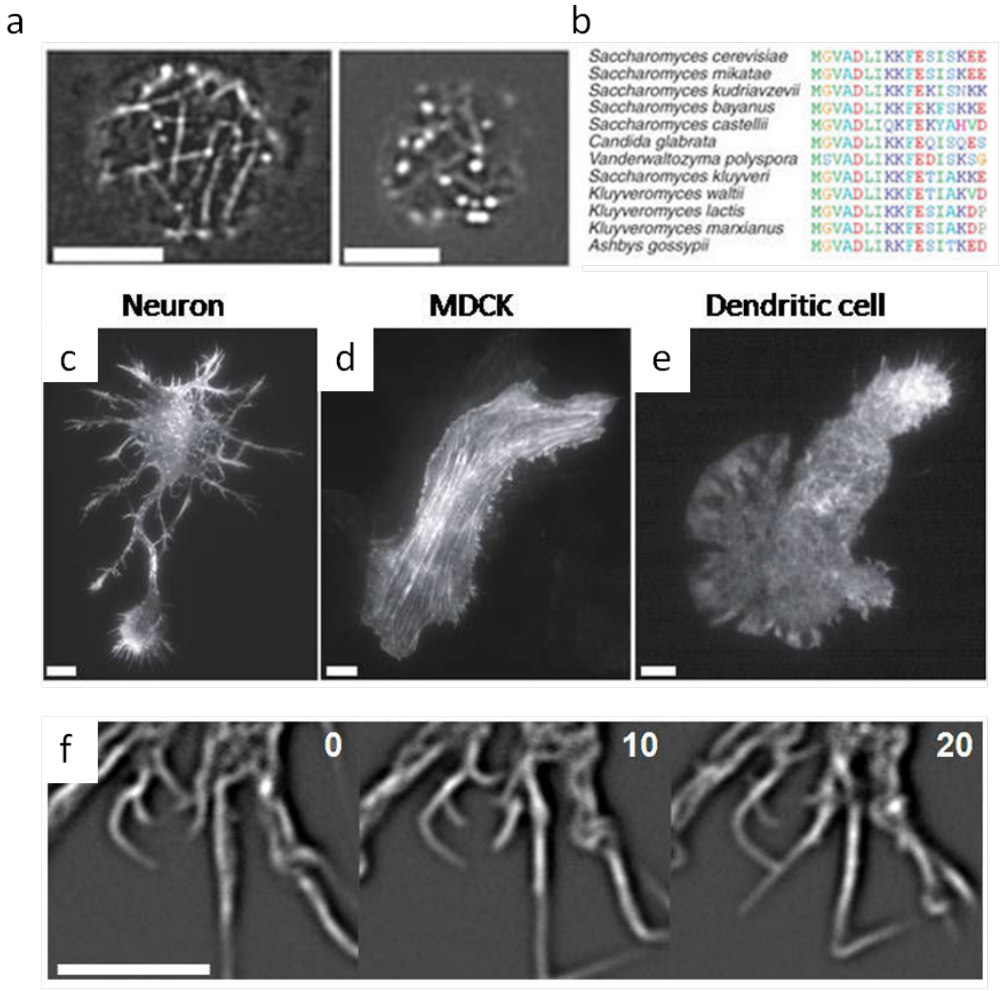

Figure 2.5 Identification and characterization of Lifeact.

(a) TIRF image of Abp140-GFP in an unpolarized yeast cell (left), Epifluorescence image of Lifeact-GFP in a yeast cell (right). (b) First aa alignment of the actin-binding sequence in fungi. (c) TIRF microscopy images of Lifeact-GFP transiently expressed in rat hippocampal neurons, (d) in MDCK cells, (e) in mouse dendritic cells, and its time series of filopodial dynamics in (f). Scale bars, 5 µm except 1 µm in (f). Adapted from [80].

2.2 Cell Migration

In the last section, the major players and the molecular basis involved in cell motility have been introduced. The process of cell migration and how these components physically coordinate both spatially and temporally will be given in this section (Figure2.6).

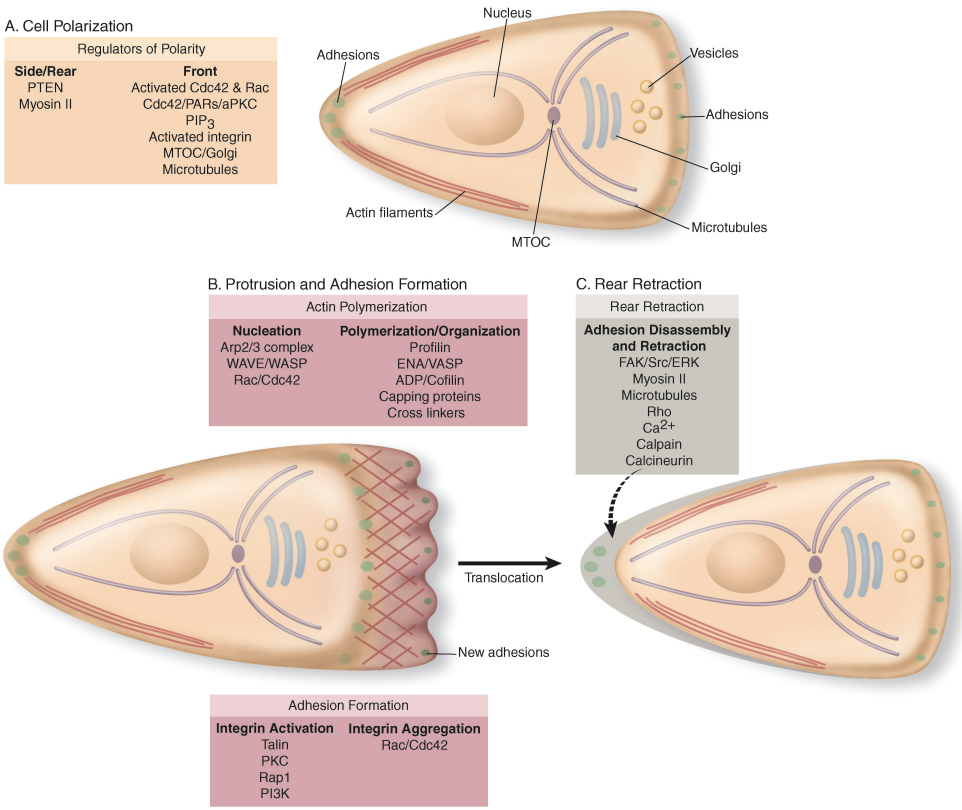

Figure 2.6 The progress of cell migration.

(A) Polarization: the first step to a migrating cell. (B) Cell migrates with the formation of membrane protrusions and is stabilized by the formation of adhesions. (C) Retraction: adhesions disassemble at the cell rear. Some possibly related components are indicated in the progress. Adapted from [4].

2.2.1 Morphological Polarization and Protrusions

The first step for a cell to migrate is polarization, which means cell must break the spatial symmetry to generate a polarized morphology, i.e., different molecules process between the cell front (the leading edge) and rear (the tailing edge). The polarization of eukaryotic cell can either spontaneously occur [81] or be guided by the extracellular environment. The interaction with the substratum or the lateral contacts with other cells can stimulate polarization [82]. Actually, cell polarization can be guided by various extracellular polarization cues, such as external forces (mechanotaxis), external electrical or magnetic fields (electrotaxis, galvanotaxis)[83, 84], gradients of surface stiffness or structure of the substrate (haptotaxis)[85], or the gradients of soluble (chemotactic) [86]. Chemotactic is the most studied cues in

cell migration. The stimuli promote polarized signals, resulting in a generation of a protrusion at the front of cell.

The membrane protrusion is driven by the actin filaments, which are a pointed end and polarized with a barbed end (introduced in Section 2.1). The dynamic polymerization of actin pushes the membrane forward. Actin filaments contribute to the physical backbone of the protrusion, thus, the organization of actin filaments determine the shape of the cell. They display distinct morphologies depending on the type of actin-binding proteins and amounts of filaments. The usual morphologies are filament bundles or the branched dendrites, which lead to different extension of active membrane, including filopodia and lamellipodia.

Filopodia

Filopodia are cylindrical, thin, needle-like protrusions, which mainly emerged by filament treadmilling mechanism (discussed in Section 2.1). Filopodia consist of unbranched, long, parallel actin filament organizations, which are highly oriented tight bundles instead of branched nucleation organizations. Many proteins are enriched in filopodia, the important regulators are the small Rho GTPase, Cdc42 (see below). Filopodia execute an exploratory function for cells, which serve as sensors and enable to probe the local environment [87, 88].

Lamellipodia

Lamellipodia are flat, broad, sheet-like protrusions, unlike filopodia, they contain a branching dendritic network. Therefore, actin filaments in lamellipodia are generated by the Arp2/3 complex, which supports the formation of branched daughter filament from the mother filament. In current view, the small GTPase Rac and the WASP/WAVE family control the localized activation of Arp2/3 complex (see below). Through the activation of Arp2/3 complex, lamellipodia enable to grow in a specific direction, which provides the basis of the cell migration. Most motile cells have a thin lamellipodium (~ 1μm) at the leading edge [89, 90].

As mentioned above, the generation of cell polarity and the extension of both filopodia and lamellipodia in response to migratory stimuli are coupled with local actin polymerization, which are mediated by a set of regulators in cells, such as the GTPase Rho family proteins.

Rho family proteins

Rho family, small guanosine triphosphate (GTP)- binding proteins, were first proposed to have roles in cell migration over 20 years ago[91]. Most Rho GTPases are active when bound to GTP and interact with the downstream target proteins, including kinases and the Arp2/3 complex, When they bound to GDP, they are inactive [91]. Rho, Rac and Cdc42 are three best-studied Rho family members of eukaryotic cells. They act together to control the formation of filopodia and lamellipodia and contribute to migration. Cdc42 is an essential regulator of cell polarity in eukaryotic organisms and it also spurs actin polymerization to the leading edge of cell [92]. Cdc42 can localize the position of the nucleus and orient Golgi apparatus in front of the nucleus and the microtubule-organizing center (MTOC) towards cell front, then, microtubules can carry out the vesicles driven by Golgi to the leading edge. This process provides the necessary proteins and membrane for protrusion forwards. Both Rac and Cdc42 are key mediators that regulate acin polymerization in protrusion. They act as activators of the WASP/WAVE family of Arp2/3 complex. Rac promotes the extension of lamellipodium by activating WAVE proteins, while Cdc42 stimulates the Arp2/3 complex to produce crosslinked actin network [93]. Rho GTPase is inactivated by GTPases activating proteisns (GAPs) and activated by guanine nucleotide exchange factors (GEFs). The activity of Cdc42 and Rac will also be regulated when WASP/WAVE proteins binds to GEFs or GAPs, resulting in negative or positive feedback to induced-actin polymerization. Rho and Rac suppress each other. Rho is more active at the rear and sides of the cell and meanwhile inhibits the activity of Rac, preventing protrusion generated by Rac at other directions except the leading edge. Rac is active at cell front and inhibits the actitity of Rho.

2.2.2 Formation of Adhesions

The occurred protrusions of migrating cell are stabilized by the formation of adhesions, which is the physical interaction of cell-cell or cell-extracellular matrix (ECM). Cell-matrix adhesion is the best-studied form in cell migration and is the focus of this section.

The surrounding environment of cell is not only composed of other cells but also the extracellular surroundings, which is called extracellular matrix (ECM). The ECM constructs the substratum on which cells are migrating. The fibrous of ECM consist of four major proteins, collagens, laminins, elastins, and fibronectins. Briefly, collagen is the most plentiful protein of ECM [94]. It can provide tensile strength, guide tissue growth and regulate cell adhesions. The flexible and elastic protein elastins and the heterotrimeric protein laminins directly take part in the formation of cell adhesions, similar with fibronectin. Fibronectins provide binding sites for integrin, which is an essential transmembrane protein of cell adhesions [95].

Integrins consist of α and β chains with large ligand-binding extracellular domains and short cytoplasmic domains. Integrins are the principal receptors for binding the ECM and cell interior, acting as the “feet” of a migratory cell. When integrins bind to a ligand of the ECM, conformation changes in the receptor by changing the interaction between the α and β chains, lead to further integrin clustering. This event initiates intracellular signals and finally regulates the formation of adhesions [96].

Adhesions, initially called focal adhesions, make the protrusions attach to the substratum. In fact, several types of cell-matrix adhesion have been pointed over the years. Nascent adhesions –small and highly transient-preferentially form at the leading geometry edge of filopodia and lamellipodia. They increase in size as cell migrates over them and persist until they reach the rear of cell. Compared to nascent adhesion, focal complexes are larger adhesions, and rely on the myosin II for their formation at the boundary of the lamellipodium [97]. The existence of

nascent adhesions and focal complexes is an essential marker of highly migratory cell. Both of them would further disassemble or grow into focal adhesions. Focal adhesions are mature adhesions that are usually connected to actin filament stress fibers. Nascent adhesions, focal complexes and focal adhesions are similar in terms of molecular composition. Several signaling proteins are present in adhesions, for example, focal ashesion kinase (FAK), tensin, paxillin are best characterized and prominent phosphoproteins [98, 99].

The mechanism of adhesion assemble is only beginning to be identified. There is convincing evidence that the formation of adhesions involves Cdc42, Rac and Rho as well as myosin-induced contractility [100].

2.2.3 Traction and Retraction

A migrating cell requires at least two distinct types of forces, traction and retraction. Firstly, at the front of migrating cells, protrusive force generated by actin polymerization implements the extension of membrane processes. As introduced earlier, at the leading edge, actin polymerized and organized under the regulation of Cdc42, Rac, Rho and independent of myosin motor activity. Once the protrusion adheres to the substratum, meanwhile, integrins serve as traction sites by binding the intracellular cytoskeleton to the ECM [101]. The interaction of myosin II with actin filaments attached on the adhesion sites drives the traction[4]. Actually integrins also act as mechanosensors, transferring the information of ECM to cell inner and changing cell dynamics [102]. The traction of cell translocation is affected by the density of the adhesions and the adhesion receptors, and the affinity of the receptors with the ligands of the ECM [103].

Secondly, the translocation of cell body forward requires the retraction force. This force depends on the activity of myosin family motor proteins, especially myosin II. Myosin II plays an important role in contractile process of migrating cell. The activity of myosin II is regulated by myosin light-chain kinase (MLCK) or Rho kinase (ROCK). As we mentioned in Section 2.1, myosin II can connect to actin filaments

and employ them as tracks to produce motion. Hence myosin II can mediate the contraction of actin filaments and promote actin filaments to bind to integrins that connected to the ECM. Then, the contractile force could facilitate the bond disruption potentially either at the integrin- ligand of the ECM or at the integrin-intracellular cytoskeleton, relying upon which bond is unstable [103, 104]. This process possibly leads that the adhesions disassemble and cells move forward.

In migrating cell, adhesion disassembly occurs both in the anterior, where it accompanies with the formation of new protrusions, and in the posterior of the cell, where it facilitates cell tail retraction. The traction and the retraction can generate independently each other. In the anterior of migrating cell, some adhesions in the bottom of protrusion disassembly as new adhesions generate, and some adhesions remain and grow into larger, mature adhesions. The migration cycle starts with the polar protrusion and complete as the cell rear retracts.

2.3 Cell Migration on Micropatterns

A key challenge of cell migration is to design experimental protocols and specific analytical methods to unravel the contribution of each parameter that controls cell behavior. Micropatterning provides researchers with an accurate and affordable tool. It reduces the use of live animals, standardizes environmental parameters in vitro assays and supports quantitative studies of how these parameters affect cell behavior.

2.3.1 Cell Migration on Micropatterned Lines

Cell migration as a fundamental cell behavior occurs in a complex tissue environment, which includes many biochemical and mechanical factors. In attempting to disentangle the complexity, researchers have to tune those parameters quantitatively and independently of each other. Taking a step further

on the simplified path, micropatterned long lines provide a stereotype trajectory for cell migration assays.

Such micropatterned line could be used as a cell racetrack in the first World Cell Race in 2011, in which a large-scale comparison of migration among over 50 different cell lines was performed under standardized conditions (Figure 2.7a). The statistical analysis revealed higher instantaneous cell speed correlates with cell persistence in the same direction irrespective of cell origin [30]. Pauthas *et al.* showed the evidence that the Golgi complex and the centrosome are located behind the nucleus not at the leading edge of the cell, when cell polarizes on thin microlines [105]. Doyle *et al.* demonstrated that in contrast to 2D, the topography of cell migration on 1D thin micro lines is closely to it on 3D fibrillar cell migration (Figure 2.7b). Moreover, cells migrate on later with a higher velocity [106]. Similar lines can be used to investigate the morphology of cells. Picone et al. limited cells on 1D micropatterned lines and showed the evidence that a characteristic steady-state length of the cell is independent of cell size or pattern width but dependent upon the orientation of microtubules [107] (Figure 2.7c). However, Levina et al. compared the epitheliocytes cell lines with fibroblasts on linear strips, showed a slightly different result that the control of cell length is cell-type-specific [108].

These versatile applications of micropatterned lines, as easy to use as conventional Petri dishes, can control important environmental parameters and are therefore likely to be as common as any other cell culture method in the modern cell researcher's evolving toolbox, which predicted by Lautenschläger et al.[29].

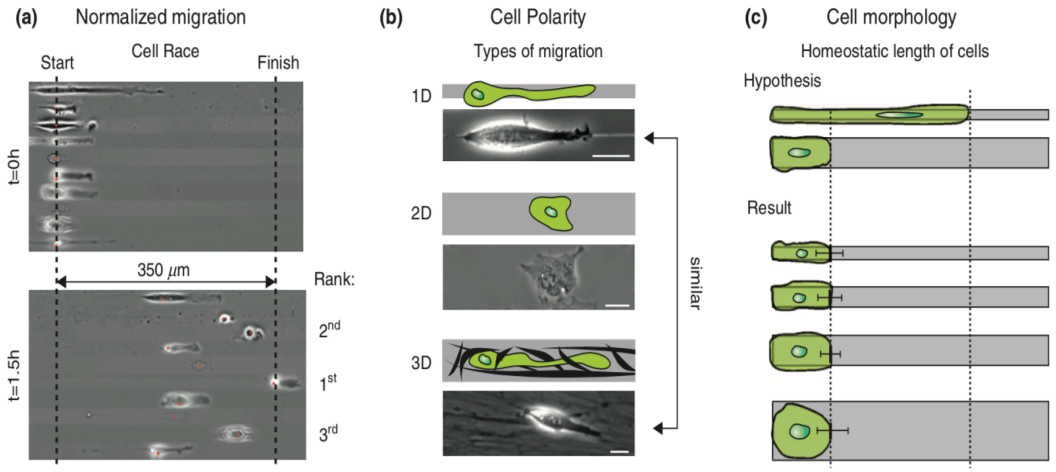

Figure 2.7 The versatility of micropatterned lines.

(a) The First Worlds Cell Race: different cell lines migrating on micropatterned lines of fibronectin. Adapted images from [30]. (b) The difference of morphology of cell on 2D micropatterned areas compared with 1D-1.5 mm thin micro patterned lines and 3D-fibrillar derived matrix. Adapted from [106]. (c) Schematic of cells on pattered lines showing the extension of cell independent of line width. Adapted from [107]. Whole Figure is adapted from [29].

2.3.2 Cell Migration on Various Specific Geometries

Micropatterning is a highly efficient tool to create specific 2D or 3D microenvironmental cues. By manipulating the shape of the micropattern，the sensitivity and response of cell to the geometries can be investigated in more details. Cell can precisely adapt its cytoskeletal structure to the geometrical and mechanical constraints from its microenvironment. Remodeling of actin and microtubule networks is involved in the adaptation of the entire cell polarity to external constraints. These modifications further affect cell migration [109].

Jiang et al. reported that teardrop-shaped asymmetrical micropattern polarizes the morphology of the attached mammalian cells. After released from the confinement, the cells migrate toward the blunt end of the teardrop, which implies that the polarity determines the direction of cell motility [110] (Figure 2.8a). Mahmud et al. showed that when confined to ratchets, random walking cells could be rectified. The imposed ratchet-shaped patterns make the cells reconfigure their internal

migration machinery and provide a possibility to sort mixed cell populations [35] (Figure 2.8b). When a cell confined to a small micropattern, a primary cilium grows on its dorsal surface. In contrast, on enlarged pattern, the ventral surface of cell has no primary cilium [111] (Figure 2.8c). Basic micropattern shapes can be brought together to achieve a multidimensional effect on cell behavior. Kushiro et al. designed a spear-shaped micropattern that was a hybrid of stripe and teardrop geometry. Through the modular reconstruction of the micropattern, cell velocity and persistent could be predictably enhanced and certain unexpected synergistic effects of cell migration can be also obtained [112]. Brückner et al. developed dumbbell-shaped micropattens in which cells undergo repeated stochastic transitions characterized by intricate nonlinear migratory dynamics [36]. In circular micropatterns, Segerer et al. found that the persistence of coherent angular motion increases with the number of cells, exhibiting a pronounced discontinuity [113]. By using a specific crossbow-shaped fibeonectin micropattern, Théry et al. demonstrated that geometric cues determine the orientation of cell polarity axes. The direction of the nucleus-centrosome can be replicated to the cell adhesion edge. In response to adhesion conditions, the anisotropy of the cell cortex does not affect the localization of the centrosome at the cell centroid [114].

Micropatterns become extremely popular in cellular research. Herein, some of them were briefly presented. These studies highlight the important role of the mechanical and the geometrical features of the microenviroment in cell physiology, from intracellular organization to multicellular morphogenesis. Although the basic progress of cell migration on micropatterned surfaces have been studied extensively, there is still a paucity of data on a lot of core mechanism of morphorgenesisi, for example the repolarization dynamics at barriers in a quantitative manner, which would be addressed in this thesis.

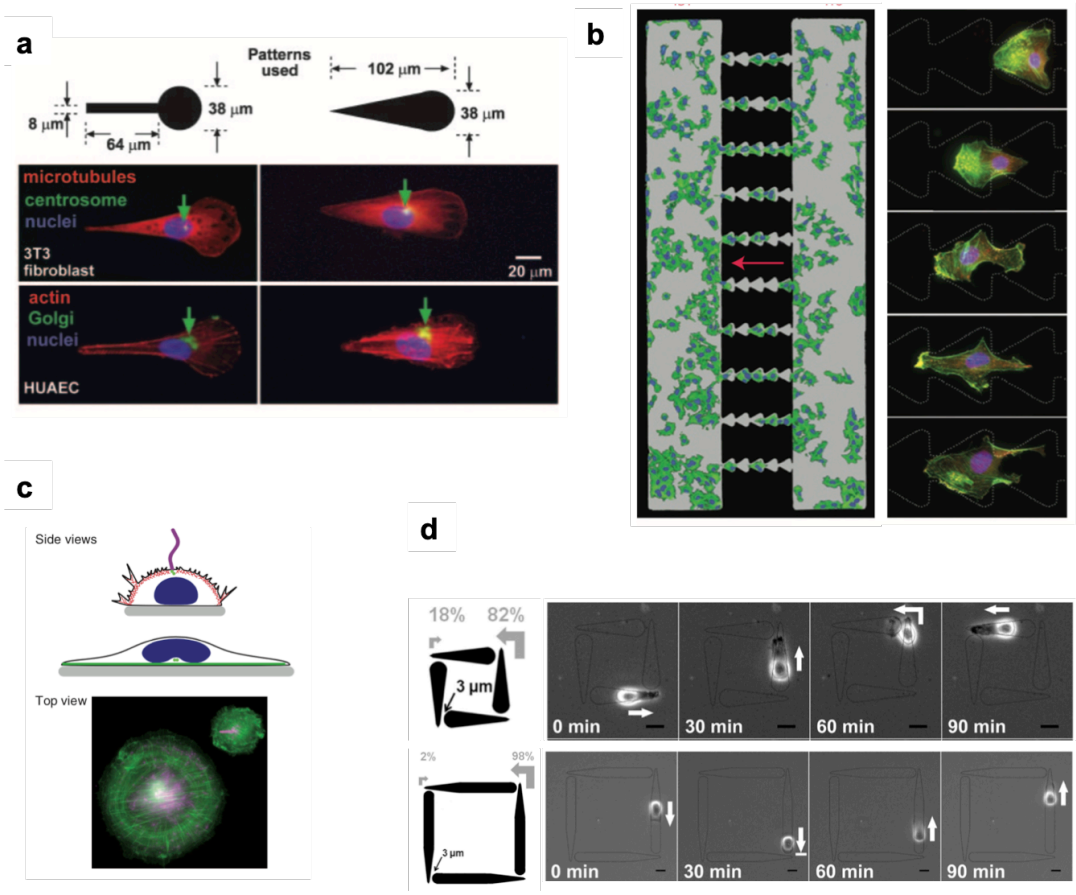

Figure 2.8 Cell migration on various specific micropatterns.

(a) The centrosome and the Golgi are localized in the region of the blunt end of the asymmetric patterns. Adapted from [110]. (b) B16F1 cell migrating on connected-triangle ratchets. The organization of Arp2/3 (yellow) and actin (green) are shown. Adapted images from [35]. (c) Cell grows on a smaller micropattern vs. a larger micropattern with the tubulin (magenta) and the actin (green) as a marker of the primary cilium. Adapted from [111]. (d). Directional cell migration on a hybrid spear-shaped micropattern. Compared to the original teardrop-shaped patterns, migration bias spear-shaped patterns is greatly enhanced. Adapted from [112].

2.4 Theoretical Description of Cell Migration

The previous sections discuss cytoskeleton dynamics in migrating cells. Cell migration is complex. Analyzing and understanding the rules of cell behavior require the underlying theoretical descriptions and models. Thus, this section begins with the introduction of the common mathematical assessment of motion patterns. Based on these patterns, more complicated mathematical models could

establish, in order to understand and reproduce the mechanisms of cellular dynamics.

2.4.1 Langevin Equation and Mean Square Displacement

Without external guidance, a typical trajectory of single wild type migrating cells on a 2D substrate resembles those of thermally driven Brownian particles. A mathematical description of the Brownian motion is the Langevin equation. Briefly, for a particle moves in x-axis direction:

$$v = \frac{dx}{dt}, \tag{2.1}$$

According to Newton´s second law of motion

$$m\frac{dv}{dt} = F, \tag{2.2}$$

Where v is the velocity and x is the displacement of the particle within time t, m is the mass of the particle, and F denotes the total force acting on the particle. F can be split into two forces, a drag force (frictional force) and a stochastic force. The frictional force is a viscous force proportional to the velocity of the particle (Stokes' law). The stochastic force $F_s(t)$ is a noise term, which is independent of the particle´s displacement and represents the collision of the fluid molecules on the particle.

$$F = -\lambda\frac{dx}{dt} + F_s(t), \tag{2.3}$$

Here, λ is the damping coefficient. The force $F_s(t)$ has a Gaussian probability distribution with correlation function:

$$\langle F_{si}(t)F_{sj}(t')\rangle = 2\lambda k_B T\delta_{i,j}\delta(t-t'), \tag{2.4}$$

Where < > denotes expectation value, $F_{si}(t)$ is the *i*-th component of the force $\mathrm{F_s(t)}$, t and t' are different time steps, $\mathrm{k_B}$ is Boltzmann constant, T is the temperature, δ denotes Dirac delta function. The Fourier transform of equation (2.4) displays the power density spectrum, which is a constant in a certain frequency range and is perceived as white noise. Then equation (2.2) can be written as:

$$m\frac{dv}{dt} = -\lambda\frac{dx}{dt} + F_s(t), \tag{2.5}$$

Equation (2.5) is known as the original Langevin equation describing Brownian motion. Based on the equation, more motion models can be enlightened. As a standard reference, the Ornstein-Uhlenbeck (OU) process, which is a model inspired by Brownian motion, can be regarded s a modification of the random walk in continuous time [115, 116].

$$\frac{dv}{dt} = -\frac{1}{t_p}v + \frac{\sqrt{2D}}{t_p}\varepsilon(t), \tag{2.6}$$

Where t is time, $\mathrm{t_p}$ represents the persistence time of the motion, $\varepsilon(t)$ is white Gaussian noise, D is the diffusion coefficient, and sometimes is regarded as the motility coefficient of microorganism, D is involved in the Stokes-Einstein equation [117].

$$k_B T = 6\pi\eta a D \tag{2.7}$$

For the mean square displacement (MSD) of a motile organism Fürth's formula[118] remains a standard, with which experimentally observed migration patterns can be analyzed [119].

$$MSD(t) = 2nD(t - t_p\big(1 - e^{-t/t_p}\big)), \tag{2.8}$$

Mean square displacement is defined as the displacement at a certain time relative to at a zero time $x(t) - x(0)$, averaged over amounts of time points. Here, n

indicates the dimension of the space, D is the diffusion coefficient of the Ornstein-Uhlenbeck (OU) process.

2.4.2 Fourier Transform

In the practical case, single cell could be look as an individual particle. Its trajectories can be recorded over a series of time steps and be regarded as a signal, which is viewed in the form of a frequency spectrum, then, more information about the cell motion can be extracted. The Fourier transform (FT) decomposes a function of time (a signal) into constituent frequency components. Fourier analysis has been used in wide applications, such as optical, electrical or mechanical signal [120]. In this work, Fourier transform is applied to analyze the behavior of single cell migration. Here, the basic principle of Fourier transform is briefly introduced [121-123].

Let $x(t)$ be any real-valued signal with a period T seconds, then $x(t)$ can be expanded as a sum of sines plus cosines, which are called as Fourier Series.

$$x(t) = a_0 + \sum_{n=1}^{\infty} [a_n cos\left(\frac{2\pi nt}{T}\right) + b_n sin(\frac{2\pi nt}{T})] \tag{2.9}$$

Here, $\frac{1}{T}$ Hertz is the fundamental frequency, $f_0 = \frac{1}{T}$, because sine and cosine function have frequencies with integer multiples of it, $f = \frac{n}{T}$. The coefficients a_0, a_n, b_n are the amplitude of each component.

$$a_0 = \frac{1}{T} \int_{-T/2}^{T/2} x(t)dt \tag{2.10}$$

$$a_n = 2\,\langle x(t)cos\frac{2\pi nt}{T}\rangle = \frac{2}{T} \int_{-T/2}^{T/2} x(t)cos\frac{2\pi nt}{T}dt, \quad \text{interger n} \geq 1 \tag{2.11}$$

$$b_n = 2\,\langle x(t) sin\frac{2\pi nt}{T}\rangle = \frac{2}{T}\int_{-T/2}^{T/2} x(t) sin\frac{2\pi n\tau}{T} dt\,, \quad \text{interger n} \geq 1 \tag{2.12}$$

This Fourier series in form of sines plus cosines represents the even and odd parts of $x(t)$ separately. This can be represented as a complex exponential type, which is analogous to the Discrete Fourier Transform (DFT)[124].

$$x(t) = \sum_{n=-\infty}^{+\infty} a_k e^{i\frac{2\pi nt}{T}} \tag{2.13}$$

Where the Fourier coefficient a_k is determined by the following formula:

$$a_k \overset{\text{def}}{=} \frac{1}{T}\int_{-T/2}^{T/2} x(t) e^{-i\frac{2\pi nt}{T}} dt \tag{2.14}$$

Then the Fourier series synthesis formula is:

$$x(t) = \sum_{n=-\infty}^{\infty}\left[\frac{1}{T}\int_{-T/2}^{T/2} x(t) e^{-i\frac{2\pi nt}{T}} dt\right] e^{i\frac{2\pi nt}{T}} \tag{2.15}$$

When taking the limit $T \to \infty$, then fundamental frequency $f_0 = \frac{1}{T} \to 0$ and can be written as df, resulting in $f = \frac{n}{T}$ serving as the new continuous variable. We may write the above equation in:

$$x(t) = \int_{-\infty}^{+\infty}\left[\int_{-\infty}^{+\infty} x(t) e^{-i2\pi ft} dt\right] e^{i2\pi ft} df. \tag{2.16}$$

Hence, Fourier transform (FT) can be defined as:

$$\hat{x}(f) = \int_{-\infty}^{+\infty} x(t) e^{-i2\pi f t} dt \tag{2.17}$$

The inverse FT:

$$x(t) = \int_{-\infty}^{+\infty} \hat{x}(f) e^{i2\pi f t} df \tag{2.18}$$

The function $\hat{x}(f)$ is the equivalent of the Fourier coefficients in the Fourier series (2.13). $\hat{x}(f)$ is a function in the continuous frequency domain where $f \in (-\infty, +\infty)$. In many practical cases, we should consider the Fourier transform in a discrete time domain, instead of an infinite continuous time domain. For example, in this thesis, there are n equal time samples,

$$t_j = j\Delta t \ (j = 0, 1, 2, \dots, n-1) \tag{2.19}$$

Here, Δt is the interval time between two adjacent time points, then $f_0 = \frac{1}{\Delta t}$ is the sampling frequency which is the video camera´s resolution (frames number per minute or second) in this work.

$$f_k = \frac{1}{T} = \frac{1}{k\Delta t} \ \ (k = 0, 1, 2, \dots, n-1), \tag{2.20}$$

Thus, for the finite discrete data signal $x(t_j)$, the discrete Fourier transform (DFT) is:

$$\hat{x}(f_k) = \sum_{j=0}^{n-1} x(t_j) e^{-i2\pi f_k t_j}, \qquad k = 0, 1, 2, \dots, n-1 \tag{2.21}.$$

DFT can be carried out by fast Fourier transform (FFT), which is a computational algorithm for efficiently performing DFT[125]. FFT increases the computing speed for huge data sets. In this thesis, it was used for the Fourier analysis.

2.4.3 Models for Cell Migration

Cell migration is a complicated phenomenon that is driven by the interaction with the cytoskeleton and the plasma membrane. A well-defined simulation model is critical for addressing the relationship between intracellular dynamics and cell morphology and movements.

Reaction-diffusion model

The basic idea of some models resides in a well-known property of reaction-diffusion systems with bistable kinetics. The reaction-diffusion system is a mathematical model that takes the form of a semi-linear parabolic partial differential equation.

$$\partial_t \mathrm{q} = \mathrm{D}\nabla^2 q + R(q) \qquad (2.22).$$

Here, q represents the unknown vector function, D is the diagonal matrix of the diffusion coefficients, and R represents all local reactions. The solution of the reaction-diffusion equation shows a wide range of behaviors, including the formation of traveling waves and wave-like phenomena as well as other self-organized “Turing patterns".

In recent decades, in order to depict and explore the dynamics and machinery, the process of cell migration has been simulated with many models based on the reaction-diffusion system [126]. A stochastic model that develops cell-edge dynamics was used to validate that protrusion-retraction switches during polarization depend on the distance from the cell center, instead of on the orientation [127]. Using a predictive mathematical modeling, Byrne et al. show that bistability in a network containing Rac1, RhoA, and PAK, which governs the cell morphology and cell motility switches [23]. Wilson et al. presented a conceptual model that the F-actin network polymerizes from the free membrane at the leading edge bio Arp2/3 nucleation [128]. Maiuri et al. developed a minimal theoretical

model that explains a universal coupling between cell speed and cell persistence, and predicts a phase diagram of cell trajectories [16]. Burnette et al. developed a model of how arc contraction causes the cell to flatten. Their model provides a possibility that the understanding of how cells use the contraction/adhesion system to configure themselves to complex spaces [129]. Barnhart et al. now proposed a a set of mechanochemical feedback loops underlying actin-driven motility and wave generation in keratocytes, which may constitute a general module for understanding actin oscillating in other cell contexts [130]. Krause et al. demonstrate that the positive and negative feedback loops describing the protrusion and retraction cycles in cell migration results in oscillatory behavior and determines the lamellipodial persistence [131]. These findings drew a sufficiently simple map to develop a mathematical model of the cell migration.

Cellular Potts model

Each model possess its exceptional benefits and meanwhile disadvantages. For the models concentrated in the intracellular kinetics machinery, they are usually short of simulating the motility of large cell group. For models focusing on the large scale locomotion of collective cells, they often lack of describing the cellular component signaling of single cells. James Glazier and François Graner proposed a modeling approach, so-called cellular Potts model (CPM), which is a respectively intermediate way to fast simulate fairly large aggregates of cells and realize the position and diffusion of intracellular dynamics [132, 133]. The CPM extended large-Q Potts model has been widely applied in further cell research. Its principle is briefly introduced as follows.

The Cellular Potts model originally aims at cell sorting, and describes N cells by regular lattice spins σ (i,j), where i,j determines a lattice site. The energy of bonds between different cells and bonds between like spins is given by the Hamiltonian.

$$H_P = \sum_{(i,j)(i',j')neighbors} I - \delta_{\sigma(i,j),\sigma(i',j')} \qquad (2.23).$$

For cell sorting, an elastic-area constraint, the cell type τ, was added to the Hamiltonian of the system. Then the modified Hamiltonian :

$$H_{sort} = \sum_{(i,j)(i',j')neighbors} J\left[\tau\left(\sigma(i,j)\right), \tau(\sigma(i',j'))\right]\left[I - \delta_{\sigma(i,j),\sigma(i',j')}\right] + \lambda \sum_{\sigma}\left[A(\sigma) - A_{\tau(\sigma)}\right]^2 \quad (2.24).$$

Where J is the interaction between spins of cell type τ, λ is the Lagrange multiplier denoting the area constraint. A indicates area of cell σ. The first item of represents the energy between neighbor cells, the second item is the elastic energy of a cell.

The simulation of CPM carries out a Monte Carlo step (MCS) and implements a succession of "elementary events", in which a randomly chosen lattice site $\sigma(i,j)$ is tried to be copied to one of its neighbors $\sigma(i',j')$ (Figure2.10). For such elementary event, the energy changes

$$\Delta H = H_{CPM}^{after} - H_{CPM}^{before} \quad (2.25).$$

The probability of the accepted copy case P is:

$$P = \begin{cases} e^{(-\Delta H)}, & \Delta H > 0, \\ 1, & \Delta H \leq 0 \end{cases} \quad (2.26).$$

The standard CPM has been widely extended in various applications. In this thesis, our simulation model adopts the basic concept of CPM to describe the single cell dynamics, which will be introduced in Chapter 5.

Chapter 3 Methods and Materials

In this chapter, the basic experimental techniques and main materials that were used in this thesis are introduced. The research results of this work will be described into two Chapters, Chapter 4 and 5. The research image data come from the time-lapse microscopy and the fluorescence microscopy, which is introduced in Section 3.1. Micropatterning is an important tool to create specific microenvironment for studying of cell behavior in this work. Two micropatterning methods, plasma induced patterning and micro contact printing, were used and briefly introduced in Section 3.2. All of the essential techniques for cell culture and preparing the cell samples were provided here. For study of actin dynamic, the transfection of cells with Lifeact-GFP mRNA plasmids is briefly described in the section. Moreover, the optical evaluation and analysis of cell tracking are the core techniques in this dissertation.

3.1 Experimental Setups

3.1.1 Phase-contrast and Fluorescence Microscope

Phase-contrast and fluorescence images are performed by a TI Eclipse (Nikon) microscope or an iMIC (Till Photonics) microscope.

With a phase-contrast microscope, the difference in phase among cells is interpreted into distinct brightness with variation in refractive indices or thickness. Objects can be detectable by eye in unstained condition. A phase-contrast microscope is consistent with condenser lens system and objective. There is an annular hole in the rear focal plane of objective to control the illumination.

Fluorescence microscopy is an essential tool in cell and molecular biology research. It expands the properties of traditional optical microscopy due to visualization of fluorescence, which makes it possible to recognize cells and cellular structures using specific fluorescent probes. Understanding the principle of fluorescence microscopy is useful when trying to solve imaging problems.

The main components of the microscope are shown in Figure 3.1. Fluorescence microscopy demands the objects of interest fluoresce, the light source and the specialized filter elements. Fluorescence is the emission of light that comes from the mercury lamp, which emits white light. The light directly passes through an exciter filter that isolates one specific wavelength of the white light and blocks out other color components. Then a dichroic mirror, which is fixed at such an angle that reflects the excitation light towards the fluorescent specimen and allows the emission light pass through. The emitted light goes backward, firstly passes through the objective then through the dichroic mirror, and is filtered again by an emission filter, then guided by a beam splitter cube. Finally, the eye or the Charge-Coupled Device (CCD) camera perceives the filtered fluorescent light against a jet-black background.

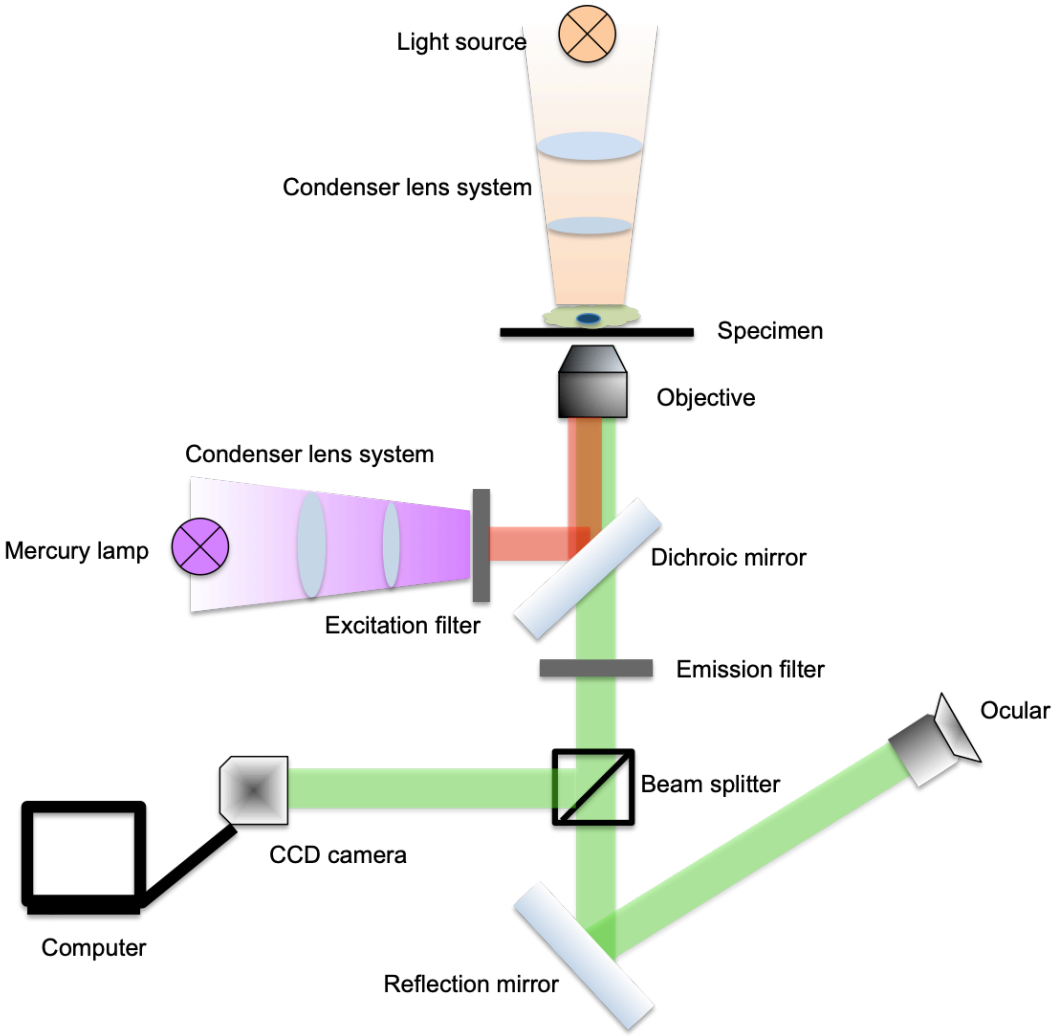

Figure 3.1 Schematic of the principle of fluorescence microscopy.

3.1.2 Time-Lapse Microscopy

Scanning time-lapse measurements in this work are performed using a phase contrast and fluorescence microscope. An inverted microscope (iMIC, Till Photonics) equipped with a 10x Zeiss objective and a 40x Zeiss objective is used. An Oligochrome lamp (Till Photonics) and an ORCA-03G camera (HAMAMATSU) were also fitted in the microscope. In this work, the fluorescent image of cells was illuminated with the Oligochrome lamp for 100 ms with 25% intensity. The cells during the measurements are kept at 37°C using a temperature controlled mounting frame (Ibidi temperature controller, Ibidi). The sample stage moves and images can be acquired automatically in a certain time intervals using Live

Acquisition software. If no special notes, the interval time is 10 min. To analyze the actin activities at the tips of the micropatterns, the 40x objective was used and original images were acquired every 5 sec – 1 min.

3.2 Surface Patterning for Cell Research

3.2.1 Production of Stamp Masters

In terms of promoting cell migration in vivo, it involves influencing cell-substrate interactions through topographical or biological signals. The biological signals often take the proteins of the ECM such as the fibronectin, laminin and collagen to direct cell adhesion. One approach to the production of topographical surfaces is the use of photolithography to fabricate stamp masters firstly.

To prepare the stamp master for micropatterning, a silicon wafer (SI-Mat) was coated with an adhesion promoter (TI Prime, MicroChemicals GmbH) by spincoating (SAIJSS, MicroTec) at a rate of 500 rpm for 5s initially then speeding up to 5000 rpm for 30s. The wafer is further baked on a heating plate at 120°C for 2 min. A photoresist (AZ40XT, AZ Electronic Materials) was then spincoated at 800 rpm for 3s and then accelerating to 3000 rpm for 30 s. The thickness of the photo resist layer is about 15 µm. The wafer is further baked at 80°C, 100°C and 125°C for 1 min respectively. The wafer was further illuminated with ultraviolet (UV) light using a laser direct imaging device (Protolaser LDI, LPKF) to write the desired pattern in the photo resist. The laser spot of 1 µm with a spot spacing of 0.2 µm and a 450 mJ/cm^2 illumination dose were used. In the following step, the wafer was baked for 1.5 min at 105°C and then the wafer was placed into a developer (MIF 826, AZ Electronic Materials) for about 2 min to remove the photo resist which was exposed to the UV light. Afterwards, the wafer was washed with miliQ water and then silanized with Trichloro(1H,1H,2H,2H-perfluorooctyl)silane (Sigma-Aldrich) by silane evaporation to prevent sticking of PDMS when it was used.

3.2.2 Production of Stamps

To fabricate the stamp, polydimethylsiloxane (PDMS) monomer (Sylgard, Dow Corning) and crosslinker (DC 184 elastomer Kit, Biesterfeld Spezialchemie GmbH) were mixed in a 10:1 ratio (w/w), degassed in a vacuum oven for 20~30 min and pured onto the stamp master. After another degassing step, the PDMS is incubated at 50°C for 10h or overnight. The crosslinked PDMS layer was peeled off and manually cut into stamps.

3.2.3 Fibronectin Labeling

To observe the patterning structures, fibronectin was labeled by dyes. 50 µl 1M carbonate buffer solution was added into 500 µl of 1 mg/ml fibronectin solution to regulate the PH to the optimal reaction condition, PH=8.5. For 10 dye/protein and reaction efficiency of 25%, 40 times dye per protein. The dye was dissolved in 3 µl dimethyl sulfoxide (DMSO) and was added into the protein solution. To let the dye protein react, the mixed solution was stored at room temperature in the dark for at least 4h or overnight. Finally, the free dye and labeled proteins were separated by gel filtration Chromatography (PD Minitrap G-25, GE Healthcare).

3.2.4 Plasma Induced Patterning

Micropatterning techniques can fabricate well-defined functional spatial arrangements for cell adhesion. Patterns with cell friendly areas and unfriendly areas could be achieved. One of the micropatterning methods is plasma-induced patterning. This technique was used in the initially test in this work. Here some regions of our sample were partially covered by the PDMS stamp of desired pattern. Then, the sample was exposed to plasma oxygen atmosphere at a power of 40 W with a pressure of 0.2 mbar for 3 min by the plasma cleaner (Femto, diener electronics). This changes the surface chemical properties (e.g. a hydrophilic surface) of the exposed area. Subsequently, a droplet about 2 µl of a 2 mg/ml poly(l-lysine)(20kDa)-graft[3.5]-poly(ethylene-glycol)(2kDa) (PLL-g-PEG) in 10 mM

HEPES (pH=7.4) and 150 mM NaCl solution was put near the edge of each stamp to let it draw into the free spaces between the substrate and stamps by capillary action. After 30 min of incubation at room temperature, the stamps were removed and the substrate was washed with PBS to remove the free PLL-g-PEG solution. Afterwards, a fibronectin / fibrinogen solution (50 µg/ml in PBS) was added for 45-60 min. Finally, the patterns were rinsed for three times with PBS and they are ready to use.

3.2.5 Micro Contact Printing

The produce of stripe-shaped microlanes was mostly used by microcontact printing in this thesis. The procedure was simply illustrated in Figure 3.2. Firstly, PDMS stamps were exposed with UV-light (PSD-UV, novascan) for 5 minutes. Then the stamps were immersed in a solution 40 µg/ml fibronectin (Yo Proteins) containing 10 µg/ml Alexa Fluor 488 dye (Life Technologies) labeled fibronectin for 45 minutes. Secondly, the stamps were washed with ultrapure water. Stamps were dried under filtered airflow and then stamped onto a hydrophobic uncoated µ-Dish (Ibidi GmbH) bottom, which was through UV exposure for 15 minutes before. The stamps were slightly pressed with tweezers for few seconds to remain in contact with the bottom. Thirdly, to fabricate the cell-repelling areas, 30 µL of 2 mg/ml poly-L-lysine-grafted polyethylene glycol (PLL-g-PEG) (2 kDa PEG chains, SuSoS) solution, which was dissolved in 10 mM Hepes and 150 mM NaCl solution, was added. After the removal of the stamps, a glass cover slip was placed on the printed bottom to assure complete coverage with PEG solution, incubated for 30 min at room temperature. Finally, the printed bottom was washed with phosphate buffered saline (1 x PBS) for three times and stored in PBS for further cell seeding. Unless otherwise specified, the pattern consisted of a uniform strips 20 µm in width. Protein such as fibronectin coated surface structures will be created by micro contact printing. On such surfaces we can easily change the geometry and surface coating and perform the following cell experiments.

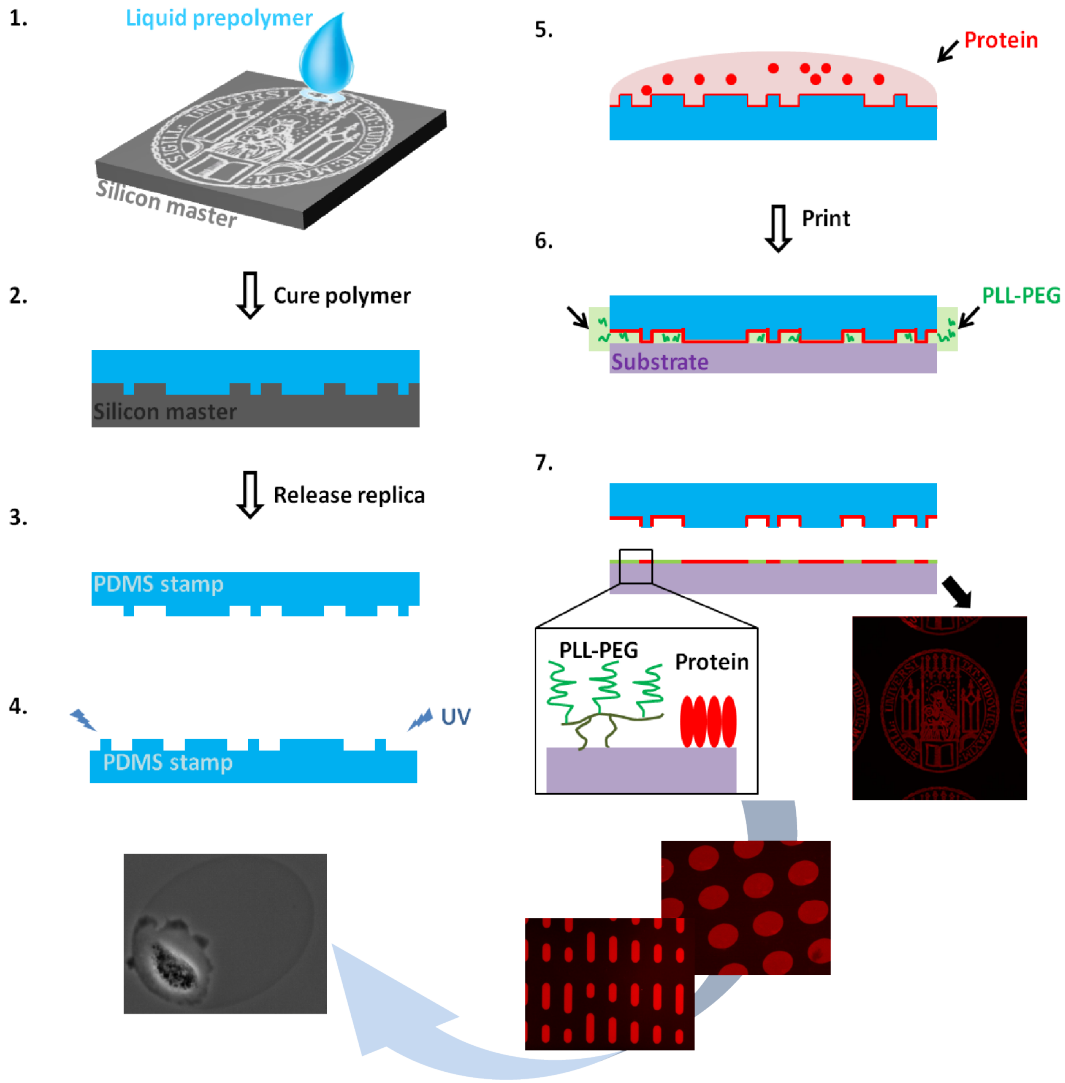

Figure 3.2 Procedure of the fabrication of micro-patterns using for cell adhesion.

(1-4). Production of PDMS stamp by using a silicon master. (5-7). Procedure of micro contact printing.

3.3 Cell Culture Methods

3.3.1 Cell Cultivation

Madin-Darby Canine Kidney (MDCK), human liver cell (HuH7), and Human breast cancer cell (MDA-MB-231) cells were used in this work. If no specific note, cells were cultured in supplemented medium with 10% fetal calf serum (FCS, Invitrogen) and 2-4 mM L-glutamin (c.c.pro) and kept in an incubator with a humidified

atmosphere of 5% CO2 and 95% air at 37°C. The cell lines used in this work and their culture medium are given in the following Table 3.1.

Cells were splitted twice a week in a ratio of 1:3 to maintain them at a confluence of about 70%. For the trypsinization, the old medium was removed and the cells were washed with PBS to discard all traces of serum that would inhibit the detaching reagent in subsequent steps. 1 ml of a 0.25% (w/v) Trypsin solution was added to the flask to detach the cell. Trypsin is a proteolytic enzyme that breaks down the adhesion of cells each other and cells to the flask. To stop the trypsinization, 5 ml of culture medium was added. The cell suspensions were transferred into a 15 ml conical tube for centrifugation at 1000 rpm for three minutes. The upper medium containing Trypsin was removed, and 6 ml of 37°C culture medium was added to re-suspend the cells. 2 ml of cell suspension was diluted with 3 ml new culture medium into a culture flask, and then cultivated in the incubator.

Table 3.1 Cell lines and their corresponding media.

Cell Type	Organism	Tissue	Medium
MDCK	canine	kidney	MEM+ 4 mM L-Glu
Huh7	human	liver	RPMI+ 2 mM L-Glu
MDA-MB-231	human	breast	DMEM-F12+ 2.5 mM L-Glu

3.3.2 Freezing and Thawing of Cells

In this work, cells were always used from the passage 6^{th} to passage 36^{th}, therefore, it is necessary to freeze and thaw cells sometimes. For cell freezing, generally cells were centrifuged and old medium was completely discarded as what we did in procedure of splitting. Then, cells were resuspended in ice-cold freezing medium containing DMSO, and were transferred to a Cryo-tube (Greiner bio-one GmbH, Germany) and immediately placed on ice. Cells were firstly stored at -80°C overnight, and finally stored in liquid nitrogen for long-term maintenance.

For cell thawing, cells which were taken out of liquid nitrogen tank were firstly thawed in a 37°C water bath for about 1 min, and then they were immediately poured into 8 ml culture medium. After 3 min centrifugation of the cells, the old medium was discarded and cells were suspended in new culture medium and plated into a culture flask. After 12h incubation, the medium containing the dead cells which didn´t attach to the substrate were removed and changed into new culture medium.

3.3.3 Cell Quantification and Seeding

For experiments, to keep a consistent number of the cells during subculture routines and to obtain about one cell per patterning structure, about 1 x 10^4 cells were seeded per dish. Therefore, it is necessary to quantify the number of cells before seeding. A counting device called hemocytometer was used in this procedure. As shown in Figure 3.3, the hemocytometer consists of two rectangular indentations forming the counting champers in which cells suspension can be filled. When mounted with a cover glass on the top, cells can be counted with an optical microscope. Because the depth of the chamber is 0.1 mm and it consists of nine 1 x 1 mm (1 mm^2) squares, the volume is fixed. Therefore, it is possible to calculate the concentration of cells in suspension. The concentration of cells can be calculated as the equations below:

$$N_{cell/mL} = \frac{n_{cell}}{n_{squares}} \times f_d \times 10^4 \qquad (3.1).$$

Where $N_{cell/mL}$ indicates the number of cells per milliliter, n_{cell} is the number of cells counted, $n_{squares}$ is the number of large squares counted, f_d represents the dilution factor.

To prepare the sample for experiments, 1 x 10^4 cells mixed with 1 mL of growth culture medium, seeded in a petri dish with a glass bottom (ibidi, Φ35mm, thickness 0.17 mm) and kept in the incubator. After 2.5h cell adhered and the

medium was gently removed and changed into 1 mL of CO_2 independent Leibovitz's L-15 Medium (c.c.pro) containing 10% FCS and 25 nM Hoechst 33342 nuclei dye (Invitrogen) and incubated for 1h at 37°C before imaging.

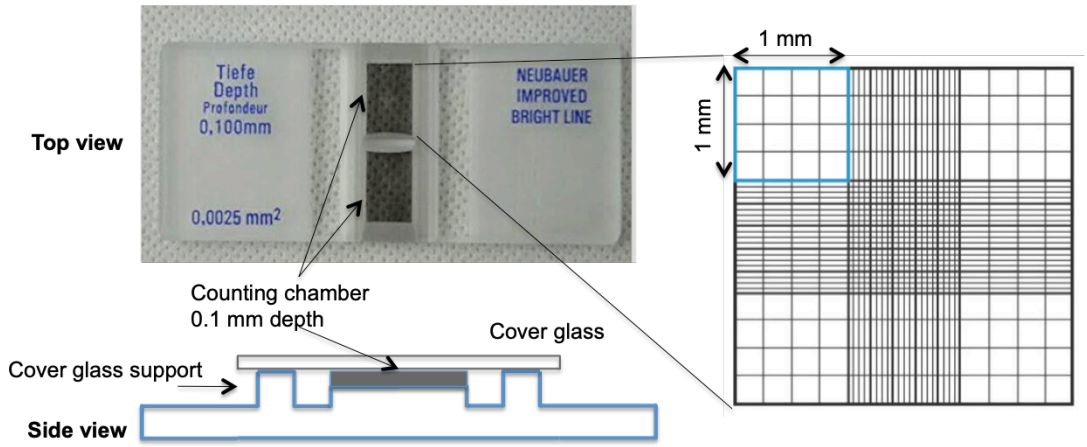

Figure 3.3 Structure and calculation principle of the hemocytometer.

3.3.4 Cell Transfection

For actin dynamic study, seeded cells were further transfected with Lifeact-GFP mRNA plasmids. Briefly, ~1x 10^4 cells were seeded into a 35mm µ-Dish and incubated 2.5h at 37°C in 5% CO_2 for cell adhesion. 1.25µl Lipofectamine MessengerMax Reagent (Invitrogen) was diluted in 123.75µl OptiMEM (Life Technologies) transfection medium and incubated 10 min at room temperature. 500 ng mRNA (0.5 µl x 1000ng/ µl) was diluted in 124.5µl OptiMEM. (Note that mRNA should be kept on ice after thaw, RNAse-free pipette-tips should be used in operation.). Both solutions were mixed and incubated for 5 min at room temperature for lipoplex formation. Adhered cells were washed with 1xPBS, and carefully added the 250µl transfection mix. After a 1h incubation at 37°C in 5% CO_2, the cell transfection mix was replaced by 1 ml Leibovitz's L-15 Medium (c.c.pro) containing 10% FCS before proceeding to time lapse imaging.

3.4 Evaluation and Analysis of Cell Tracks

3.4.1 Single Cell Tracking and Image Processing

The phase contrast videos of cells on patterning structures were recorded for a certain period by the time lapse microscope, and the further analysis of cells images in video files were carried out by ImageJ (National Institutes of Health, NIH). Firstly, to research the migration behavior of single-cells without effects of other cells or cell-cell interactions, only circle/ ellipse/stripe-shaped patterns that contain isolated cells are chosen by eye. Secondly, only cells which move at least one period (from one side to another side and then back) are considered to analyze, non-moving cells such as dead or dying cells were excluded. Thirdly, when the cells run out of or partly span over the micropatterns, the following record images are excluded. Fourthly, only cells migration tracks that last for at least 18 hours are considered. In particular, if no specific note, single cell with two nuclei was also excluded. Finally, images of those qualified isolated cells migrating in the micro-patterns were manually cropped. The trajectory of each stained nucleus was preprocessed by first applying a bandpass frequency filter and a fluorescence intensity threshold to the fluorescence images, and the geometric center of mass of nucleus was subsequently evaluated. The geometric mean of the nucleus position was considered as the cell position. As a result, ImageJ reads out the spatiotemporal displacements of the nucleus in two dimensions in the form of $x(t_i)$ and $y(t_i)$, $i = 0, 1, 2, \dots, N$. i is the number of frames in the video.

3.4.2 Data Analysis

Trajectories of individual cells were analyzed in Matlab (Math-works). If not noted otherwise, the center of the stripe was defined as origin of linear coordinate system, such that the coordinate y for the position might be either positive or negative, and the cell velocity was evaluated from the component along the long edges of the stripe (the migrating direction),

$$v_i = (\varphi_{i+1} - \varphi_i)/\ \Delta t, \qquad (3.2).$$

Where φ_i indicates the cell position at time i and Δt is the intervals. The statistical analysis, curve fitting as well as turn-around time were processed with handwritten Matlab code.

Chapter 4 Guiding Micropatterns to Study Single-Cell Migration

Cells are highly sensitive to geometrical and mechanical constraints from their microenvironment. Micro-patterning techniques can provide a soft, 3-dimensional, complex and dynamic microenvironment for individual cells arrangements. By imposing defined boundary conditions, cells can precisely adapt their cytoskeleton architecture to the geometry of their microenvironment. Moreover surfaces presenting signal molecules can further impact cell adhesion, morphology, and migration. Understanding cell motility may be profoundly important for the study of chemotaxis, embryogenesis, and cancer metastasis. Section 4.1 shows that single MDCK cells on circle-shaped micro-patterns exhibit a spontaneous oscillatory motion behavior. In a second step, Section 4.2 demonstrates the effect of geometries, such as circle, ellipse and stripe, on the spontaneous oscillatory motion. Section 4.3 describes the oscillatory motion of different cell lines, such as MDCK, Huh7, and MDA-MB-231 cells. The last two sections summarize the cell motions and choose an appropriate cell line and micropattern to the highly reproducible and controllable oscillation behavior serving for upcoming study in Chapter 5.

4.1 The Emerging of Spontaneous Oscillations on Micropatterns

Spontaneous molecular oscillations are ubiquitous in biology. Oscillations play an important role in many dynamic cellular processes. Understanding cell oscillatory motility may be profoundly important for the study of chemotaxis, embryogenesis, and cancer metastasis. Cells are highly sensitive to geometrical and mechanical constraints from their microenvironment. Moreover, surfaces presenting signal molecules can further impact cell adhesion, morphology, and migration. Herein, our central hypothesis is that by imposing defined boundary conditions, single cells can precisely adapt their cytoskeleton architecture to the geometry of the micropatterns and generate oscillatory motion inside it.

In order to study the single cell migration behavior in a well defined and a standardized environment, in a first set of experiments, MDCK cells are seeded on micro-structured fibronectin-coated circles surrounded by a PEGylated area. Consequently, cells that are on the specific structures always stay on the micropattern and do not get in contact with other cells. The main advantage of circles is that they are isotropic. We find that some cells exhibit an oscillatory mode of migration.

Single cells located on a circle were used for studying individual cell behavior until they divide. To avoid that multiple cells on the observed structure and to observe cells over several days, cells have to be seeded at rather low concentrations. Figure 4.1(a,b) shows a typical trajectory of a MDCK cell migrating over a period of 3 days in a circle-shaped micropattern. The diameter of one circle was chosen to be 75 µm. On these, cells exhibited a morphology closely resembling that cells on an open 2D surface, but they were still sufficiently guided. It is unclear how the curvature might influence the migration behavior, which will therefore be studied. The cell nuclei were fluorescently stained, and thereby the trajectory of the geometric center of mass of the nucleus was evaluated in ImageJ [134]. It is not easy to recognize the

distinct phases of the random motions and the oscillations from the two dimensional trajectory. In order to discriminate different modalities, an automated tracking of the cell position along the x-axis over time is shown in Figure 4.1(c). Distinct phases of motion and morphology are discernible, as shown in Figure 4.1(c and d). Four characteristic cell modes of migration and morphology were found: (A) A random walking mode with a roundish cellular morphology. The cell starts to migrate randomly after being seeded on the surface resembling a cell migrating on an open 2D surface. This state lasts about 2500 min. (B) A circling mode with a fish-like shape, an asymmetric, polarized morphology. This morphology occurs just after the random mode and persists as shortly as ~300 min. In this phase, the cell probing the boundary of the micropattern. (C) An oscillation mode with a polarized morphology with lamellipodia at the leading edge. The cell traverses the micro-pattern from one side directly to the opposite side. This kind of back and forth motion, which was called “oscillation”, persists ~1500 min. (D) Gradual reorientation with a random walk following the oscillation.

In fact, multi-modality in cellular migration has reported before [135-137], however among those migration modalities, the spontaneous oscillation of whole cell was few reported. Oscillation is the simplest cell motion, which could be the ideal model for studying cellular behavior [138].

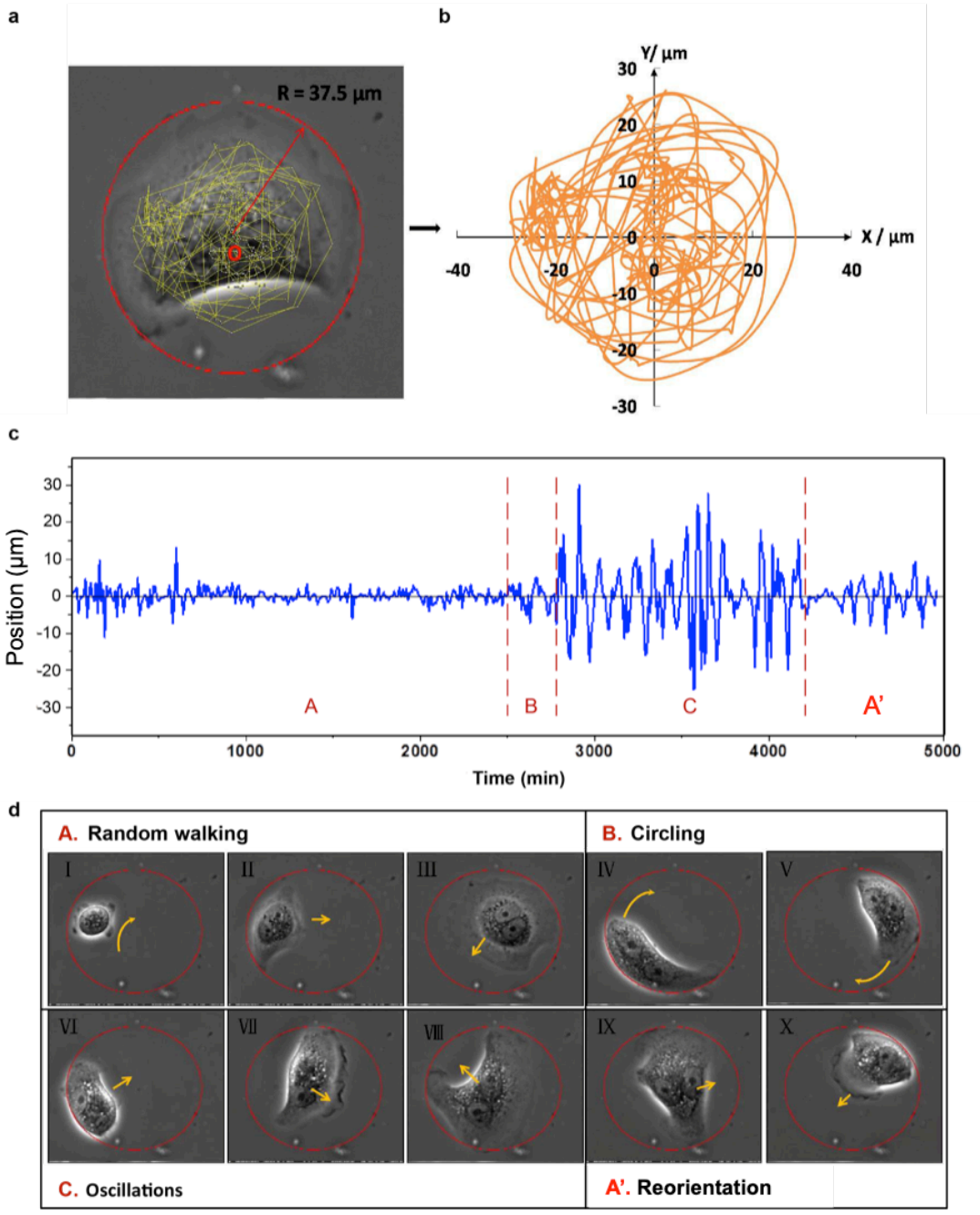

Figure 4.1 Cell migrations in a circle-shaped micropattern.

(a) Phase contrast images of a single MDCK cell migrating in a circle-shaped micro pattern (radius=37.5 µm). Yellow lines indicate the trajectories of the geometric center of mass of the cell nucleus, which was imaged every 10 minutes. (b) XY-trajectories of the cell nucleus. The origin is the center of the circle micropattern. (c) The position of the nucleus against time. The trajectories predominantly fall into four classes A-B-C-D. (d) Cell morphologies correspond to the four classes in (c): A. Random walking, B. Circling, C. Oscillations, D. Reorientation. Yellow arrows indicate the direction of motion of the cell.

In order to quantify the oscillations observed within the tracks and gain more detailed understanding on the oscillatory migration, it is useful to analyze the velocity of the cell.

$$|v_{int}| = \sqrt{(x_{i+1} - x_i)^2 + (y_{i+1} - y_i)^2}/\Delta t \quad (4.1).$$

Here, v_{int} denotes the instantaneous velocity, which is the cell position from one frame to the next within a specific interval time, Δt. The resulting velocity plot of the cell depicted in Figure 4.1 is shown in Figure 4.2(a). Oscillations are evident in-between the red dashed lines. The velocity during the oscillatory state is very high, reaching 3.0 – 4.0 μm/min. Moreover, there are at least three periods of oscillations during the observation time of 72h. For the random walking state, the velocity of the nucleus exhibits small fluctuations and is mostly less than 1.0 μm/min, which is much slower than the oscillatory state. Figure 4.2(b) shows a snapshot sequence of the typical oscillation morphology of cell in a circle micro-pattern in Figure 4.1. Cells move periodically from one side to another and back. Along the way it shows a clearly polarized phenotype with protrusions or a clearly visibly leading edge and a retracting end. As the cell hits one side of the micro-pattern, the cell body is compressed until a newly formed lamellipodium (indicated by a red arrow) appears at the opposite end of the cell body.

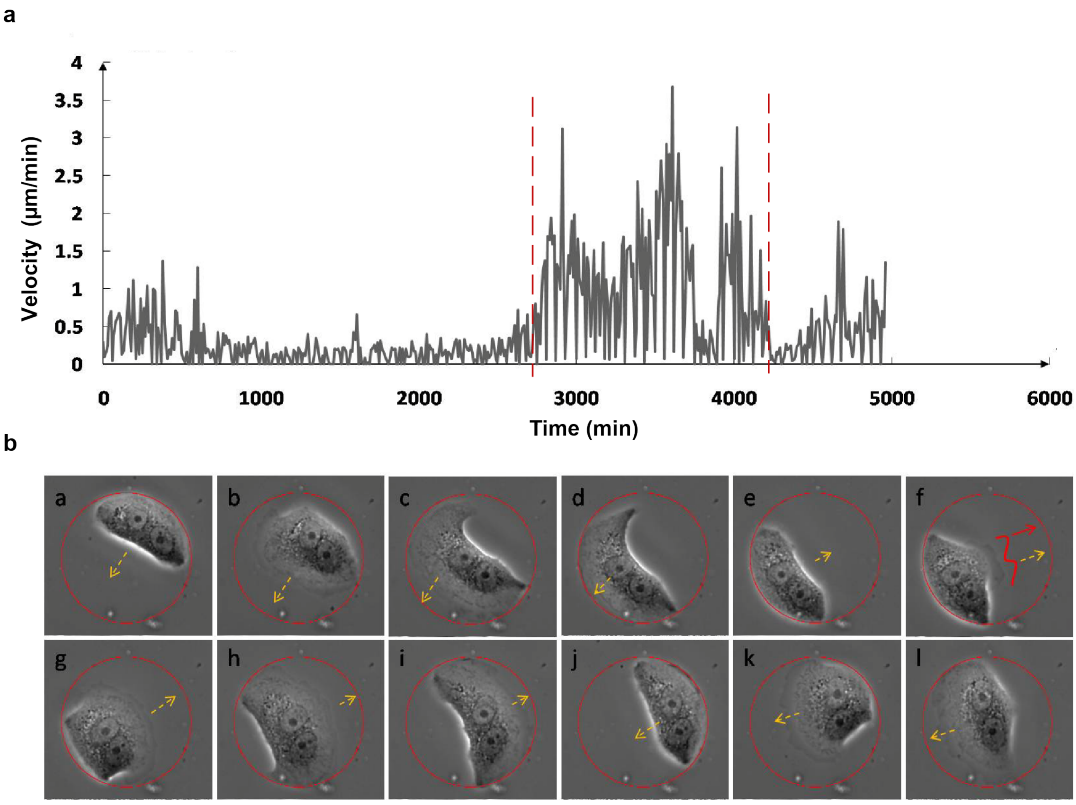

Figure 4.2 Oscillatory migrations of a MDCK cell on a circle-shaped micropattern.

(a) Velocity of the single MDCK cell in a circle-shaped micro pattern (radius=37.5 μm). The period of ``oscillations`` are indicated by the two red dashed lines. (b) Time-lapse series of phase contrast images of cell oscillatory morphologies in the circle (3140-3250 min, Δt = 10 min). The yellow arrow indicates the direction of motion of the cell nucleus. The red arrow and curve indicate the direction of cell membrane protrusions.

4.2 Effect of Global Geometry and Aspect Ratio

In a first set of experiments, MDCK cell oscillation was achieved on circle patterns with a radius of 37.5 μm. Does the dimension of the patterns affect the migration behavior? Distinct radiuses of circle patterns were used to detect the occurrence frequency of oscillatory motion. As can be seen in Figure 4.3, the oscillatory migration was seldom observed, occurring on less than 5% on circle patterns and its frequency increases with decreasing size of the circle patterns. However, the random walking an occurrence of at least 78% is the main migration behavior on the circle pattern. The cells, which circled around the inner edge of the pattern, account for less than 15% of migration behavior on each kind of patterns. The

results indicate, nonetheless, the increased adhesion area provided by larger circle micro-pattern reduces the occurrence of oscillatory migration.

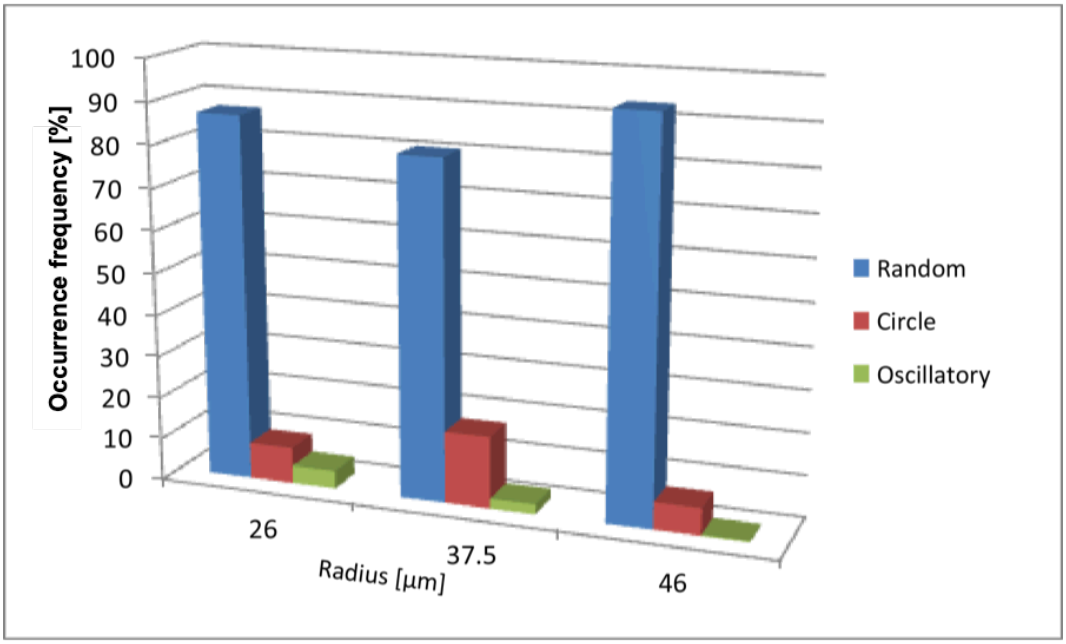

Figure 4.3 The dimension of a micropattern affects the migrating morphology.

Occurrence of distinct migratory morphologies as a function of the radius of circular micropatterns: random migration (blue), circle migration (red), oscillatory migration (green). Single MDCK cells in circle-shaped micropatterns with distinct radius, R= 26 μm, 37.5 μm, 46 μm were analyzed. ~100 cells were observed in each kind of micro-pattern.

Even though single MDCK cells on the circle micro-patterns performed random walking a lot, there are still some cells circling around the edge or oscillating along one direction of the diameter. It means that the shape of the micro-pattern has an effect on the direction of cellular migration. To apply a shape disturbance to the cell migration, ellipse shaped micropatterns were introduced. In doing so, we tested if the direction of oscillatory migration could be controlled. In Figure 4.4, a phase contrast image of a MDCK cell confined to an ellipse-shaped micropattern is shown. As we anticipate, the cell firstly fluctuates and then performs oscillatory migration along the direction of the long axis of the ellipse pattern, which can be seen from the trajectories in Figure 4.4(b). There are at least two phases of oscillations during the observation time of 24h. The persistence time of oscillations is about 9 hours and 7 hours, respectively. The velocity along the long axis averaged

over the intervals is shown in Figure 4.4(c), the velocity of the oscillations is around 2.0-4.0 μm/min, and can be as high as 5.0 μm/min. This value is considerably larger than the velocity of a randomly walking cell, which is usually about 0.5-1.0 μm/min. To further confirm whether the system behaves in an oscillatory manner, a spectral analysis (fast Fourier transform (FFT)) of the velocity was performed. The result shows two peaks at the period of 1.04 h and 1.26 h respectively, this matches to the two phases of cell oscillations. Hence, oscillatory migration can be induced on micro patterns by geometrical constrains.

For circle-shaped and ellipse-shaped micro-patterns, about ~100 MDCK cells were observed in each experiment. Taken together, MDCK cells exhibit obvious oscillation behavior, however, they have also drawbacks that have to be taken into account. One point is that MDCK cells divide quickly, about 12h after seeding. This results in short observation time. Also, many MDCK cells have two nuclei. MDCK cells sometimes break out of the observed micropattern. It is therefore necessary to find an appropriate cell line for upcoming experiments. This leads naturally to another question: does the oscillatory behavior depend on the cell type?

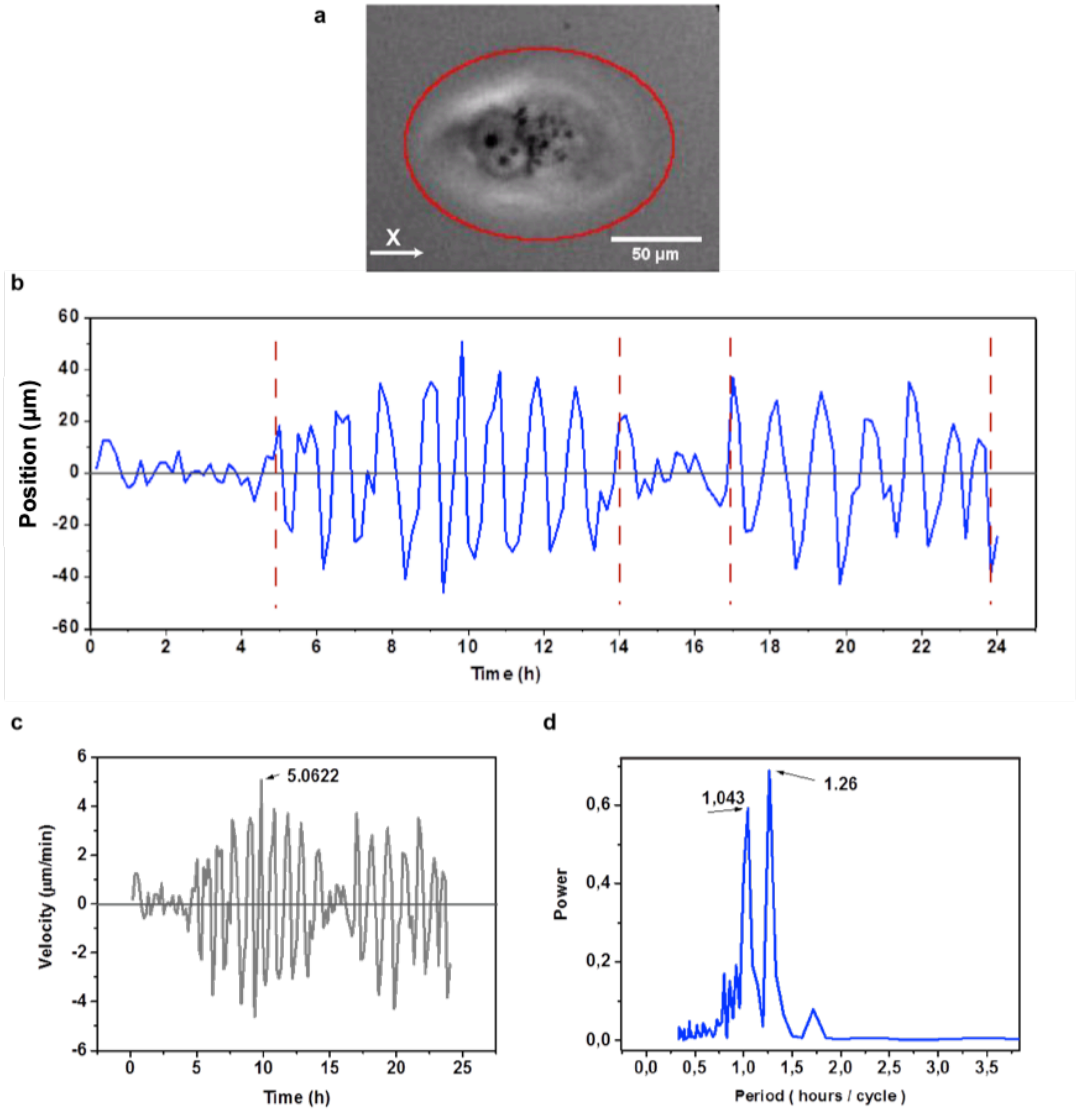

Figure 4.4 Oscillatory migration of a single MDCK cell on an ellipse-shaped micro-pattern.

(a) A phase contrast image of a single MDCK cell migrating in an ellipse-shaped micro-pattern (long axis=100 µm, short axis=80 µm). (b) Trajectory of the geometric center mass of the cell nucleus along the long axis X-axis over 24h. The origin is the center of the ellipse micro-pattern. Between the red dashed lines oscillation phases are visible. (c) A velocity-time plot of the track of the cell nucleus. (d) The periods of the oscillations were calculated by FFT.

4.3 Distinct Cell Lines on Circle and Ellipse

To find out whether other cell lines also show a spontaneous oscillatory behavior on the micropatterns. Huh7 cells and MDA-MB-231 cells were tested. The Huh7 cell

line exhibits a substantially lower probability of spontaneous oscillatory behavior, typical examples of behaviors are shown in Figure 4.5. In order to explore the migratory behavior of Huh7 cells, ellipse-shaped micro-patterns with distinct aspect ratios (a/b) were introduced to the setup. Two possible outcomes were observed: either the Huh 7 cells randomly walked on the ellipse, or the cells circled around the edge of the ellipse from time to time. Only a few oscillatory behaviors can be found in the setup with aspect ratio of 160/80 (µm/µm). Additionally, Huh7 cells have a considerably lower run velocity. Hence, a longer observation time in the experiments is needed.

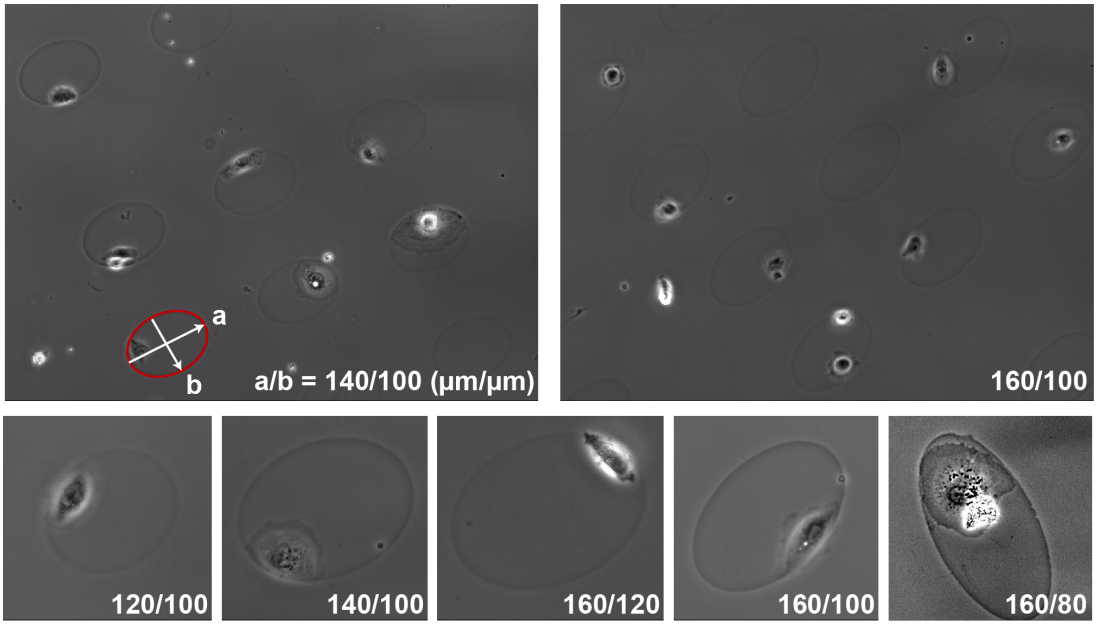

Figure 4.5 Typical behaviors of Huh7 cells in ellipse-shaped micropatterns.

Phase contrast images of single Huh7 cells migrating in ellipse-shaped micropatterns with different aspect ratio (long axis/short axis=a/b, µm/µm).

In contrast, the MDA-MB-231 cell line exhibits a substantially higher probability of spontaneous oscillating as well as circling. As shown in Figure 4.6, three migration states of MDA-MB-231 cells can be found: the random walking, the orbiting around the inner edge and the oscillating state. Typical trajectories of the cell nucleus' positions further display the three characteristic migration modes on the circle shaped micropattern (circle radius R= 50 µm). The highlights indicated a sequence of the oscillating morphology. As can be seen, the single MDA-MB-231

cell traverses the pattern from one edge directly to the opposite edge and is then reflected back with an asymmetric polarized morphology. A series of micropatterns with different dimensions were introduced into the setup to statistically analyze the occurrence of the distinct migration states. As shown in Figure 4.6(g), compared to the circle shaped micro-pattern with R= 50 μm, a smaller circle shaped micro-pattern (R= 25 μm) leads to less oscillating and circling but to more random walk. It reveals that it is necessary to provide enough area for oscillating or circling. Moreover, by using ellipse shaped micropatterns, we found that a higher aspect ratio results in more oscillatory motion. This result indicates that one might achieve a higher frequency of oscillatory behavior by narrowing down the shape of the micropattern. Polarization by contact guidance will increase oscillatory migration.

In addition, to compare the morphology of MDA-MB-231 cells on an ellipse shaped micro-pattern, a typical phase-contrast image of each of the three characteristic states is shown in Figure 4.7. It further clarifies that when the cell is at a state of random walking on the ellipse, it has a quasi-roundish morphology with scattered lamellipodia in many directions. As the cell is at a state of circling or oscillating, it has a polarized morphology with a lamellipodium limited to the cell front and the nucleus is located at the rear.

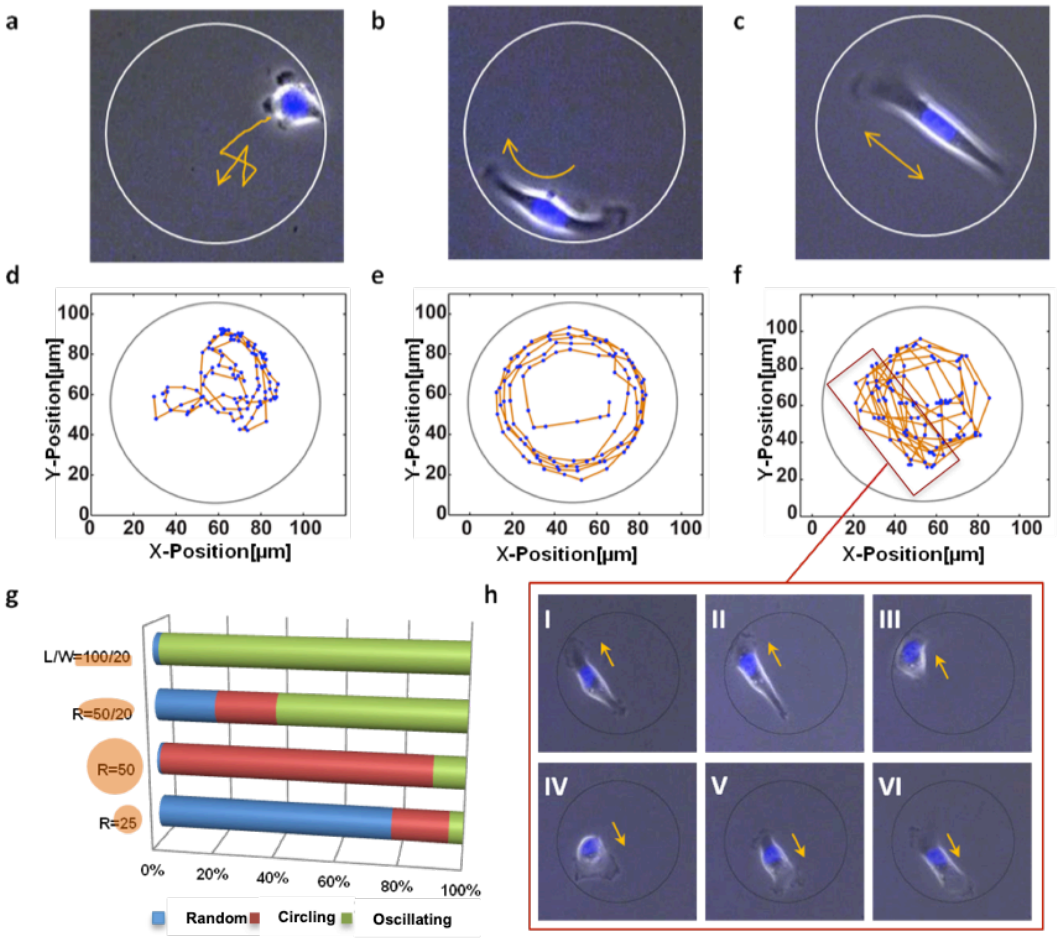

Figure 4.6 Three migration states of single MDA-MB-231cells on circle and ellipse shaped micro-patterns.

Phase contrast images of single MDA-MB-231 cells on circle-shaped micropattens, radius R=50 µm, (a) Random walking (b) Circling (c) Oscillatory motion. The nucleus is labeled with Hoechst 3334 stain and is shown in blue. (d-f) Trajectories of the cell nucleus tracked for 18h with images taken every 10 minutes, corresponding to the three migration states from (a-c). (g) The frequency of occurrence of the different migration modes in four micropatterns of different dimensions. (h) A sequence of images showing an oscillating cell in the circle micro patterns.

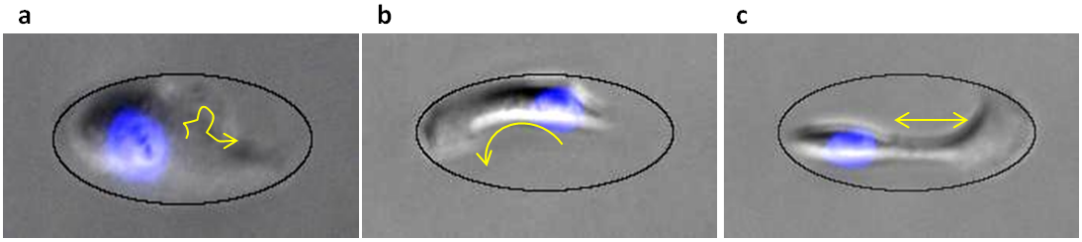

Figure 4.7 Three migratory morphologies of single MDA-MB-231cells on ellipse shaped micro-patterns.

(a) Random walking, (b) Circling around the edge, (c) Oscillation. The ratio of the long axis and short axis of the ellipse is a/b=100 µm /40 µm.

Taken together, the MDA-MB-231 cell line is the most suitable for the following experiments. The MDA-MB-231 cell line was chosen for five reasons: Firstly, MDA-MB-231 cells are more likely to perform oscillations than MDCK cells and Huh7 cells. Secondly, MDA-MB-231 cells have a longer lifetime than MDCK, most of them divide after 36 hours. Thirdly, only a few MDA-MB-231 cells have two nuclei. Fourthly, MDA-MB-231 cells are better confined on the micro-pattern than MDCK cells. They almost never leave the field of view. Moreover, MDA-MB-231 cells run faster than Huh7 cells on the micro-patterns. Thus, MDA-MB-231 cells exhibit a high amount of oscillatory events in a shorter observation time.

4.4 MDA-MB-231 Cells on Stripe-shaped Micropatterns

According to the above findings that the probability for cells to be in an oscillatory state is increased by narrowing the confining geometry of the micropattern, we hypothesize that polarization by contact guidance will increase directed oscillatory migration. To test this hypothesis, we introduce stripe-micro patterns with circle shaped tips to the setup. The appropriate geometry for an assay for an oscillation study has to be identified first. To this end, as shown in Figure 4.8, stripe-shaped micropatterns that have different lengths from 30 µm to 120 µm were designed. The second important parameter to choose is the width of the stripe. To this end, a series of micropatterns with distinct widths from 5 µm to 50 µm were tested. In order to avoid cell-cell interaction, the gap between each stripe is 60 µm.

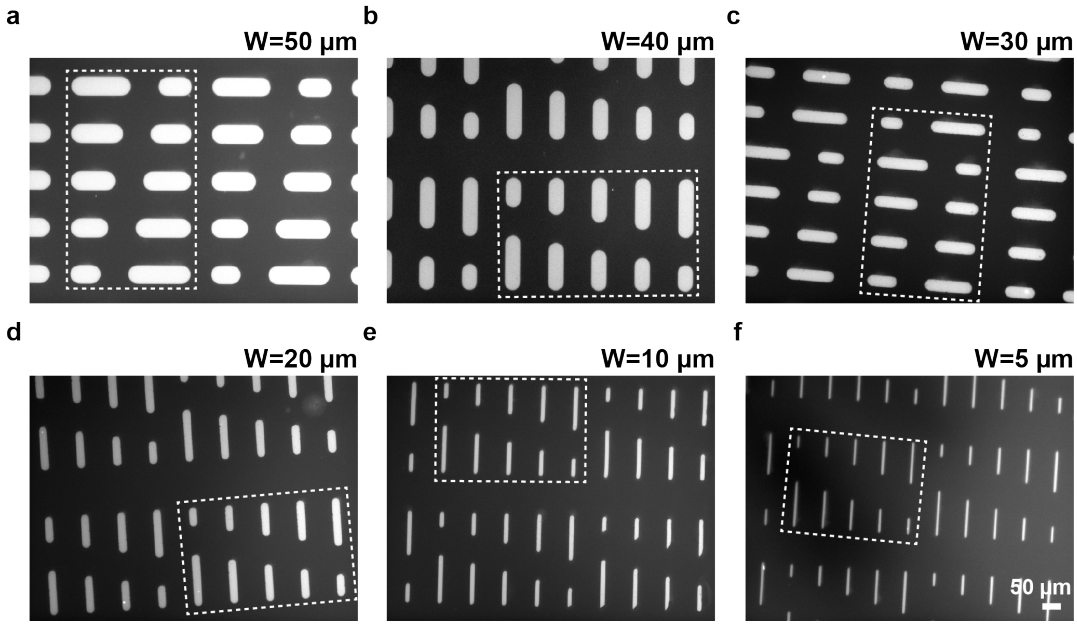

Figure 4.8 Stripe-shaped micro-patterns with different sizes.

(a-f) The width of the structures is 50, 40, 30, 20, 10, 5 µm respectively. The length L=30, 40, 50, 60, 70, 80, 90, 100, 110, 120 µm.

As shown in Figure 4.9, for a width of the stripes less than 10 µm, MDA-MB-231 cells migrating on the stripes are likely to run out of the confining patterns. For a width of the stripes of more than 30 µm, cells have a certain probability to circle around the inner edge of the pattern or randomly walk on the pattern. Moreover, for a width of the stripes of more than 40 µm, it is likely to have more than two cells on one stripe. Hence, the width of the stripe was chosen to be 20 µm, which is about as wide as a MDA-MB-231 cell. In this case, MDA-MB-231 cells exhibit a morphology closely resembling that during one-dimensional movement regardless of the stripe length (Figure 4.9c). In particular, previous studies showed a dependence of migration velocity and cell shape on the width of the micro-pattern [106].

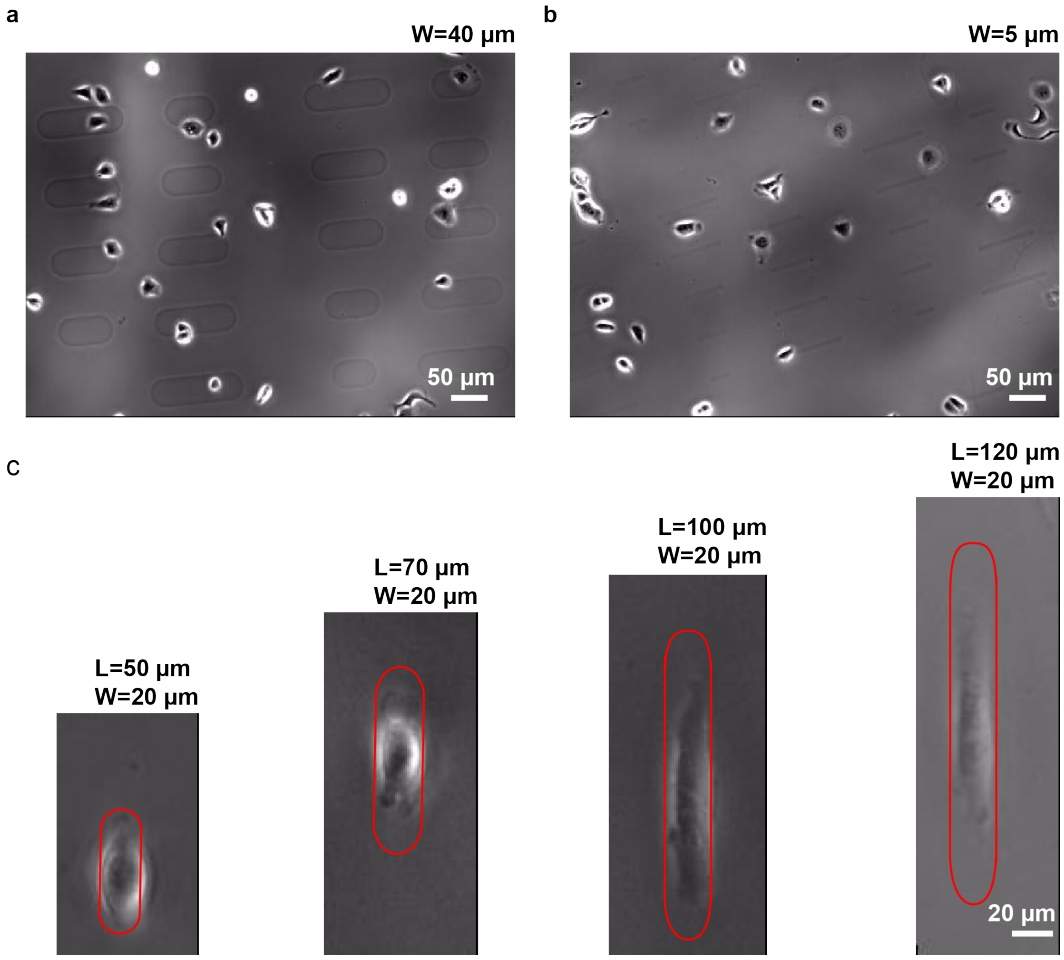

Figure 4.9 Morphology of MDA-MB-231 cells on stripe-shaped micropatterns.

An appropriate width of the stripe for an assay for oscillation study was found. a) Cells on stripes with a width of 40 µm. b) cells on stripes with a width of 5 µm. c) Cells on stripes with a width of 20 µm, and the length of the stripe was 50, 70, 100, 120 µm respectively.

To increase the amount of oscillation events, another important parameter to choose is the length of the stripe. For the width = 20 µm, distinct cellular movement states were found on the stripes with different length. As shown in Figure 4.10, the tracks of the cell position and the velocities indicate that when single MDA-MB-231 cell migrate on the shorter stripes (L=30 µm and L=50 µm), the velocity of cells and the center of mass of the nucleus fluctuate slightly. There is no oscillation behavior, because there is not enough space for the cell to move on the shorter stripes. When a single cell migrates on the longer stripe (L=100 µm), it fluctuates slightly in the center of the stripe and then migrates back and forth after

10 hours with a fast velocity, which could be up to 3.0 µm/min, and this are the phases of the oscillations.

As the cell behavior clearly changes with the length of the stripe, more constant conditions for single-cell oscillations have to be considered. Whether single cells oscillates on the stripes with the length between 50 µm and 100 µm needs to be clarified. As shown in Figure 4.11, the cell position and the velocity of cell on stripes with length of 50, 60, 80, 100 and 200 µm are compared. When a single cell migrates on a stripe less than 100 µm, e.g. L=60, 80 µm, it fluctuates most of time, the tendency to oscillate does not increase. In contrast, as the stripe length increases, e.g. L=100, 200 µm, oscillations became pronounced. Here, for L=200 µm, the maximum of the velocity is 4.2 µm/min.

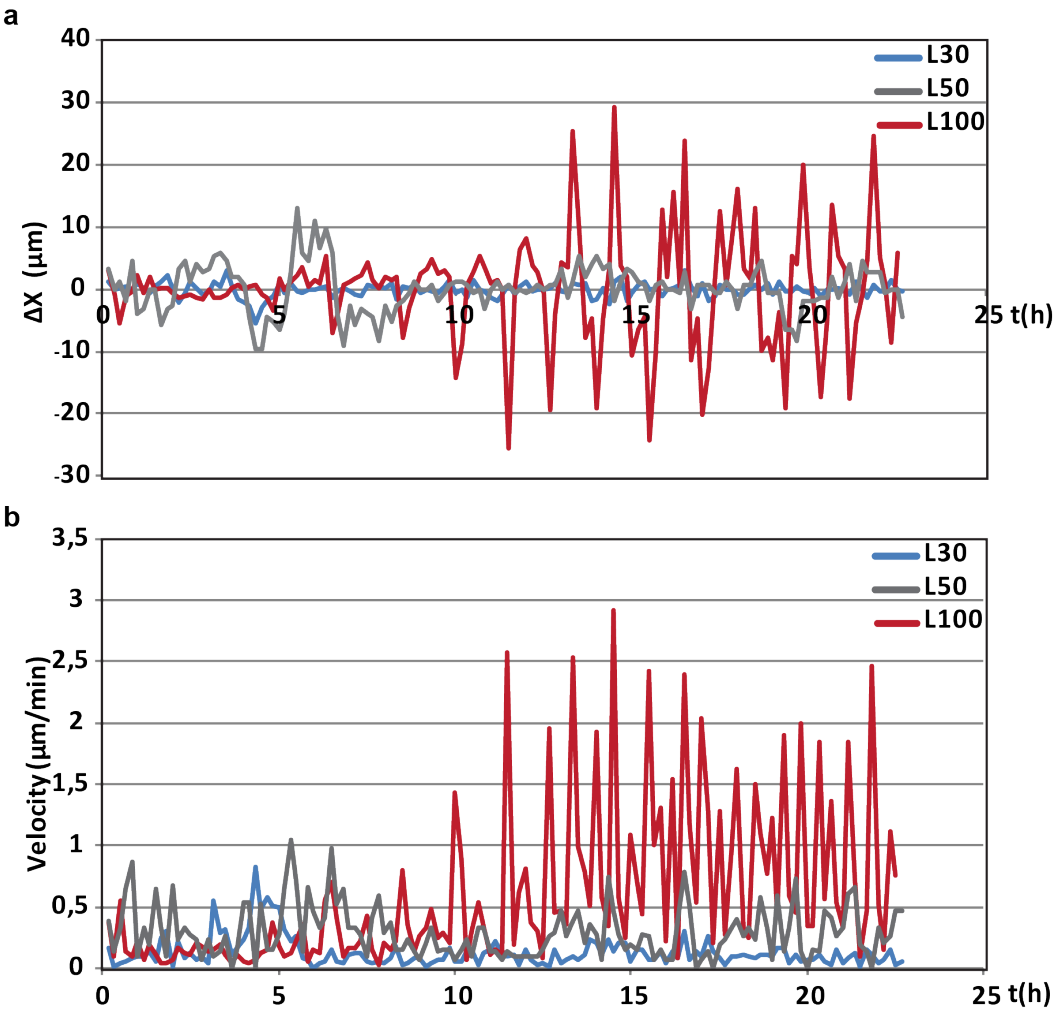

Figure 4.10 Initial observations of single MDA-MB-231 cells on short and longer stripe-

shaped micro-patterns

a) Trajectories of the geometric center of mass of the cell nucleus on the stripe shaped micro-pattern. The origin is the center of the stripe-shaped micro-pattern. b) A velocity-time plot of the track of the cell nucleus. The length of the stripe was 30 µm, 50 µm, 100 µm, respectively. All stripes had a width of 20 µm.

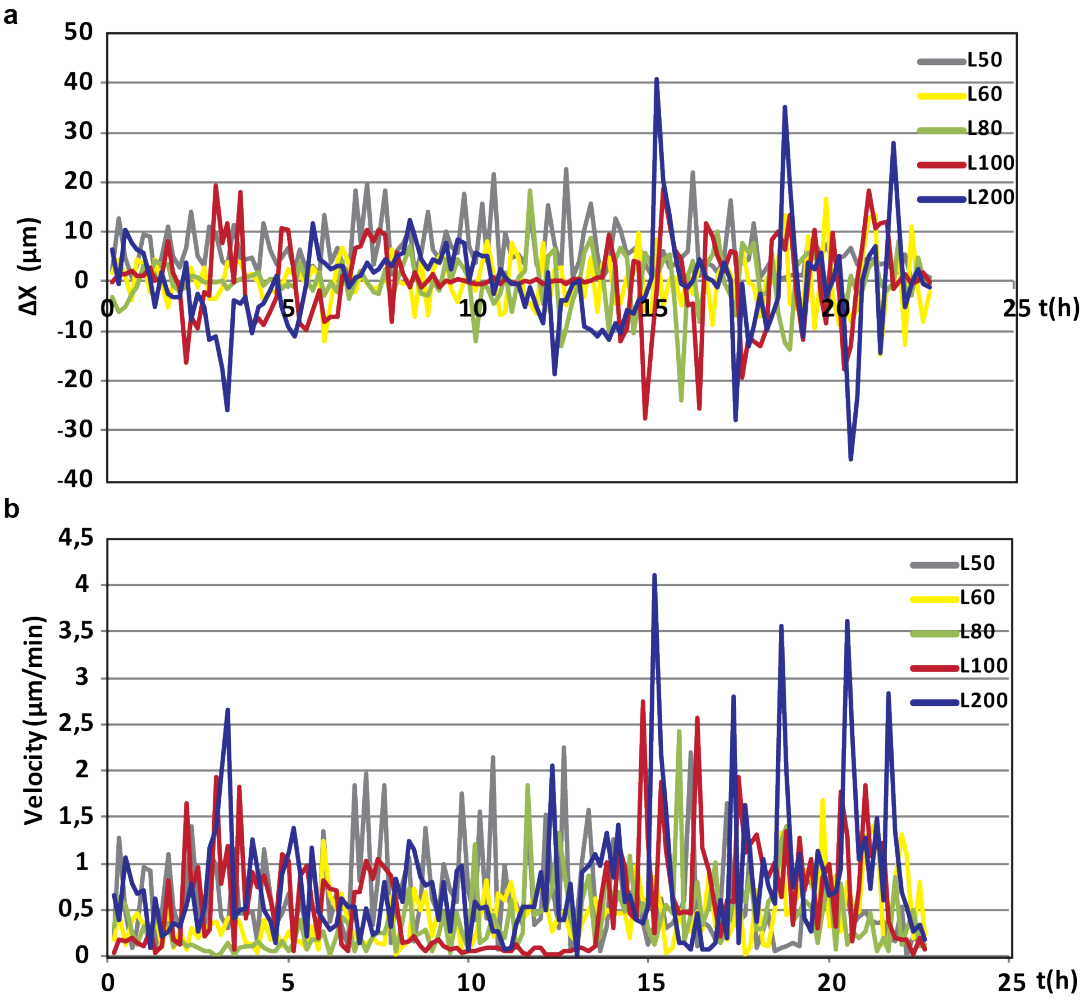

Figure 4.11 Analysis of single MDA-MB-231 cells on stripe-shaped micro-patterns with distinct length

a) Trajectories of the geometric center of mass of the cell nucleus on the stripe shaped micro-pattern. The origin is the center of the stripe-shaped micro-pattern. b) A velocity-time plot of the track of the cell nucleus. The length of the stripe was 50 µm, 60 µm, 80 µm, 100 µm, 200 µm, respectively. All stripes had a width of 20 µm.

Taken together, the results of this section show that the arrays of stripe-shaped micro-patterns are a suitable platform to study cell oscillatory behavior. These findings indicate that it is possible to observe many oscillatory motions on longer

stripes (such as, L>=100 µm) with a width of 20 µm. For spontaneous oscillations, the increasing velocity might be due to the fact that, after some time, cells move over a surface where they already have been before. More importantly, the results show that there would be a threshold of size of micropattens that generates oscillations; otherwise, a random migration is the main mode. On small sizes, a polarized state of cell is not supported, but as the cell spreads on larger micropattern, the polarized state and homogeneous state could reach a balanced bistability. For a cell of fixed size, the threshold decreases with the increasing cell area. Spontaneous oscillation is such kind of state that repeats polarization-repolarization reaction to respond external perturbation. For a cell in a 1D system, periodic oscillations can happen if an external perturbation is beyond a certain threshold, which was earlier by B. Camley et al [139].

4.5 Actin Morphologies in An Oscillating Cell

Eukaryotic cells can utilize different arrangements of actin filaments to perform distinct processes. In order to investigate the actin morphologies in an oscillatory cell we used LifeAct-transfected MDA-MB-231 cells. The actin binding peptide-GFP fusion construct, Lifeact, is known to not interfere with actin dynamics [140, 141]. As preliminary results, distinct actin morphologies are found in cells during oscillation or migration, such as finger-like protrusions, sheet-like protrusions, long tails, microvilli or filopodia, which are shown in Figure 4.12. There are usually three types of actin structures: parallel bundles, antiparallel bundles and dendritic networks. The processes performed by the different actin filament structures can generally be divided into two categories: Protrusions leading to the expansion of the cell membrane, or contractions leading to shrinkage. In particular, the long tails might be the cell fragments, which have no nucleus and no microtubules but are still able to move[142]. The tails might be the simplest model system for actin driven locomotion[143]. Moreover, actin might have a distinct conformation in the oscillatory cell as it moves on different micropatterns. In the next chapter, further work is dedicated to the study of actin dynamics.

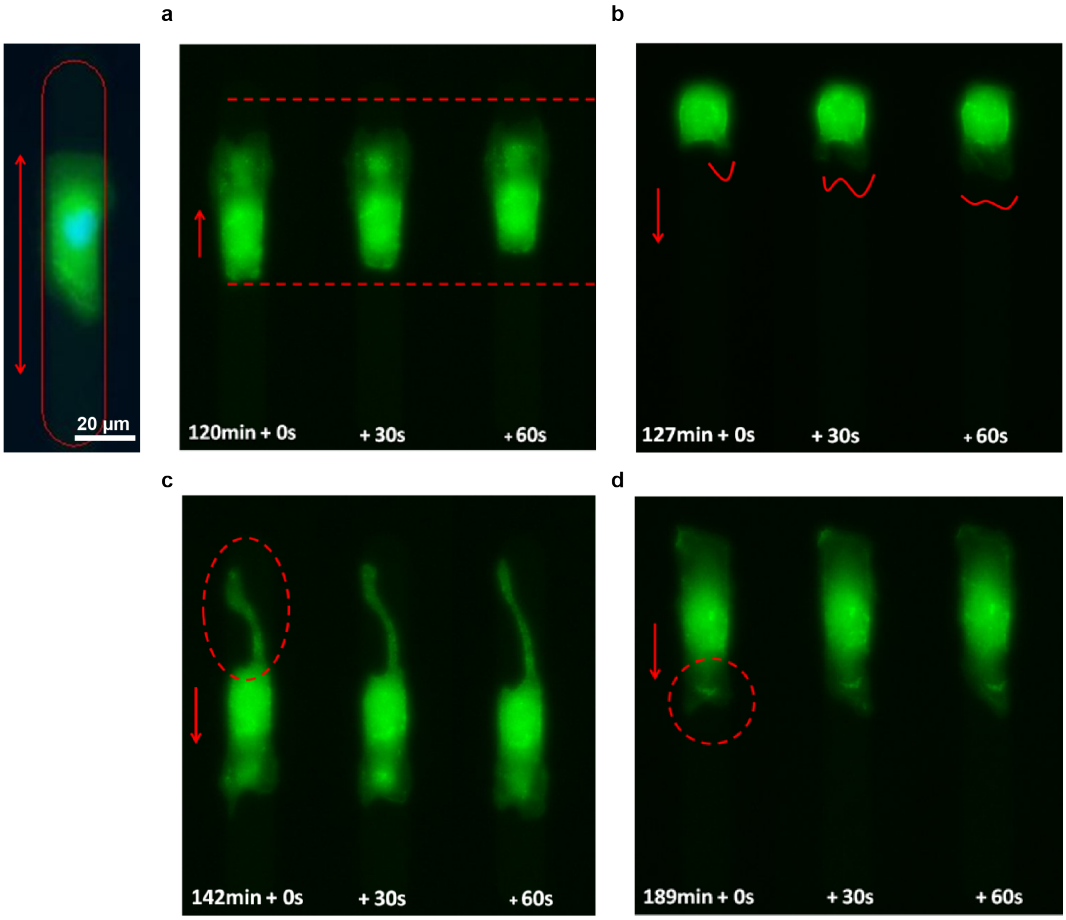

Figure 4.12 Distinct actin morphologies of a LifeAct-GFP labeled MDA-MB-231 cell oscillating on a microlane.

(a) Contractions leading to shrinkage (b) Finger-like protrusions leading to the expansion of the cell membrane (c) Moving tails behind the cell body (d) microvilli and filopodia. Stripe length L=100 µm, width W=20 µm. The red arrow indicates the direction of the motion.

Chapter 5 Quasi-Oscillations and Actin Dynamics of Single Cell on Microlanes

Cell migration on microlanes represents a suitable and simple platform for the exploration of the molecular mechanisms underlying cell cytoskeleton dynamics. In this Chapter, the quasi-oscillatory movements of single MDA-MB-231 cells confined in stripe-shaped microlanes. We observed cell behavior in form of alternating states of directional polarized migration in the middle of the microlane and depolarized-repolarized reorientation at the pole. The spatial velocity distribution and frequency spectrum are analyzed, that provide a set of parameters that succinctly describe cell quasi-oscillation. By introducing distinct geometric ends into the microlanes and using LifeAct-GFP transfected MDA-MB-231 cells, we found that local deformation of the leading edge has almost no effect on the reversal time (repolarization time) but has an effect on the actin arrangements. Applying a computational Potts model that includes a minimal dynamical cytoskeleton model allows probe distinct scenarios of repolarization and actin dynamics at the end of microlanes.

5.1 Typical Quasi-oscillatory Motion of Single Cells on Microlanes

In the first set of experiments, we investigated whether cells captured on microlanes exhibit oscillatory migration (Chapter 4). One typical oscillating migration of single cell on stripe-shaped microlane was shown in Figure 5.1. Breast cancer cells (MDA-MB-231), which were chosen as the representative cell type in the following study, were seeded on arrays of 20µm wide and 100µm long, fibronectin coated micro-lanes surrounded by PEGylated, cell repellent surface. The fabrication of the micro-pattern follows previous protocols and is described in detail in the methods section. Cells adhere, spread and remain confined in the microstructures during the entire period of the experiment. Movies were taken in time-lapse mode recording images every 10 minutes over 36 h. During this time, cells migrate in a guided manner and always align their front-rear polarity axis along the main axis of the microlanes. We observe repeated cycles of directed motion, termination of the motion at the ends, and cell repolarization in the opposite direction. The recurring sequence of events leads to quasi-periodic migration as shown in the time sequences in Figure 5.1a. Cells exhibit a typical migratory morphology with an actin-rich lamellipodium at the leading edge, seen as dark rim in phase contrast, and a retracting tail at the rear. As cells reach the end of the micro-lanes, they take a shortened, almost round appearance with no lamellipodium until a newly formed lamellipodium appears at the opposite end of the cell body. These migratory and resting phenotypes coincide with distinct regimes of the center of mass motion of the cell nucleus. Figure 5.1b shows an exemplary trajectory of a cell nucleus over 36 hours. The cell shows phases of directed motion followed by pausing and repolarization, hence resulting in a quasi-periodic movement. The migration pattern is quasi-periodic in the sense that the timing of reorientation is stochastic and hence leaves to variability in the period of the back-and-forth motion. Figure 5.1c and d show exemplarily for the particular sequence the time dependence of the cell body length. Two states of cell body could be discriminated, a compressed state and a prolong state. When a cell's

position in the end of microlane, the feature of this behavior becomes evident in the formation of rest phase which exhibits a slower or zero velocity. When the cell leaves the end of micro-lane, the feature of its morphology becomes evident in the formation of polarized phase which exhibits a faster until highest velocity in the center position of the micro-lane. The advantage of stripe-shaped microlanes is that the conversion of polarization-depolarization of single cells could occur repeatedly in the same view field. Hence hundreds of repolarization progress can be a*nalyzed in parallel.*

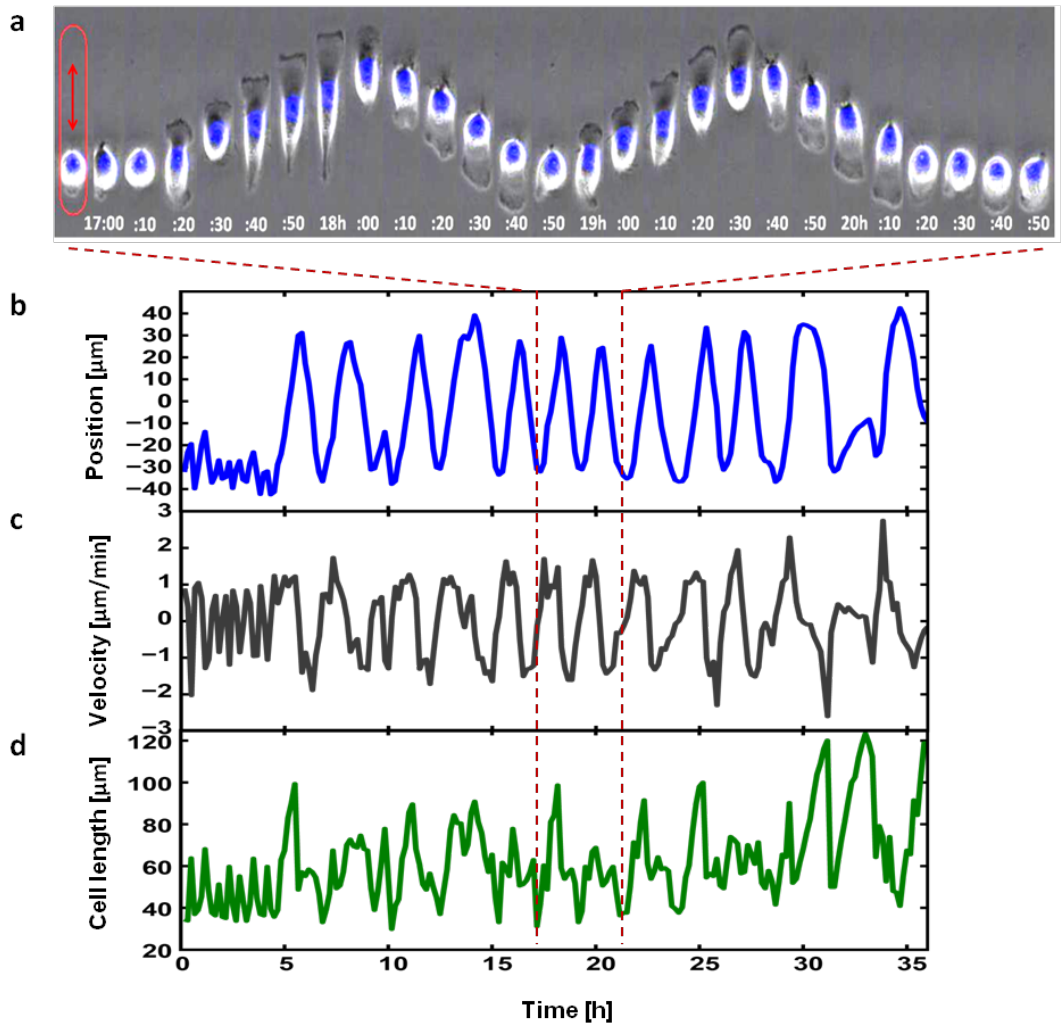

Figure 5.1 Typical oscillatory migration on a stripe-shaped microlane

(a) Time sequence of a cell (MDA-MB-231) migrating on a stripe-shaped micropattern (Stripe length L = 100 µm, width W = 20 µm, 10 min time intervals). Images are taken in phase contrast and with fluorescence microscopy. The nucleus is labeled with Hoechst 3334 as indicated in blue. (b) Trajectory of cell nucleus tracked over the course of 36 h showing

quasi-periodic alternations between directed migration and repolarization. (c) Velocity of cell is in directional state (vertical direction). (d) Transformation of cell length.

5.2 Effective Periodicity and Its Dependence on Lane Length

Next, we study how cells reverse direction at the ends of the microlanes. In order to better distinguish phases of directed migration from the phases of reorientation we fabricated micro-lanes with different lengths (Figure 5.2).

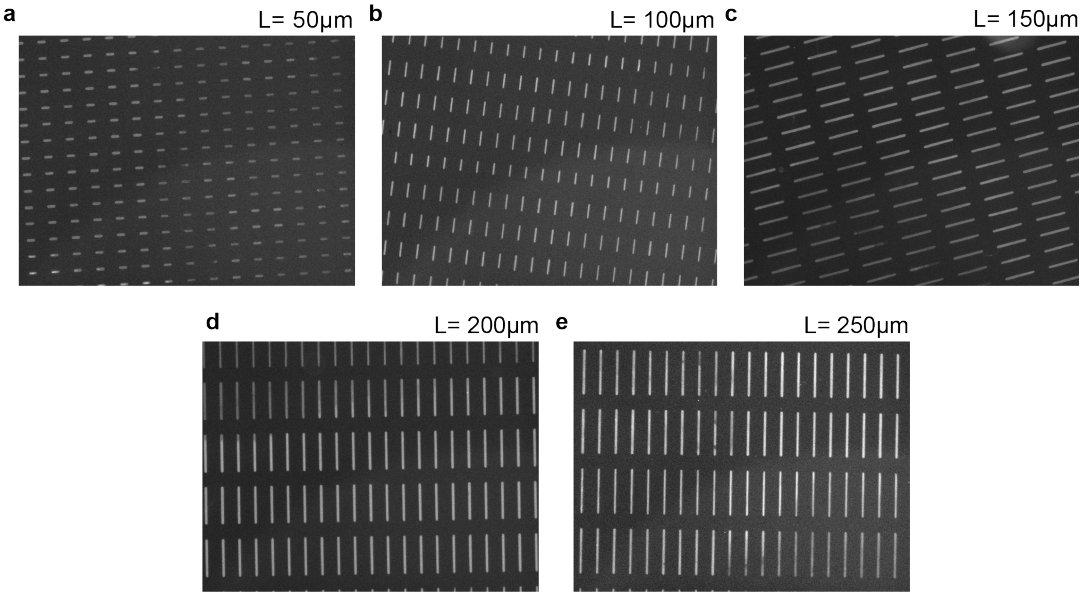

Figure 5.2 Microlanes with different lengths.

(a-e) Fluorescence image of the pattern consisting of labeled fibronectin (bright) and PLL-PEG (dark). Length, L=50, 100, 150, 200, 250 µm respectively. All the width of the structures are 20 µm.

Sufficient statistics of many hundreds of cells in parallel was sampled using automated tracking of the fluorescently labeled nuclei. The automated image analysis yields cell trajectories $x(t)$ as described in the method section. The instantaneous velocities are determined as, $v(t) = [x(t + \Delta t) - x(t)]/\Delta t$, where $\Delta t = t_{i+1} - t_i$, denotes the 10min intervals of two subsequent frames. Figure 5.3 shows exemplary single cell trajectories, together with the spatial distribution of

cell positions and velocities (we have sampled an ensemble of over 100 cells for each microlane length). These distributions are determined by binning the cell positions into 5 µm wells along a stripe, and then computing the fraction, $p(x)$, and the mean absolute velocity, $\langle|v|\rangle(x)$, of cells found in each bin. It appears that cells in the shortest microlane (L=50 µm) don't exhibit periodic motion and remain in a symmetric morphology with two lamellipodium extending to the ends. Evidently, there is not enough space for directional migration on short microlanes. In contrast, quasi-periodic migration is observed in longer microlanes (L=100 to 250µm). Figure 5.3 shows that the detection frequency of cell nuclei decreases towards the micropattern tips and becomes flat in the middle of the microlanes. Similarly, the mean absolute velocity distributions decline towards the micropattern tips and show a distinct plateau behaviorat the case of longer stripes. In the center of longer microlanes, we find that the cells migrate with a mean absolute velocity of approximately 0.4 - 0.6 µm/min. Note that for L=150µm the probability density of the nucleus position as well as the spatial distribution of the mean absolute velocity has two obvious peaks, which also can been faintly seen in the L=200 µm and L=250 µm lanes. The peaks indicate that the cells start to spend more time in the microlane ends due to the repolarization. In the same duration, compared to the length 100, 200 and 250, more pronounced quasi-oscillatory events could be observed at length 150µm, a fact that we will use length 150 µm in the following experiments.

In order to differentiate the center of the microlanes, where cell speeds are distributed uniformly (plateau), from the micropattern tips, where cell repolarization takes place, we look more closely at the mean absolute velocity distribution. We approximate the spatial velocity distribution by a trapezoidal profile, where two velocity ramps at the micro-lane tips are connected by a plateau in the micro-lane center. We determine the transition points between the ramp (repolarization) and plateau (run) regions (see black dash lines in Figure 5.3).

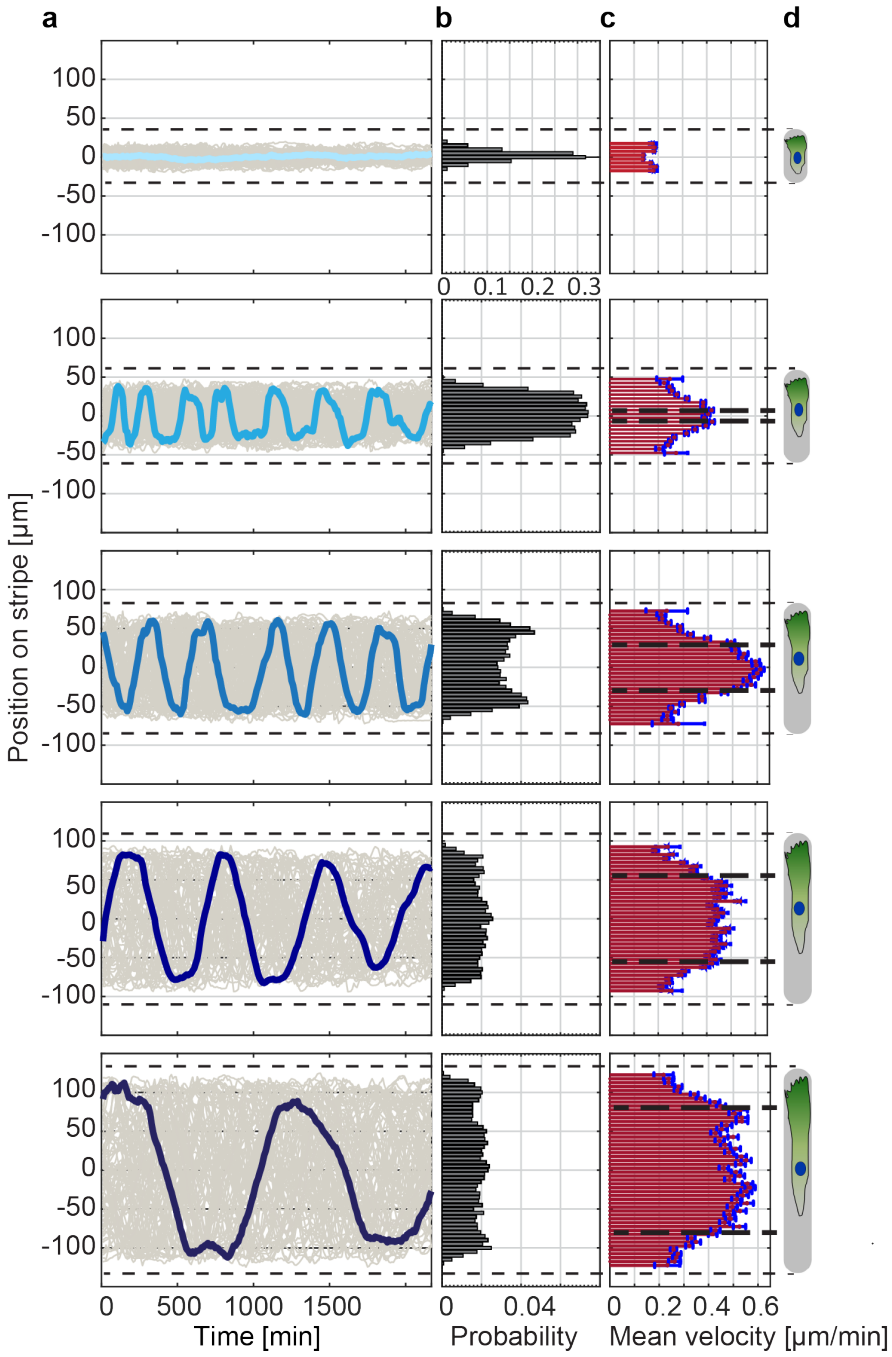

Figure 5.3 Migration pattern as a function of lane length.

From left to right: (a) Time courses of cell nucleus position of cells within microlanes. (b) Spatial distributions of nuclei. (c) Spatial distributions of mean absolute cell velocity. Blue lines are SE for the binned data. (d) Schematic drawing of the microlanes with length L = 50, 100, 150, 200, 250 µm and width W = 20 µm. Dashed lines indicate the transition between microlane tips and microlane center. These results were obtained by binning the cell positions (5µm bin width). For each micro-pattern stripe length, we tracked roughly 100 cells. The positions of the cell nuclei were tracked over a time course of 36h, with images taken every 10 minutes.

Table 5.1 Number of analyzed cells for different lengths of microlane with round tips

Length (µm)	L=50	L=100	L=150	L=200	L=250
N_{cell}	95	114	100	80	103

5.3 Definition of Reversal Area

To study the cell repolarization at the edges separately from the free cell migration in the middle of the micro-pattern, we identify the transition points between the ramp (repolarization) and plateau (run) regions. A reversal area A_0 at the tips of the microlane was defined.

We observed that the distance of the nucleus to the tip of the stripe during repolarization varies quite a lot for different cells. Thus, it is not trivial to find the value of reversal boundary. On the one hand, it has to be large enough that for all cells the center of the nucleus is inside the reversal area when touching the tip of the stipe. On the other hand, it has to be as small as possible to get a good separation between running and repolarization of cells.

To find an appropriate reversal area A_0 and the boundary ξ_0 for the microlane with round tips, we looked at the mean velocity along the stripe positional axis (Figure 5.3), which shows a plateau in the center and decreasing velocity towards the ends, a schematic example was depicted in Figure 5.4. In the area where the velocity decreases, the cells presumablyinteract with the end, thus we use this to define the reversal area. To make the transition easier to detect, we calculate the mean velocity by binning the cell position into 5 µm wells along the lane. . Considering cells do not polarize and thus there is no clear repolarization in the short microlane, here we apply the analysis to the four longer microlanes. We use the "findchangepts" function in Matlab, which uses a maximum likelihood approach to find the most probable change point (CP) between two linear regimes. The resulting value is ξ_0= 55 µm for the round geometry, leading to a reversal area A_0 =

1057 µm² for all geometries. Here, the calculation procedure was briefly described as follow:

v_{mean}: The mean velocity of a cell migrating in a bin-range (each bin step = 5 μm) along the lane, $v_{mean} = \langle|\langle v_i\rangle_{step\ k}|\rangle$. Where v_i indicates the cell velocity at time i, $v_i = (\mathrm{x}_{i+1} - \mathrm{x}_i)/\ \Delta\mathrm{t}$, x_i indicates the cell position at time i. The error range given is the standard error of the mean. (Figure 5.5)

A symmetry cumulative sum by the center of the stripe was used to mirroring the v_{mean} distribution along the stripe position, therefore ξ =0 corresponds to the end of the lane, the max value of ξ depends on the different half-length of the stripes.

Afterwards, the trapezoid distribution of v_{mean} can be fitted to a linear regression for the repolarization region and yields the mean velocity value of the motility region.

For long stripe (L=150-250 μm) the CP positions were calculated at ξ= 50~60 μm. Therefore, a uniform reversal region, where ξ_0=55 μm away from the round tip of the microlane was defined, leading to a constant reversal area A_0 = 1057 µm² for cells on all microlanes with geometric tips.

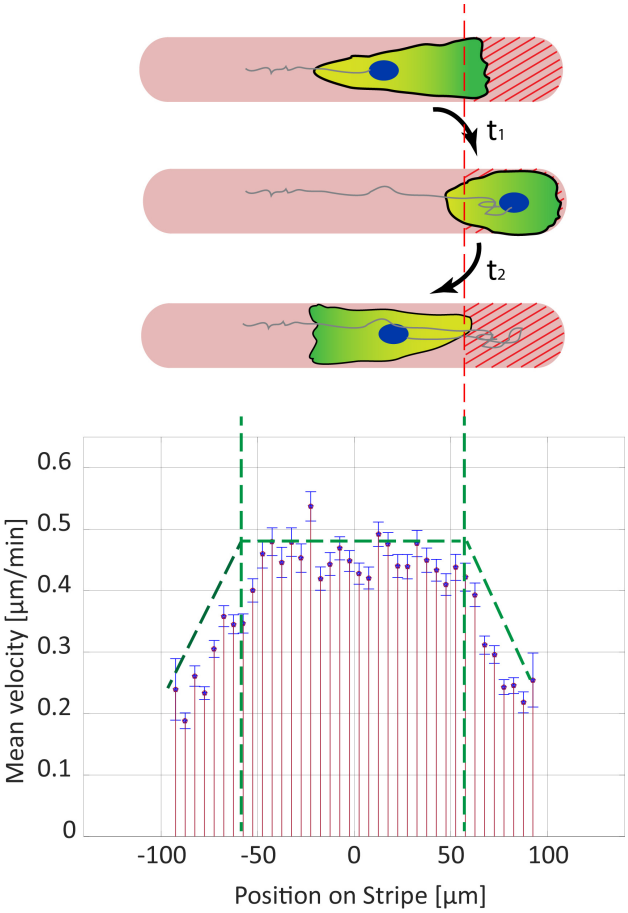

Figure 5.4 Schematic diagram of the determination of reversal area.

Cells on microlane with the length L=200 µm was taken for an example, a clear plateau of constant velocity is visible towards the middle of the stripe. The transition from the plateau to the tips was found by dotted lines (green), which provide the likelihood regimes for CP analysis in the following step. The shaded region indicates the tip area used to define the time points, t_1 and t_2 of entry and exit of the cell.

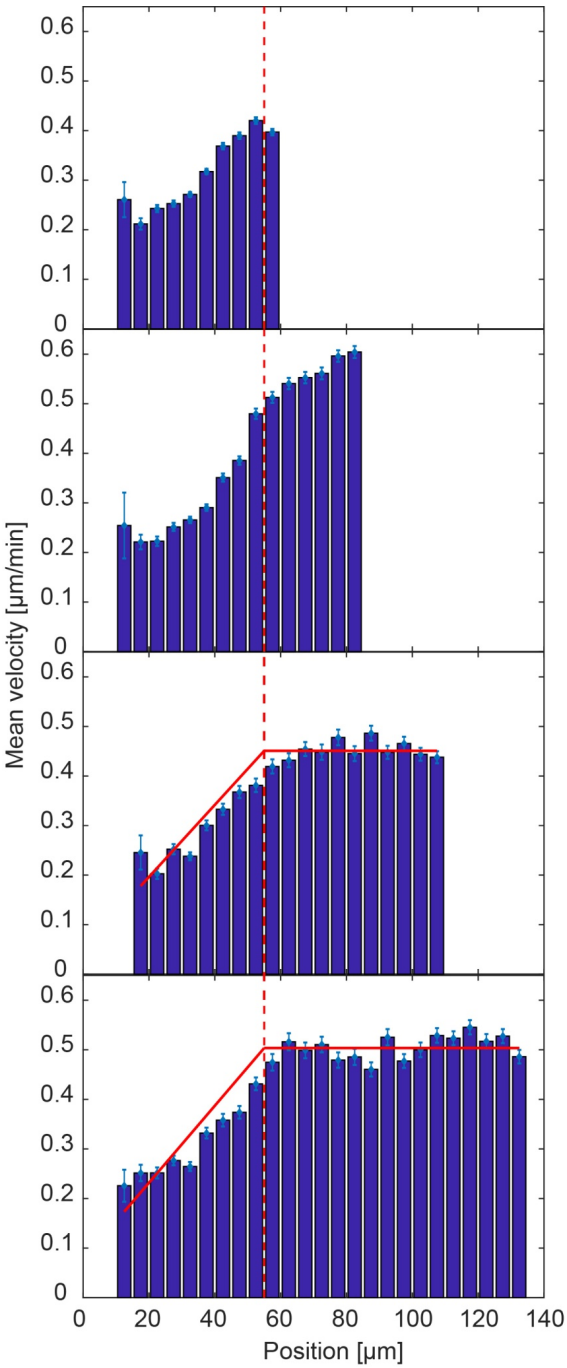

Figure 5.5 Determination of reversal line.

Mean cell velocity as a function of the distance to thenearest tip on microlanes of different length (top to bottom: 100, 150, 200, 250 µm). The velocity is averaged over the whole cell population in regions of width 5µm. The transition from the plateau to the reversal area (dotted line) is found by a maximum likelihood CP analysis that finds changes between different linear regimes (red lines).

5.4 Velocity Distribution and Sustained Oscillations

We further quantify the quasi-periodic migration of cells. First, we determine the overall distribution of absolute cell velocities (Figure 5.6a). We find that for microlanes long enough to show persistent cell migration (L=100-250µm), the cell velocity distributions collapse onto an exponentially decaying master curve. Short microlanes, where we don't observe persistent cell migration, show a distinctly narrower velocity distribution. This can be explained as follows: we have seen earlier that the cell begins to repolarize at a distance of 55µm from the micro-pattern tips. If the micro-lane is shorter than this distance, then the cell is in a constant state of repolarization, which leads to diminished oscillatory motion.

Then, we performed a discrete Fourier transform of the cell velocity time-traces for different stripe lengths, which yields the frequency distribution corresponding to the quasi-periodic cell migration. We find that the frequency spectrum follows a log-normal distribution. Furthermore, the dominant frequency (f_{max}, peak of the frequency spectrum) shifts to lower frequencies for longer stripe lengths. This indicates that cells move with a constant velocity across the micro-lane. To demonstrate this hypothesis, we plot the period of migration, $T = 1/f_{max}$, against the stripe length (Figure 5.6c). We find that the period of migration increases linearly with the stripe length, at a slope $dT/dL = 0.054 \pm 0.0058\,h/\mu m$, corresponds to a constant average velocity of pole-to-pole migration, $v_c = 0.62\mu m/min$, which is in good agreement with the velocity plateau in the stripe centers (cf. Figure 5.3).

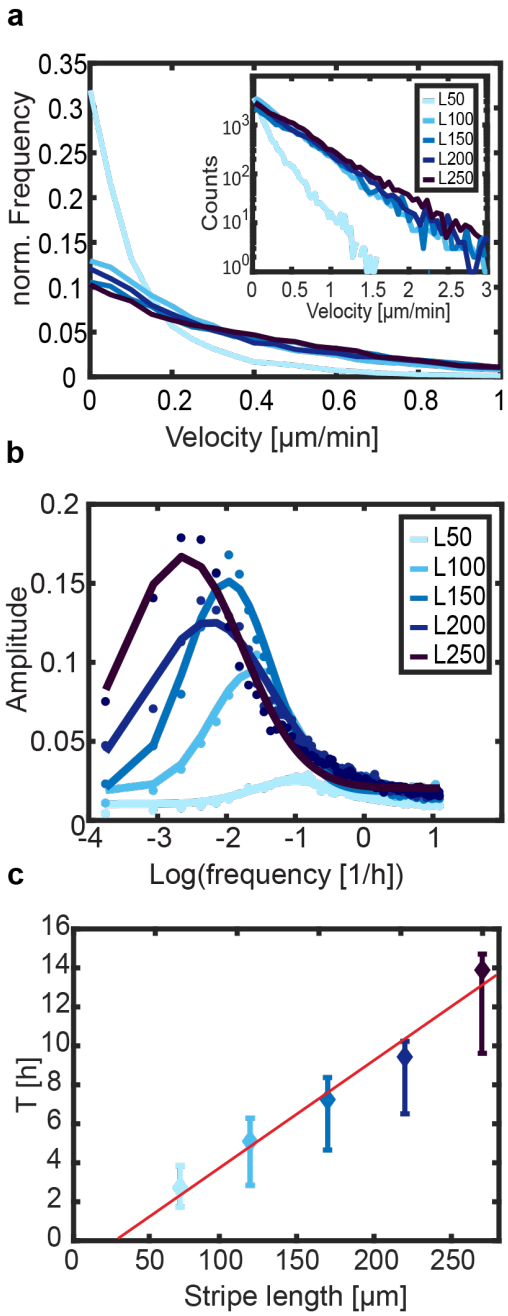

Figure 5.6 Overall spectral analysis of the large ensemble of cell traces.

(a) Normalized distribution of absolute cell velocities, $\langle|v|\rangle$, for single MDA-MB-231 cells migrating in stripe-shaped micro patterns of five different lengths and fixed width (W=20 µm). Inset: Non-normalized (counts) velocity distribution in a logarithmic plot. (b) Discrete Fourier transform of the time-dependent directional velocities, fitted by a log-normal distribution (lines). (c) The migration period (T=1/frequency) of single cells increases linearly with the stripe length. The error bars correspond to the peak width of (b).

5.5 Repolarization Time

In the following we address the repolarization of cells and the way directed migration is reversed at the ends of the microlanes. We observe that cells depolarize when the protruding lamellipodium encounters the confining PEG-layer. Then, the cell shrinks as its trailing edge continues to move. Finally, the trailing edge stalls, the cell begins to expand again, and repolarizes towards the opposite, free, cell edge. This repolarization manifests itself in a new lamellipodium that emerges at the free cell edge. Note that this phenomenon of internal repolarization is rather specific for cells confined on tracks. The more general appearance of mesenchymal cell migration in 2D as well as 3D appears to redirect existing lamellipodia or exhibit several competing lamellipodia. However, in the experiments presented here, the appearance of lamellipodia is restricted to two sides of the cell due to its lateral confinement by the microlanes. Hence, reorientation of crawling cells occurs via a relatively well-defined cycle of depolarization and repolarization. This feature allows us to examine the 'reversal time', which is a measure for the time scale of depolarization and repolarization when a cell reaches the end of a microlane. To this end, we define a distance ξ_0 from the ends that marks the positions where the velocities are seen to decrease (Figure 5.7a). Using the trapezoidal velocity profiles shown in Figure 5.3, we determine this boundary to be ξ_0 = 55 µm. During a depolarization-repolarization cycle, a cell traverses this transition point twice: once at $t = t_1$, when it approaches the micro-lane tip, and once at $t = t_2$, when it leaves the micro-lane tip. Therefore, we define the reversal time as $t_R = t_2 - t_1$, and determine its distribution for four different micro-lane lengths (Figure 5.7b). We note that the distributions are independent of the stripe length. Although the exact value of the average reversal time will typically depend on the particular choice of the reversal area, we consistently find an average depolarization and repolarization time of approximately 100 min.

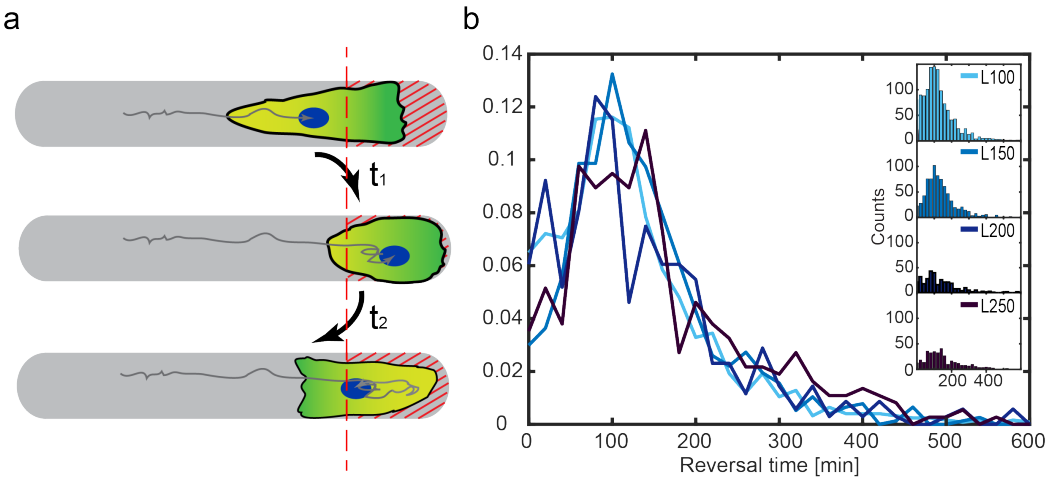

Figure 5.7 Distribution of reversal time of the cells on micro-lanes with distinct lengths.

(a) Schematic drawing of a cell entering the microlane tip region (A_0), arresting and then returning from the tip region, with the leading edge of the cell shaded in dark green. The red dashed line indicates the position of cell entry into the tip region, at time t_1, and exit of the tip region, at time t_2. (b) The normalized distribution of the reversal times $t_R = t_2 - t_1$for four different microlane lengths.

5.6 Developed Cellular Potts Model (CPM)*

The data presented so far are taken from large ensembles of cells and hence the distribution functions of the quasi-oscillatory motion present a robust, generic test bed for comparison with mathematical modeling. We have recently developed a computational model, based on a 2D Cellular Potts Model (CPM), to provide valuable insights into the temporally and spatially resolved evolution of shape and position of cellular ensembles[34, 144]. Cellular Potts Model (CPM) was originally implemented by J. Glazier and F. Graner [132, 133] In this work cell migration was represented with linear coordinates, rather than polar coordinates as the previous study [4], for the reader´s convenience, we concisely present the simulation in this section. This section is to a large part based on the publication of F. Thüroff et al*, and A. Goychuk* [34, 144, 145].

In the cellular potts model (CPM), each cell is represented by a simply connected set of lattice sites $\mathrm{D}^{(\alpha)} = \{\vec{\mathrm{x}} | \mathrm{c}(\vec{\mathrm{x}})\}$ (referred to as the domain of cell α). The

indicator function $c(\vec{x})$ gives the index of the cell occupying grid site $\vec{x}$. Each grid site $\vec{x}$, can be occupied by at most one cell. The time evolution of a cell's domain $D^{(\alpha)}$ proceeds via a succession of *protrusion events* and *retraction events*, which will be collectively referred to as "elementary events" $\mathcal{T}$. The dynamic of the system proceeds via a succession of Monte-Carlo steps (MCS). Each MCS consists of a series of attempts to perform elementary events, in which a certain of "source" grid site $\overrightarrow{x_s}$ is randomly chosen. During a retraction event, cell α expels one of the grid sites to its border, $\overrightarrow{x_s} \in B^{(\alpha)}$: $D_{old}^{(\alpha)} \rightarrow D_{new}^{(\alpha)} = D_{old}^{(\alpha)} \setminus \{\overrightarrow{x_s}\}$. During a protrusion event, cell α incorporates one grid site $\overrightarrow{x_t} \in N^{(\alpha)}$ ("target grid site") from its neighborhood $N^{(\alpha)}$: $D_{old}^{(\alpha)} \rightarrow D_{new}^{(\alpha)} = D_{old}^{(\alpha)} \cup \{\overrightarrow{x_t}\}$. (Shown in Figure 5.8). The probability $P(\mathcal{T})$ for such elementary event is determined by a "Hamiltonian":

$$P(\mathcal{T}) = min\left\{1, e^{-\frac{\Delta H}{K_b T}}\right\}$$

The constant term, $K_b T > 0$, can be justified in the activity of the system. Where ΔH indicates the energy response in the successful elementary event. Here $H = H_{cont} + H_{adh} + H_{cyto}$, which takes into account the effect of cell contractility (H_{cont}), cell – cell adhesion (H_{adh}), and polymerization – depolymerization of the cytoskeleton (H_{cyto}). More detailed and in-depth description of the model can be referred to [144].

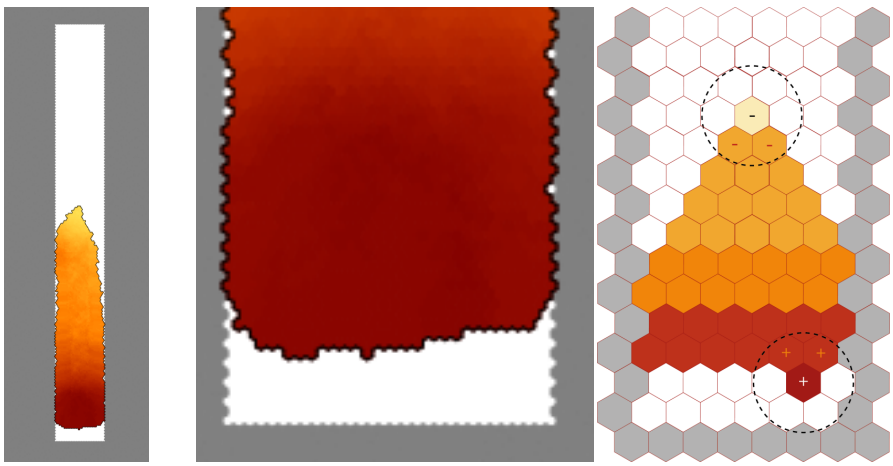

Figure 5.8 Illustration of the sets of Cellular Potts Model.

Grid sites occupied by cell α are indicated by orange. Within a feedback radius (dotted), an elementary event of protrusion (red) and retraction (light yellow) of the cell on the grid, the regulatory factors $F(\overrightarrow{x_n})$ are incremented (+) or decremented (-) respectively. The inner field variable is modified accordingly, thus promoting or inhibiting further migration in this area.

In the model, we consider the time evolution of the contact area between a cell and the two-dimensional surface that the cell migrates on. From now on, we will refer to this contact area simply as "cell", which has area A and perimeter P. We discretize each cell into a simply connected set of hexagons and associate its configuration with an energy, $H = H_{\text{cont}} + H_{\text{cyto}}$, which has contributions from cell contractility and from cell polarizability. Cell contractility is captured by the term

$$H_{\text{cont}} = \kappa_A A^2 + \kappa_P P^2,$$

which assigns an energetical cost for increasing cell area or cell perimeter. Cell-substrate adhesions as well as forces exerted via actin polymerization and actomyosin contractility are captured by the term

$$H_{\text{cyto}} = -\sum_{\text{x}} \epsilon(\boldsymbol{x}, t),$$

Where $\epsilon(\boldsymbol{x}, t)$ is a spatially resolved scalar *protrusion field*. We assume that the protrusion field has both an upper bound (due to limited protein availability) and a lower bound (minimal adhesion energy): $\epsilon(\boldsymbol{x}, t) \in [\epsilon_0 - \Delta\epsilon/2 \dots \epsilon_0 + \Delta\epsilon/2]$. Then, the time evolution of the cell is governed by a Metropolis algorithm with an effective temperature T and gradually approaches the minimum of its associated energy H, by making new cell-substrate contacts (protrusion) or by detaching from the substrate (retraction).

We break detailed balance by introducing two prototypic feedback loops that serve to approximate the underlying chemical pattern formation:

(i). Protrusions and the associated positive mechanochemical signaling reinforce the protrusion field (cell adhesions and cell cytoskeleton) within a radius R. There, the protrusion field exponentially approaches its upper bound, $\epsilon \to \epsilon_0 + \Delta\epsilon$, with a rate μ.

(II). Retractions and the associated negative mechanochemical signaling weaken the protrusion field (cell adhesions and cell cytoskeleton) within a radius R. There, the protrusion field exponentially approaches its lower bound, $\epsilon \to \epsilon_0 - \Delta\epsilon$, with a rate μ.

In the absence of mechanochemical signals, the protrusion field exponentially approaches its neutral state, $\epsilon \to \epsilon_0$, with a rate μ.

Micropatterning of the substrate is achieved in the simulations by superimposing the protrusion field with a second spatially varying scalar field φ, which reflects an offset in the cell-substrate binding energy. Here, we implement the micropattern by introducing no-go areas, $\varphi \to -\infty$, which the cell cannot explore.

Our extended Cellular Potts model has several control parameters. The average protrusion field, ϵ_0, and the bulk stiffness, κ_A, jointly determine cell size. Cell dynamics is controlled by the ratio between the polarizability of the cell, $\Delta\epsilon$, and the membrane stiffness, κ_P, as well as the signaling range, R, and the cytoskeletal rate, μ. The overall stochasticity of the system can be tuned by the effective temperature, T, which can also be absorbed by rescaling the membrane stiffness and the perimeter stiffness. In our previous work, we have investigated how cell behavior depends on these parameters [144]. In the current project, a finer cell discretization of the cell than that in [144] was necessary to resolve the micropattern tips. We achieved this by increasing the average protrusion field compared to our previous work; note that it is equally valid to decrease the bulk stiffness [144]. Then, to account for the observed persistent cell motion and stochasticity in the experiments, we increased cell polarizability and the effective temperature. Furthermore, we reduced the signaling radius so that cells can form

multiple competing lamellipodia. Lastly, we decreased the polarization update rate to account for a higher temporal resolution of the simulations.

Table 5.2 Parameters used for the computational simulation in this work, the simulation conditions are used to all single cell.

Name	Function	Value
R	signaling radius	4
$\Delta\epsilon$	cell polarizability	75
κ_P	cell contractility (perimeter stiffness)	0.06
μ	cytoskeletal response rate	0.02
ϵ_0	average protrusion field	1500
κ_A	cell contractility (area stiffness)	0.18
T	effective temperature	25

5.7 CPM Recapitulates Quasi-oscillatory Motion

The extended Cellular Potts model is capable of describing spatiotemporal dynamics of cells in 2D[34, 144], which can recapitulate the quasi-oscillatory migration. In particular, we model the contact area of a cell with a planar substrate, which is described by a set of discrete adhesion sites on a 2D lattice. In addition to a simplified description of the mechanical properties of cells[146-148], we also account for a minimal mechanism of cell polarization. Specifically, we include an internal self-regulating *polarization field* within each individual cell, which emulates effective protrusive forces due to actin polymerization, as well as actomyosin contractility and cell-substrate adhesions. This polarization field is regulated via intracellular signals that are assumed to have a fixed range. In more detail, we simplify all intracellular signaling, which is mediated by the Rho GTPase family of proteins for example, into two prototypic feedback loops: (i) cell protrusions

reinforce the protrusion field and lead to further protrusions and (ii) cell retractions weaken the protrusion field and lead to further retractions[34, 144]. Then, we simulated individual cells with fixed parameters and constant average area on stripe-shaped microlanes. Note that this premise already marks a striking difference to the experiments: in the simulations we investigate a population of clonal and therefore identical cells, while the cells used in the experiments show a wide variation in morphology and migratory behavior. Therefore, we expect all variances in the simulations to be under-estimated compared to the experiments. Furthermore, we adjusted the duration of a Monte Carlo step so that the average absolute velocity of simulated cells, $\langle|v|\rangle = 0.6\ \mu m/min$, matches the experiments.

We find that the model reproduces the quasi-oscillatory motion observed in our experiments, with the simulated cell trajectories being in good agreement with experimental data (Figure 5.9). Then, we evaluated the distribution of cell reversal times in the simulations analogously to the experiments, finding a pronounced peak at 100 min (Figure 5.9c). Furthermore, the simulated cells show a similar spatial velocity distribution as in the experiments (Figure 5.9d). In addition, we also performed more intuitive comparisons between simulation and experiment. In particular, we found similar morphologies of (i) polarized and persistently migrating cells with a flat leading edge and a tapered rear part, (ii) cells that contract after running into a dead end on the micro-lane, and (iii) repolarized cells (Figure 5.9a). In addition, to assess actin distribution during cell migration, we transfected live cells with a fusion construct of the actin-binding peptide LifeAct and GFP (LifeAct-GFP). Intuitively comparing the representative kymographs for both a simulated cell and an experimental LifeAct-GFP transfected cell, both demonstrate similar oscillations on the same microlane (Figure 5.9b). Our findings suggest that the quasi-periodic migration of cells on microlanes is well described by an extended Cellular Potts model. This model predicts emergent cell polarization from stochastic occurrence and self-reinforcement of cell protrusions, which then leads to a stochastic (re)polarization time. However, we also note a qualitative difference between experiment and simulation. It seems likely that there is a sharper actin accumulation at the leading edge in experiment, in contrast to the polarization field

(which can be seen as a proxy for the cytoskeleton density) of a simulated cell decreasing progressively from front to rear.

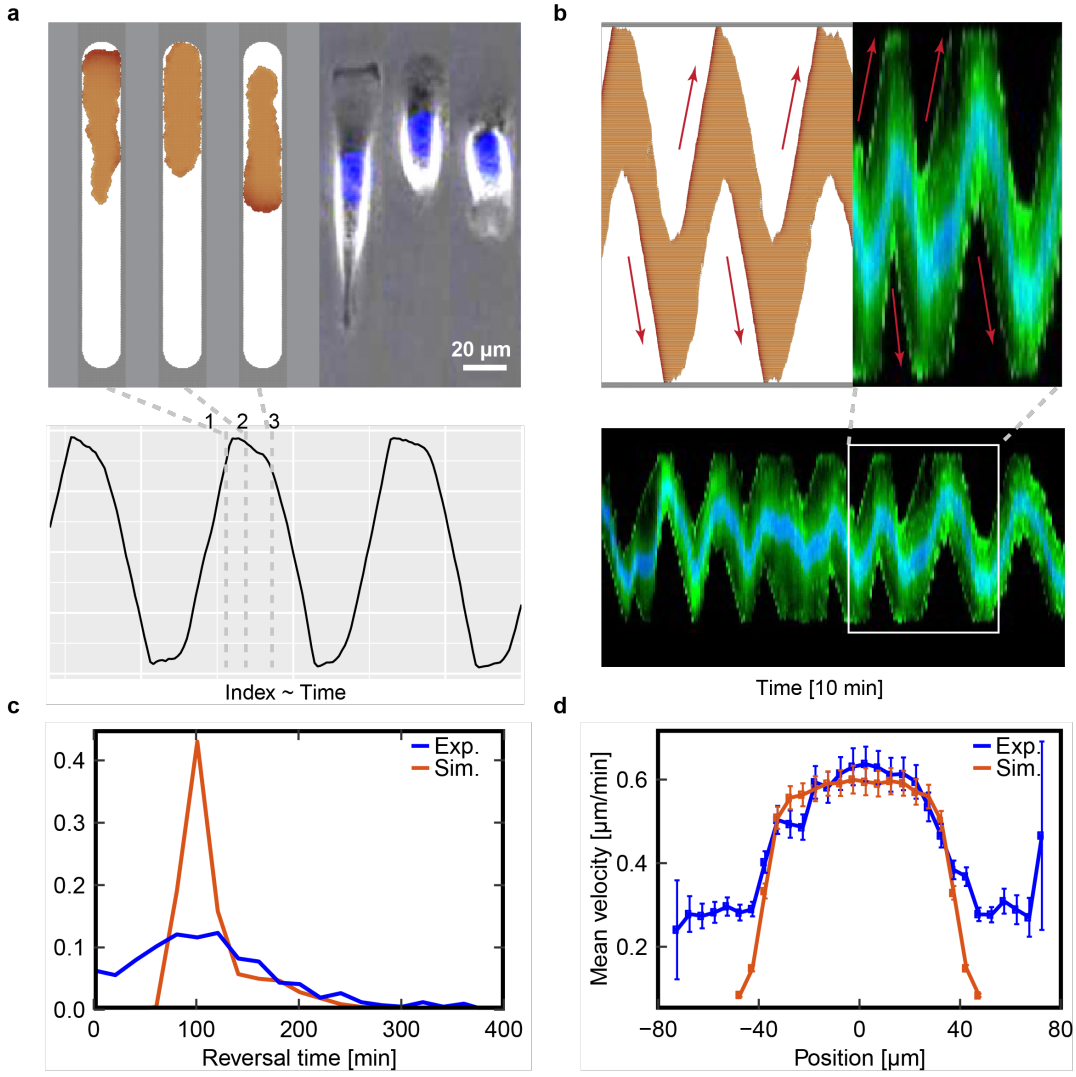

Figure 5.9 Comparison of computer simulation and experimental results. The microlane length is fixed at 150 µm with a round tip geometry.

(a) Our extended Cellular Potts model features an internal polarization field. The simulation reproduces the distinct run and rest phenotypes and yields cell center-of-mass trajectories that show quasi-periodic behavior (bottom); experimentally obtained cell trajectories are indicate on the upper right. (b) Comparison between the kymograph of a LifeAct-GFP transfected MDA-MB-231 cell with nuclear staining (bottom) and the kymograph of a simulated cell. Top: Zoom-in into a region that contains two periods of oscillation. Top left: Simulated cell. Top right: Experimental cell. Bottom: Zoom-out to the kymograph of an experimental cell that performs many periods of oscillation. Red arrows indicate actin dynamics in the front of the cells. (c) Reversal time distributions of simulated and

experimental cells. (d) Spatial mean absolute velocity distributions of simulated and experimental cells.

5.8 Effect of Curvature on Actin Dynamic

It is understood that the non-linear dynamics of actin polymerization and turnover depends on the cell shape and the geometry in which the cell migrates[24, 149]. In order to test the interplay between surface geometry and cell contour, we investigate the depolarization and repolarization of cells on microlanes with differently shaped tips. For example, a tapered tip allows us to explore how the reversal time depends on the deformation of the leading lamellipodium. To this end, we fabricated microlanes with four distinctly curved tips: round-, blunt-, sharp-, and concave-shaped. Then, we chose a constant stripe length L = 150 µm. Exemplary fluorescent images of the adhesion micro-patterns are shown in Figure 5.10b. To assure the comparability of the cell behavior on microlanes with different tips, we kept the total area of all stripes as well as the defined reversal area constant. To satisfy these constraints, we individually computed the position of the cell reversal boundary ξ_0 for each of the four tip shapes (Figure 5.10a). Across all studied geometries, we find that cells consistently perform oscillatory motion. Furthermore, the distribution of reversal times, or in other words the depolarization-repolarization times, does not significantly depend on the respective tip geometry (Figure 5.10c). All reversal times are centered around approximately 100 min, which is consistent with the results in Figure 5.7b. Evidently, tip curvature does not play a significant role in determining the reversal time for a defined tip area. A comparison between experiment and simulation, using analogous algorithms for the analysis, yields similar reversal times (Figure 5.10d). However, the reversal time distribution is typically broader in the experiments than in the simulations, indicating that our simulations might underestimate the variability of cells. Note, however, that it is equally likely that the broad distribution of reversal times in the experiments originates for cell-to-cell variability in the ensemble, which is not considered by the simulations at all.

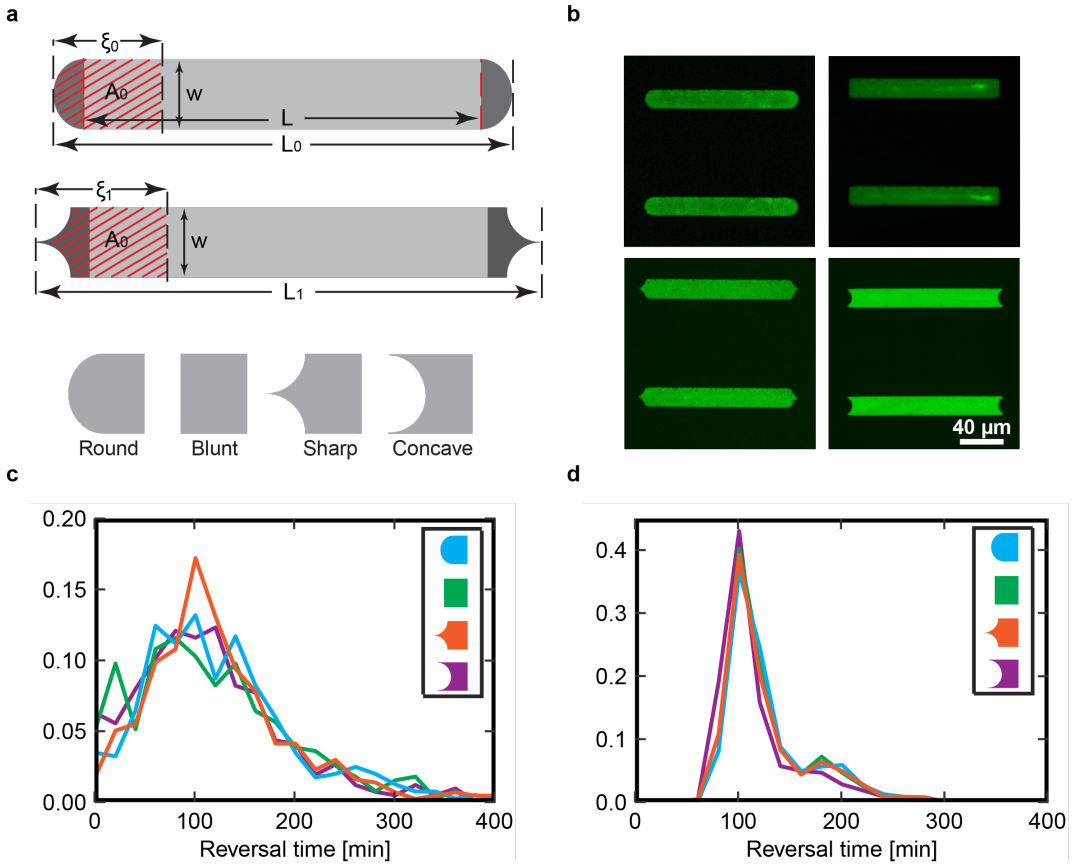

Figure 5.10 Effect of curvature on the repolarization time.

(a) Schematic diagram of micropattern geometry with four different tip shapes: blunt, concave, round, and sharp. The area of all microlanes and the reversal area A_0 are kept constant same, the whole lane length are different. (b) Exemplary fluorescent images of microlanes of width W=20 µm. (c, d) The distribution of cell reversal times (Δt) when reaching the microlane tips, for four different tip shapes. The cell enters the reversal area at a distance of ξ_0 =55 µm from the corresponding round tip of microlane. (c) Experimental reversal time distribution. (d) Simulated reversal time distribution.

To gain additional insight into the spatiotemporal actin dynamics at the leading edge of the cell, we recorded a series of live time-lapse images of LifeAct-GFP transfected MDA-MB-231 cells. LifeAct, which is an actin-binding peptide-GFP fusion construct, does not interfere with actin dynamics[80]. The deformation of the leading edge and the spatial distribution of F-actin in the protrusions are visualized in a close-up image series of the advancing lamellipodium at the microlane ends (Figure 5.11). There, we also show snapshots of the leading edge of simulated cells for a direct comparison between experiment and simulation. Both in experiment and simulation, we find that the lamellipodium splits in the concave-

shaped end and that it is focused in a sharp tip. These findings indicate that the local actin assembly is determined by the local curvature of the confining PEG-border. Furthermore, our experiments show that the cell contour is not entirely adjusted to the contour of the fibronectin/PEG interface. In many instances, we find transient actin protrusions into the PEGylated area. Because the PEGylated area does not constitute a solid mechanical boundary in our experiments, actin protrusions may lead to invasion of said region. However, there, the cell is not capable of adhering to the underlying substrate, leading to a subsequent retraction. In contrast, in our computer simulations, we strictly confined the cell contour to the micropattern. Furthermore, in the simulation, the contour of the advancing cell edge does not adopt the shape of the concave and sharp microlane tips to the same degree as in the experiments (Figure 5.11c, d). This might be due to (i) an overestimation of the perimeter stiffness or (ii) prohibiting the simulated cell from leaving the micropattern, which would allow less curved cell shapes.

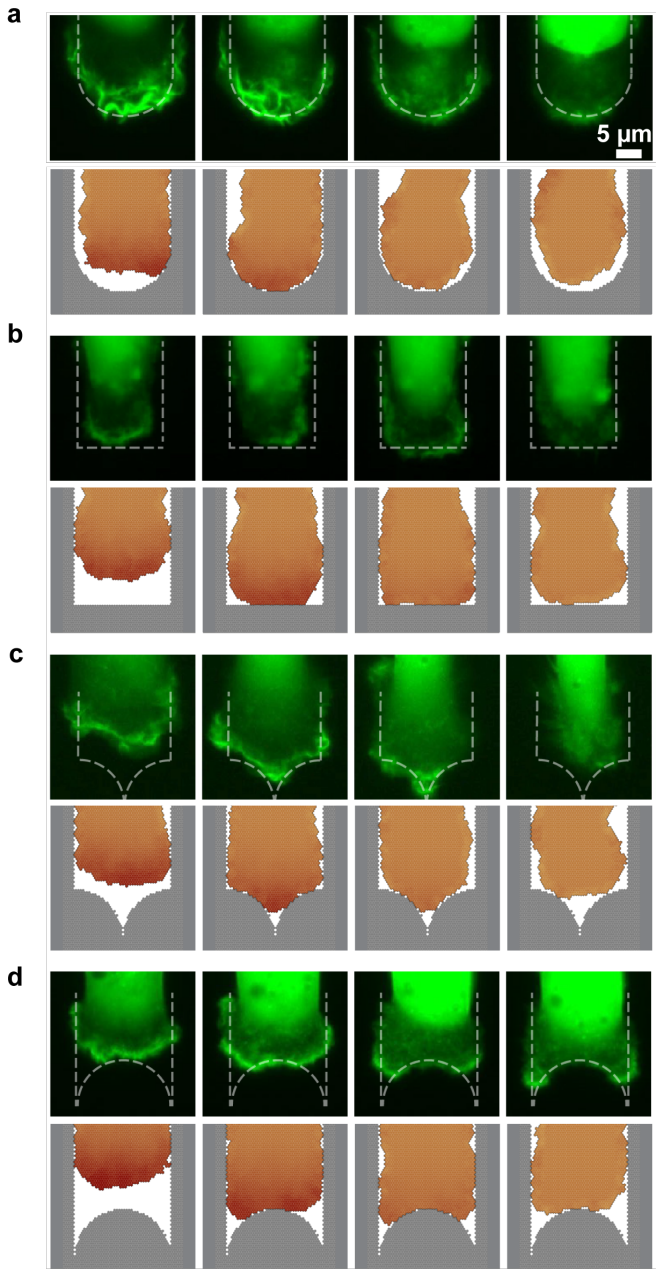

Figure 5.11 Geometry dependence of migratory arrest.

Comparison between LifeAct GFP labeled MDA-MB-231 cells and simulated cells, which migrate towards differently shaped micro-lane tips (Stripe length L=150 µm, width W=20 µm). The top row (in green) shows fluorescence time lapse data, while the bottom row shows the corresponding computer simulation for a) round-shaped tips b) blunt-shaped tips c) sharp-shaped tips and d) concave-shaped tips

Chapter 6 Conclusion and Outlook

Oscillatory motion represents an ideal and simple mode for the exploration of cell migration. Although the basic mechanisms of random cell migration are well studied, no individual model explains the complex regulation of spontaneous quasi-periodic migration, especially the repolarization and its dependence on curvatures. In this work we investigated single cells migrating in confining micropatterns. We found that cells migrate in a pronounced oscillatory manner with repetitive depolarization-repolarization processes.

Micropatterned surfaces evolved into useful tools, providing defined environments for the study of cell migration and cellular responses to external cues. In Chapter 4, µPIPP and µCP were introduced for the creation of biocompatible micropatterns. The techniques are not only quite easy to implement but also low cost. It supports defined conditions for cell adhesion and meanwhile reduces the variability from cell to cell. Combining the µPIPP with µCP allows the realization of special designed microenvironments such as surfaces with gradients proteins and structure with some chemotactic barriers [150, 151]. Micropatterns provide the possibility to capture and study the dynamic adaption of a single cell on the underlying substrates with distinct geometries. We used such patterned surfaces to independently vary the geometry to study the role of global features and local curvatures on cell behavior.

Initial studies were conducted to determine whether the shape of the micropattern is the more important factor that determines the occurrence of the cell oscillatory motion. For this, micropatterns that from isotropic shape to anisotropic shape were used to confine MDCK cells. Additionally, for each kind of pattern, the influence of its aspect ratio was tested as well. On these patterns, strong evidence for a spontaneous quasi-oscillatory behavior of single cells was found. These initial tests resulted in the following observations: (i) Single cells on the circle-shaped pattern

exhibit dominantly a random walk mode and a circling mode. The cells form lamellipodia at all regions. Few cells on the circle perform quasi-oscillatory motion that provides an interesting starting point. (ii) Cells on the ellipse-shaped pattern have a higher occurrence frequency of oscillations along its long axis, and a lower occurrence of circling mode, which leads to a hypothesis that narrower patterns might yield more oscillation events. Then, (iii) a stripe-shaped micropattern was introduced and showed higher occurrence of periodic pole-to-pole migration. The direction of those lamellipodial protrusions was well dictated by stripe-shaped islands. The results demonstrate that global geometric features in the extracellular environment can control both the internal cytoskeleton of cell and the orientation of oscillatory motion.

More important, the above study indicates that for all these geometries, there would be a threshold of size and aspect ration to generate oscillations; otherwise, a random walk is the main migration mode. We present this study primarily as an example of the complex cellular behaviors demonstrating that periodic migration is coupled to external perturbation and cell shape. When a cell confined to a small micropattern, a primary cilium grows on its dorsal surface, and the polarized state is not supported [111]. In contrast, on enlarged pattern, the ventral surface of cell has no primary cilium; the polarized state and homogeneous state could reach a balanced bistability. Earlier reports on polarity by B. Camley et al predict that in a1D system, the actin promoter density on the membrane at a homogeneous state will reach a polarized state when an external perturbation is beyond a certain threshold. For a cell of fixed size, the threshold decreases with the increasing cell area. Spontaneous oscillation is such kind of state that repeats polarization-repolarization reaction to respond external perturbation [139].

In contrast to previously mentioned that the global geometry cues can affect the cell motion, we meanwhile use different cell lines (such as MDCK, Huh7, MDA-MB-231 cells) to study whether the cells differ in their intrinsic levels of the spontaneous quasi-oscillatory migration. In the same observation time, higher occurrence frequency of quasi-oscillations can be observed for MDA-MB-231 cells.

However, MDCK cells often undergo a division state with two nuclei in a single cell, and Huh 7 cells run lower than MDa-MB-231 cells. Hence, in combination with the stripe-shaped micropatterns, MDA-MB-231 cell line were found to be the most appropriate cell line to highly reproduce the controllable oscillations for upcoming analysis in Chapter 5.

Taken together, the quasi-oscillatory motion of single cells in our setup typically includes the following processes: (i) formation of protrusion toward the direction of migration; (ii) fast motion of the bulk of the cell body at a morphological polarization; (iii) polarization quenched when the cell hits the tip of micropattern; (iv) reversal repolarization toward the opposite direction. The bimodal supports detail insights into the polarization-repolarization behavior.

As what we investigated in Chapter 4, it is possible to obtain large amount of oscillatory motion of MDA-MB-231 cells by using stripe-shaped microlanes. Next, the dominating frequency of oscillation, the spatial distribution of cell position and the persistent velocity of polarized migrating cell as a function of microlane length confirms a pole-to-pole oscillation mode in Chapter 5. We found that cells migrate in a pronounced oscillatory manner with repetitive depolarization-repolarization progresses. A morphological view of this quasi-periodic migration highlights the repetitive depolarization and repolarization of cells. At the tips of the microlanes, cell polarization and hence cell advancement is quenched due to contact with the PEGylated area. Then, spontaneous protrusions of the cell along its opposite, free, edge and subsequent polarization in the opposite direction reverses the cell motion. The reversal time does neither dependent on the length nor the geometric tips of the microlanes. We find that an extended Cellular Potts model (CPM) can recapitulate the experimentally observed pole-to-pole cell oscillatory mode. The model shows that the distribution of stochastic repolarization times might be explained as follows. Stochastic membrane protrusions explore the vicinity of the cell. Then, if the cell can adhere in the explored region, these protrusions form stable lamellipodia through a self-reinforcing feedback loop. In addition, the model also captures details of the spatiotemporal evolution of the actin polymerization

front such as lamellipodium splitting in concave tip geometries. These findings are surprising, since currently, the CPM does not take into account any molecular details of the cytoskeleton. Further, development of the CPM model including myosin and the actin regulating RhoGTPases, which has been the subject of interest in analytical reaction-diffusion models of moving cells [16, 21-24], will possibly improve the simulation of morphology and dynamics of the moving cell.

Hence the microlane assay provides a useful testbed for future refinements of CPM simulations as the setting allows the gathering of statistical data over repeated events of protrusions encountering defined obstacles. As a cell depolarizes in the different shaped ends of micro-lanes, the spatial distribution of actin activity could lead towards a better understanding of how cell adhesion and the local geometrical membrane curvature regulates actin polymerization [110, 152, 153]. In these respects, future studies combining cellular migration assays confined to micro-patterns and computational simulation, might be of value to identify mechanisms of migration phenotypes.

Cell migration can be actively driven by the arrangements of actin and myosin. Indeed, the role of actin in guiding cell polarization in response to geometry still remains under intense investigation. The intracellular signaling pathways that regulate actin cytoskeleton organization or protrusion formation are likely to contribute to the quasi-oscillatory migration. The orientation of the polymerization of F-actin, which can drive the finger-like filopodia and broad lamellipodia, are strongly influenced by the confinement geometry. The polymerization of actin is triggered by different molecular switches RhoA, Rac 1, or Cdc 42. An aspect, which could be addressed in future experiments, is how the geometrical micro-pattern affects the dynamics of the molecular switches when a cell performs an oscillatory migration.

Forming the polarization axis is important for cell migration, particularly for directionally oscillatory migration, which is regulated by the Rho GTPase family members RhoA, Rac 1 and Cdc 42, as shown in Figure 6.1. The level of Rac 1 activity

plays a central role in choosing random or directional migration [154]. During the intrinsic migration of a cell, Rac 1 is highly active at the leading edge. Rac 1 is known to trigger the local polymerization of actin and the structure formation of lamellipodia [155]. Cdc 42 are the master regulators of cell polarization that effect directional migration [156]. Rac 1 and Cdc 42 can also promote Rho A activity at the rear of the cell, meanwhile, they aid the formation of the leading edge as well as the trailing edge [157]. In fact, many current models have shown that Rac promotes membrane protrusion at the leading edge and that RhoA regulates contractility in the cell body [158-160]. Moreover, there is evidence that RhoA also regulates membrane protrusion [161, 162]. Then, to shed light on the process of cell oscillatory migration, it would be helpful to have a marker to indicate the polarization axis. Such a marker should allow the tracking of the signalling pathways throughout the whole cell.

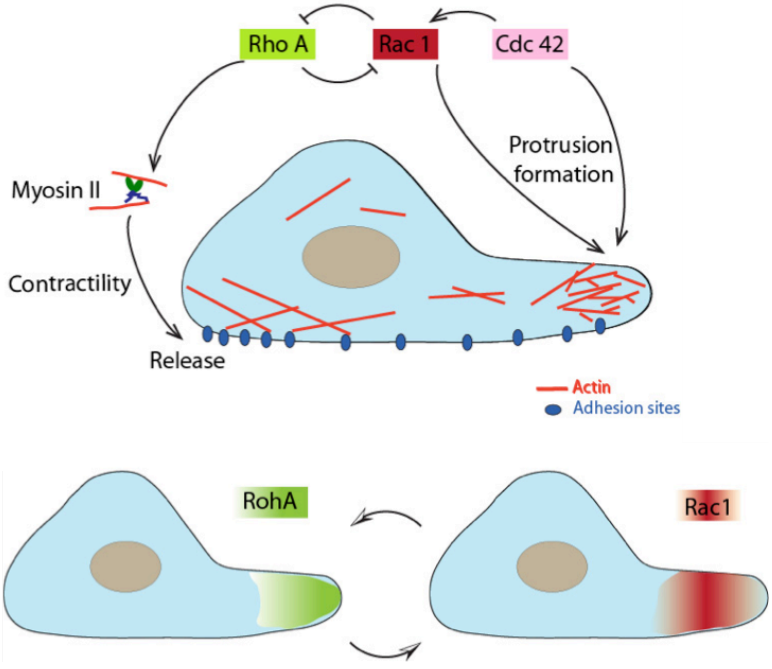

Figure 6.1 The regulating network of cytoskeleton dynamics.

Therefore, a fluorescent biomarker to visualize the spatiotemporal dynamics of RhoA activity during cell migration could be designed in future assays. Rac has

previously been shown to antagonize RhoA activity [163, 164]. However, little is known about the specific competition effects between these molecular switches. Thus, studying the effect of geometry on the dynamics of the molecular switches might complement those studies and give insights into the process of cellular polarization-repolarization.

In conclusion, the findings of this thesis shed new light on the directional migration of cells. Surfaces micropatterns constrain individual cells to distinct geometries; these geometries act as global spatial cues to govern the cells performing a quasi-oscillatory migration; the local features of geometries provides a subtle but significant effect on the repolarization of actin. The technique and setup in this work enable reliable, quantitative assays for tracking cell polarization. More importantly, the combination with the computer simulation model and the dynamics of cytoskeletal architecture (e.g., actin) of single cell contribute to the development of the understanding of cellular process.

Abbreviations

Abp140	Actin-binding protein 140
ADF	Actin Depolymerizing Factor
ADP	Adenosine-di-phosphate
ATP	Adenosine triphosphate
CCD	Charge-Coupled Device
CO_2	Carbon dioxide
CP	Change point
CPM	Cellular Potts Model
DFT	Discrete Fourier Transform
DMSO	Dimethyl sulfoxide
DNA	Deoxyribonucleic acid
ECM	Extracellular Matrix
EDTA	Ethylenediaminetetraacetic acid
FAK	Focal Ashesion Kinase
FCS	Fetal Bovine Serum
FFT	Fast Fourier Transformation
FT	Fourier Transformation
GAPs	GTPases Activating Proteisns
GEFs	Guanine nucleotide exchange factors
GFP	Green Fluorescent Proteins
GTPase	Guanosine Triphosphatase
GTP	Guanosine Triphosphate
HuH7	Human liver cell
L-Glu	L-Glutamine
MCS	Monte Carlo Step
MDA-MB-231	Human breast cancer cell
MDCK	Madin-Darby Canine Kidney
MLCK	Myosin Light-chain Kinase

mM	milli Molar
MSD	Mean square displacement
MTOC	Microtubule Organizing Center
µCP	Micro Contact Printing
µPIP	Plasma-Induced Protein Patterning
MW	Molecular Weight
OU	Ornstein-Uhlenbeck
PBS	Phosphate-Buffered Saline
PDMS	Poly(Dimethyl-Siloxane)
PEG	Poly(Ethylene-Glycol)
PLL	Poly(L-Lysine)
ROCK	Rho kinase
Tmod	Tropomodulins
UV	Ultraviolet
WASP	Wiskott-Aldrich syndrome protein

List of Figures and Tables

Figures

Tables

References

[1] S.F. Gilbert, The morphogenesis of evolutionary developmental biology, International Journal of Developmental Biology 47(7-8) (2003) 467.

[2] M. Poujade, E. Grasland-Mongrain, A. Hertzog, J. Jouanneau, P. Chavrier, B. Ladoux, A. Buguin, P. Silberzan, Collective migration of an epithelial monolayer in response to a model wound, Proceedings of the National Academy of Sciences 104(41) (2007) 15988-15993.

[3] J.A. Cooper, Mechanisms of cell migration in the nervous system, The Journal of Cell Biology 202(5) (2013) 725-734.

[4] A.J. Ridley, M.A. Schwartz, K. Burridge, R.A. Firtel, M.H. Ginsberg, G. Borisy, J.T. Parsons, A.R. Horwitz, Cell Migration: Integrating Signals from Front to Back, Science 302(5651) (2003) 1704-1709.

[5] E. Ingulli, Mechanism of cellular rejection in transplantation, Pediatric Nephrology 25(1) (2008) 61.

[6] W.-h. Guo, M.T. Frey, N.A. Burnham, Y.-l. Wang, Substrate Rigidity Regulates the Formation and Maintenance of Tissues, Biophysical Journal 90(6) (2006) 2213-2220.

[7] Three-Dimensional Cell Culture Systems and Their Applications in Drug Discovery and Cell-Based Biosensors, ASSAY and Drug Development Technologies 12(4) (2014) 207-218.

[8] T.E. Starzl, A.J. Demetris, M. Trucco, N. Murase, C. Ricordi, S. Ildstad, H. Ramos, S. Todo, A. Tzakis, J.J. Fung, M. Nalesnik, A. Zeevi, W.A. Rudert, M. Kocova, Cell migration and chimerism after whole-organ transplantation: The basis of graft acceptance, Hepatology 17(6) (1993) 1127-1152.

[9] D.A. Lauffenburger, A.F. Horwitz, Cell Migration: A Physically Integrated Molecular Process, Cell 84(3) 359-369.

[10] T.J. Mitchison, L.P. Cramer, Actin-Based Cell Motility and Cell Locomotion, Cell 84(3) (1996) 371-379.

[11] K. Keren, Z. Pincus, G.M. Allen, E.L. Barnhart, G. Marriott, A. Mogilner, J.A. Theriot, Mechanism of shape determination in motile cells, Nature 453(7194) (2008) 475-480.

[12] K. Kruse, S. Camalet, F. Julicher, Self-propagating patterns in active filament bundles, Physical Review Letters 87(13) (2001).

[13] A.E. Carlsson, Dendritic Actin Filament Nucleation Causes Traveling Waves and Patches, Physical Review Letters 104(22) (2010) 228102.

[14] G. Giannone, B.J. Dubin-Thaler, H.G. Dobereiner, N. Kieffer, A.R. Bresnick, M.P. Sheetz, Periodic lamellipodial contractions correlate with rearward actin waves, Cell 116(3) (2004) 431-443.

[15] T. Bretschneider, K. Anderson, M. Ecke, A. Müller-Taubenberger, B. Schroth-Diez, H.C. Ishikawa-Ankerhold, G. Gerisch, The Three-Dimensional Dynamics of Actin Waves, a Model of Cytoskeletal Self-Organization, Biophysical Journal 96(7) (2009) 2888-2900.

[16] P. Maiuri, J.-F. Rupprecht, S. Wieser, V. Ruprecht, O. Bénichou, N. Carpi, M. Coppey, S. De Beco, N. Gov, C.-P. Heisenberg, C. Lage Crespo, F. Lautenschlaeger, M. Le Berre, A.-M. Lennon-Dumenil, M. Raab, H.-R. Thiam, M. Piel, M. Sixt, R. Voituriez, Actin Flows Mediate a Universal Coupling between Cell Speed and Cell Persistence, Cell 161(2) (2015) 374-386.

[17] D. Shao, H. Levine, W.-J. Rappel, Coupling actin flow, adhesion, and morphology in a computational cell motility model, Proceedings of the National Academy of Sciences 109(18) (2012) 6851-6856.

[18] J. Allard, A. Mogilner, Traveling waves in actin dynamics and cell motility, Current Opinion in Cell Biology 25(1) (2013) 107-115.

[19] A.B. Verkhovsky, The mechanisms of spatial and temporal patterning of cell-edge dynamics, Curr Opin Cell Biol 36 (2015) 113-121.

[20] Y.H. Tee, T. Shemesh, V. Thiagarajan, R.F. Hariadi, K.L. Anderson, C. Page, N. Volkmann, D. Hanein, S. Sivaramakrishnan, M.M. Kozlov, A.D. Bershadsky, Cellular chirality arising from the self-organization of the actin cytoskeleton, Nature Cell Biology 17(4) (2015) 445-+.

[21] Y. Mori, A. Jilkine, L. Edelstein-Keshet, Wave-Pinning and Cell Polarity from a Bistable Reaction-Diffusion System, Biophysical Journal 94(9) (2008) 3684-3697.

[22] L. Edelstein-Keshet, W.R. Holmes, M. Zajac, M. Dutot, From simple to detailed models for cell polarization, Philosophical Transactions of the Royal Society B: Biological Sciences 368(1629) (2013).

[23] K.M. Byrne, N. Monsefi, J.C. Dawson, A. Degasperi, J.-C. Bukowski-Wills, N. Volinsky, M. Dobrzyński, M.R. Birtwistle, M.A. Tsyganov, A. Kiyatkin, Bistability in the Rac1, PAK, and RhoA signaling network drives actin cytoskeleton dynamics and cell motility switches, Cell systems 2(1) (2016) 38-48.

[24] A.F.M. Marée, V.A. Grieneisen, L. Edelstein-Keshet, How Cells Integrate Complex Stimuli: The Effect of Feedback from Phosphoinositides and Cell Shape on Cell Polarization and Motility, PLOS Computational Biology 8(3) (2012) e1002402.

[25] J. Halatek, E. Frey, Rethinking pattern formation in reaction–diffusion systems, Nature Physics 14(5) (2018) 507.

[26] O. Hoeller, J.E. Toettcher, H. Cai, Y. Sun, C.-H. Huang, M. Freyre, M. Zhao, P.N. Devreotes, O.D. Weiner, Gβ Regulates Coupling between Actin Oscillators for Cell Polarity and Directional Migration, PLOS Biology 14(2) (2016) e1002381.

[27] M. Gerhardt, M. Ecke, M. Walz, A. Stengl, C. Beta, G. Gerisch, Actin and PIP3 waves in giant cells reveal the inherent length scale of an excited state, J Cell Sci 127(20) (2014) 4507-4517.

[28] C. Beta, K. Kruse, Intracellular oscillations and waves, Annual Review of Condensed Matter Physics 8 (2017) 239-264.

[29] F. Lautenschläger, M. Piel, Microfabricated devices for cell biology: all for one and one for all, Current opinion in cell biology 25(1) (2013) 116-124.

[30] P. Maiuri, E. Terriac, P. Paul-Gilloteaux, T. Vignaud, K. McNally, J. Onuffer, K. Thorn, P.A. Nguyen, N. Georgoulia, D. Soong, A. Jayo, N. Beil, J. Beneke, J.C. Hong Lim, C. Pei-Ying Sim, Y.-S. Chu, A. Jiménez-Dalmaroni, J.-F. Joanny, J.-P. Thiery, H. Erfle, M. Parsons, T.J. Mitchison, W.A. Lim, A.-M. Lennon-Duménil, M. Piel, M. Théry, The first World Cell Race, Current Biology 22(17) (2012) R673-R675.

[31] G. Kumar, C.-C. Ho, C.C. Co, Retracted: Guiding Cell Migration Using One-Way Micropattern Arrays, Advanced Materials 19(8) (2007) 1084-1090.

[32] B. Boldajipour, H. Mahabaleshwar, E. Kardash, M. Reichman-Fried, H. Blaser, S. Minina, D. Wilson, Q. Xu, E. Raz, Control of chemokine-guided cell migration by ligand sequestration, Cell 132(3) (2008) 463-473.

[33] P. Maiuri, E. Terriac, P. Paul-Gilloteaux, T. Vignaud, K. McNally, J. Onuffer, K. Thorn, P.A. Nguyen, N. Georgoulia, D. Soong, The first world cell race, Current Biology 22(17) (2012) R673-R675.

[34] F.J. Segerer, F. Thüroff, A. Piera Alberola, E. Frey, J.O. Rädler, Emergence and Persistence of Collective Cell Migration on Small Circular Micropatterns, Physical Review Letters 114(22) (2015) 228102.

[35] G. Mahmud, C.J. Campbell, K.J. Bishop, Y.A. Komarova, O. Chaga, S. Soh, S. Huda, K. Kandere-Grzybowska, B.A. Grzybowski, Directing cell motions on micropatterned ratchets, Nature physics 5(8) (2009) 606.

[36] D.B. Brückner, A. Fink, C. Schreiber, P.J.F. Röttgermann, J.O. Rädler, C.P. Broedersz, Publisher Correction: Stochastic nonlinear dynamics of confined cell migration in two-state systems, Nature Physics 15(6) (2019) 617-617.

[37] C. Schreiber, F.J. Segerer, E. Wagner, A. Roidl, J.O. Rädler, Ring-Shaped Microlanes and Chemical Barriers as a Platform for Probing Single-Cell Migration, Scientific reports 6 (2016) 26858.

[38] J. Zhang, W.H. Guo, Y.L. Wang, Microtubules stabilize cell polarity by localizing rear signals, Proceedings of the National Academy of Sciences of the United States of America 111(46) (2014) 16383-8.

[39] S.I. Fraley, Y. Feng, A. Giri, G.D. Longmore, D. Wirtz, Dimensional and temporal controls of three-dimensional cell migration by zyxin and binding partners, Nature communications 3 (2012) 719.

[40] B.A. Camley, Y. Zhao, B. Li, H. Levine, W.-J. Rappel, Periodic Migration in a Physical Model of Cells on Micropatterns, Physical Review Letters 111(15) (2013).

[41] K.G. Campellone, N.J. Webb, E.A. Znameroski, M.D. Welch, WHAMM is an Arp2/3 complex activator that binds microtubules and functions in ER to Golgi transport, Cell 134(1) (2008) 148-161.

[42] M.A. Jordan, L. Wilson, Microtubules as a target for anticancer drugs, Nature Reviews Cancer 4 (2004) 253.

[43] D.A. Fletcher, R.D. Mullins, Cell mechanics and the cytoskeleton, Nature 463 (2010) 485.

[44] D.J. Mooney, R. Langer, D.E. Ingber, Cytoskeletal filament assembly and the control of cell spreading and function by extracellular matrix, Journal of Cell Science 108(6) (1995) 2311-2320.

[45] R. McBeath, D.M. Pirone, C.M. Nelson, K. Bhadriraju, C.S. Chen, Cell shape, cytoskeletal tension, and RhoA regulate stem cell lineage commitment, Developmental cell 6(4) (2004) 483-495.

[46] D.E. Ingber, L. Dike, L. Hansen, S. Karp, H. Liley, A. Maniotis, H. McNamee, D. Mooney, G. Plopper, J. Sims, Cellular tensegrity: exploring how mechanical changes in the cytoskeleton regulate cell growth, migration, and tissue pattern during morphogenesis, International review of cytology, Elsevier1994, pp. 173-224.

[47] C.P. Brangwynne, F.C. MacKintosh, S. Kumar, N.A. Geisse, J. Talbot, L. Mahadevan, K.K. Parker, D.E. Ingber, D.A. Weitz, Microtubules can bear enhanced compressive loads in living cells because of lateral reinforcement, J Cell Biol 173(5) (2006) 733-741.

[48] F. Gittes, B. Mickey, J. Nettleton, J. Howard, Flexural rigidity of microtubules and actin filaments measured from thermal fluctuations in shape, The Journal of Cell Biology 120(4) (1993) 923-934.

[49] C. Allen, G.G. Borisy, Structural polarity and directional growth of microtubules of Chlamydomonas flagella, Journal of molecular biology 90(2) (1974) 381-402.

[50] T. Mitchison, M. Kirschner, Dynamic instability of microtubule growth, Nature 312 (1984) 237.

[51] T.E. Holy, S. Leibler, Dynamic instability of microtubules as an efficient way to search in space, Proceedings of the National Academy of Sciences 91(12) (1994) 5682-5685.

[52] T. Watanabe, J. Noritake, K. Kaibuchi, Regulation of microtubules in cell migration, Trends in Cell Biology 15(2) (2005) 76-83.

[53] E. Fuchs, K. Weber, Intermediate filaments: structure, dynamics, function and disease, Annual review of biochemistry 63(1) (1994) 345-382.

[54] M. Hatzfeld, K. Weber, Modulation of keratin intermediate filament assembly by single amino acid exchanges in the consensus sequence at the C-terminal end of the rod domain, Journal of Cell Science 99(2) (1991) 351-362.

[55] E. Fuchs, D.W. Cleveland, A Structural Scaffolding of Intermediate Filaments in Health and Disease, Science 279(5350) (1998) 514-519.

[56] G. Wiche, Role of plectin in cytoskeleton organization and dynamics, Journal of Cell Science 111(17) (1998) 2477-2486.

[57] E.W. Flitney, E.R. Kuczmarski, S.A. Adam, R.D. Goldman, Insights into the mechanical properties of epithelial cells: the effects of shear stress on the assembly and remodeling of keratin intermediate filaments, The FASEB Journal 23(7) (2009) 2110-2119.

[58] M.-Y. Tsai, S. Wang, J.M. Heidinger, D.K. Shumaker, S.A. Adam, R.D. Goldman, Y. Zheng, A mitotic lamin B matrix induced by RanGTP required for spindle assembly, Science 311(5769) (2006) 1887-1893.

[59] T.D. Pollard, J.A. Cooper, Actin, a Central Player in Cell Shape and Movement, Science 326(5957) (2009) 1208-1212.

[60] W. Kabsch, H.G. Mannherz, D. Suck, E.F. Pai, K.C. Holmes, Atomic structure of the actin: DNase I complex, Nature 347 (1990) 37.

[61] D. Sept, J.A. McCammon, Thermodynamics and kinetics of actin filament nucleation, Biophysical journal 81(2) (2001) 667-674.

[62] A. Wegner, J. Engel, Kinetics of the cooperative association of actin to actin filament, Biophysical chemistry 3(3) (1975) 215-225.

[63] D. Drenckhahn, T.D. Pollard, Elongation of actin filaments is a diffusion-limited reaction at the barbed end and is accelerated by inert macromolecules, Journal of Biological Chemistry 261(27) (1986) 12754-12758.

[64] J.-M. Neuhaus, M. Wanger, T. Keiser, A. Wegner, Treadmilling of actin, Journal of Muscle Research & Cell Motility 4(5) (1983) 507-527.

[65] C. Dos Remedios, D. Chhabra, M. Kekic, I. Dedova, M. Tsubakihara, D. Berry, N. Nosworthy, Actin binding proteins: regulation of cytoskeletal microfilaments, Physiological reviews 83(2) (2003) 433-473.

[66] I. Sagot, A.A. Rodal, J. Moseley, B.L. Goode, D. Pellman, An actin nucleation mechanism mediated by Bni1 and profilin, Nature cell biology 4(8) (2002) 626.

[67] D. Pantaloni, M.-F. Carlier, How profilin promotes actin filament assembly in the presence of thymosin β4, Cell 75(5) (1993) 1007-1014.

[68] R.D. Mullins, J.A. Heuser, T.D. Pollard, The interaction of Arp2/3 complex with actin: nucleation, high affinity pointed end capping, and formation of branching networks of filaments, Proceedings of the National Academy of Sciences 95(11) (1998) 6181-6186.

[69] E. Kerkhoff, Cellular functions of the Spir actin-nucleation factors, Trends in cell biology 16(9) (2006) 477-483.

[70] D. Pruyne, M. Evangelista, C. Yang, E. Bi, S. Zigmond, A. Bretscher, C. Boone, Role of formins in actin assembly: nucleation and barbed-end association, Science 297(5581) (2002) 612-615.

[71] D. Sept, J. Xu, T.D. Pollard, J.A. McCammon, Annealing accounts for the length of actin filaments formed by spontaneous polymerization, Biophysical journal 77(6) (1999) 2911-2919.

[72] M. Ghosh, X. Song, G. Mouneimne, M. Sidani, D.S. Lawrence, J.S. Condeelis, Cofilin promotes actin polymerization and defines the direction of cell motility, Science 304(5671) (2004) 743-746.

[73] D.H. Wachsstock, W. Schwarz, T. Pollard, Cross-linker dynamics determine the mechanical properties of actin gels, Biophysical journal 66(3) (1994) 801-809.

[74] J.R. Sellers, Myosins: a diverse superfamily, Biochimica et Biophysica Acta (BBA)-Molecular Cell Research 1496(1) (2000) 3-22.

[75] J.S. Berg, B.C. Powell, R.E. Cheney, A millennial myosin census, Molecular biology of the cell 12(4) (2001) 780-794.

[76] K.C. Flynn, C.W. Pak, A.E. Shaw, F. Bradke, J.R. Bamburg, Growth cone‐like waves transport actin and promote axonogenesis and neurite branching, Developmental neurobiology 69(12) (2009) 761-779.

[77] H. Faulstich, D. Georgopoulos, M. Bloching, Quantitative chromatographic analysis of toxins in single mushrooms of Amanita phalloides, Journal of Chromatography A 79 (1973) 257-265.

[78] T. Bretschneider, S. Diez, K. Anderson, J. Heuser, M. Clarke, A. Müller-Taubenberger, J. Köhler, G. Gerisch, Dynamic actin patterns and Arp2/3 assembly at the substrate-attached surface of motile cells, Current Biology 14(1) (2004) 1-10.

[79] P. Lénárt, C.P. Bacher, N. Daigle, A.R. Hand, R. Eils, M. Terasaki, J. Ellenberg, A contractile nuclear actin network drives chromosome congression in oocytes, Nature 436(7052) (2005) 812.

[80] J. Riedl, A.H. Crevenna, K. Kessenbrock, J.H. Yu, D. Neukirchen, M. Bista, F. Bradke, D. Jenne, T.A. Holak, Z. Werb, M. Sixt, R. Wedlich-Soldner, Lifeact: a versatile marker to visualize F-actin, Nature Methods 5 (2008) 605.

[81] R. Wedlich-Soldner, R. Li, Spontaneous cell polarization: undermining determinism, Nature cell biology 5(4) (2003) 267.

[82] J.T. Parsons, A.R. Horwitz, M.A. Schwartz, Cell adhesion: integrating cytoskeletal dynamics and cellular tension, Nature reviews Molecular cell biology 11(9) (2010) 633.

[83] M. Zhao, Electrical fields in wound healing—an overriding signal that directs cell migration, Seminars in cell & developmental biology, Elsevier, 2009, pp. 674-682.

[84] D.J. Cohen, W.J. Nelson, M.M. Maharbiz, Galvanotactic control of collective cell migration in epithelial monolayers, Nature materials 13(4) (2014) 409.

[85] M.K. Driscoll, X. Sun, C. Guven, J.T. Fourkas, W. Losert, Cellular contact guidance through dynamic sensing of nanotopography, ACS nano 8(4) (2014) 3546-3555.

[86] P. Roca-Cusachs, R. Sunyer, X. Trepat, Mechanical guidance of cell migration: lessons from chemotaxis, Current opinion in cell biology 25(5) (2013) 543-549.

[87] P.K. Mattila, P. Lappalainen, Filopodia: molecular architecture and cellular functions, Nature reviews Molecular cell biology 9(6) (2008) 446.

[88] M.R. Mejillano, S.-i. Kojima, D.A. Applewhite, F.B. Gertler, T.M. Svitkina, G.G. Borisy, Lamellipodial versus filopodial mode of the actin nanomachinery: pivotal role of the filament barbed end, Cell 118(3) (2004) 363-373.

[89] A. Ponti, M. Machacek, S. Gupton, C. Waterman-Storer, G. Danuser, Two distinct actin networks drive the protrusion of migrating cells, Science 305(5691) (2004) 1782-1786.

[90] V. Small, Shifting views on the leading role of the lamellipodium in cell migration: speckle tracking revisited, (2009).

[91] A.J. Ridley, P.M. Comoglio, A. Hall, Regulation of scatter factor/hepatocyte growth factor responses by Ras, Rac, and Rho in MDCK cells, Molecular and cellular biology 15(2) (1995) 1110-1122.

[92] S. Etienne-Manneville, A. Hall, Rho GTPases in cell biology, Nature 420(6916) (2002) 629.

[93] M.D. Welch, R.D. Mullins, Cellular control of actin nucleation, Annual review of cell and developmental biology 18(1) (2002) 247-288.

[94] S. Etienne-Manneville, Polarity proteins in migration and invasion, Oncogene 27(55) (2008) 6970.

[95] C. Frantz, K.M. Stewart, V.M. Weaver, The extracellular matrix at a glance, J Cell Sci 123(24) (2010) 4195-4200.

[96] A. Huttenlocher, A.R. Horwitz, Integrins in cell migration, Cold Spring Harbor perspectives in biology 3(9) (2011) a005074.

[97] G. Giannone, B.J. Dubin-Thaler, O. Rossier, Y. Cai, O. Chaga, G. Jiang, W. Beaver, H.-G. Döbereiner, Y. Freund, G. Borisy, Lamellipodial actin mechanically links myosin activity with adhesion-site formation, Cell 128(3) (2007) 561-575.

[98] S.H. Lo, E. Weisberg, L.B. Chen, Tensin: a potential link between the cytoskeleton and signal transduction, Bioessays 16(11) (1994) 817-823.

[99] M.D. Schaller, J.T. Parsons, Focal adhesion kinase and associated proteins, Current opinion in cell biology 6(5) (1994) 705-710.

[100] A.J. Ridley, A. Hall, The small GTP-binding protein rho regulates the assembly of focal adhesions and actin stress fibers in response to growth factors, Cell 70(3) (1992) 389-399.

[101] K.A. Beningo, M. Dembo, I. Kaverina, J.V. Small, Y.-l. Wang, Nascent focal adhesions are responsible for the generation of strong propulsive forces in migrating fibroblasts, The Journal of cell biology 153(4) (2001) 881-888.

[102] C.G. Galbraith, K.M. Yamada, M.P. Sheetz, The relationship between force and focal complex development, J Cell Biol 159(4) (2002) 695-705.

[103] D.A. Lauffenburger, A.F. Horwitz, Cell migration: a physically integrated molecular process, Cell 84(3) (1996) 359-369.

[104] P.Y. Jay, P.A. Pham, S.A. Wong, E.L. Elson, A mechanical function of myosin II in cell motility, Journal of cell science 108(1) (1995) 387-393.

[105] F. Pouthas, P. Girard, V. Lecaudey, T.B.N. Ly, D. Gilmour, C. Boulin, R. Pepperkok, E.G. Reynaud, In migrating cells, the Golgi complex and the position of the centrosome depend on geometrical constraints of the substratum, Journal of Cell Science 121(14) (2008) 2406-2414.

[106] A.D. Doyle, F.W. Wang, K. Matsumoto, K.M. Yamada, One-dimensional topography underlies three-dimensional fibrillar cell migration, The Journal of Cell Biology 184(4) (2009) 481-490.

[107] R. Picone, X. Ren, K.D. Ivanovitch, J.D.W. Clarke, R.A. McKendry, B. Baum, A Polarised Population of Dynamic Microtubules Mediates Homeostatic Length Control in Animal Cells, PLOS Biology 8(11) (2010) e1000542.

[108] E.M. Levina, M.A. Kharitonova, Y.A. Rovensky, J.M. Vasiliev, Cytoskeletal control of fibroblast length: experiments with linear strips of substrate, Journal of Cell Science 114(23) (2001) 4335-4341.

[109] M. Théry, Micropatterning as a tool to decipher cell morphogenesis and functions, Journal of Cell Science 123(24) (2010) 4201-4213.

[110] X. Jiang, D.A. Bruzewicz, A.P. Wong, M. Piel, G.M. Whitesides, Directing cell migration with asymmetric micropatterns, Proceedings of the National Academy of Sciences 102(4) (2005) 975-978.

[111] A. Pitaval, Q. Tseng, M. Bornens, M. Théry, Cell shape and contractility regulate ciliogenesis in cell cycle–arrested cells, The Journal of cell biology 191(2) (2010) 303-312.

[112] K. Kushiro, A.R. Asthagiri, Modular design of micropattern geometry achieves combinatorial enhancements in cell motility, Langmuir 28(9) (2012) 4357-4362.

[113] F.J. Segerer, F. Thüroff, A.P. Alberola, E. Frey, J.O. Rädler, Emergence and persistence of collective cell migration on small circular micropatterns, Physical review letters 114(22) (2015) 228102.

[114] M. Théry, V. Racine, M. Piel, A. Pépin, A. Dimitrov, Y. Chen, J.-B. Sibarita, M. Bornens, Anisotropy of cell adhesive microenvironment governs cell internal organization and orientation of polarity, Proceedings of the National Academy of Sciences 103(52) (2006) 19771-19776.

[115] L. Ornstein, On the Brownian motion, Proc. Amst, 1919, pp. 96-108.

[116] G.E. Uhlenbeck, L.S. Ornstein, On the Theory of the Brownian Motion, Physical Review 36(5) (1930) 823-841.

[117] A. Eintsein, On the movement of small particles suspended in a stationary liquid demanded by the molecular-kinetic theory of heat Investigations on the Theory of the Brownian Motion, New York: Dover, 1956.

[118] R. Fürth, Die brownsche bewegung bei berücksichtigung einer persistenz der bewegungsrichtung. mit anwendungen auf die bewegung lebender infusorien, Zeitschrift für Physik 2(3) (1920) 244-256.

[119] D. Selmeczi, S. Mosler, P.H. Hagedorn, N.B. Larsen, H. Flyvbjerg, Cell Motility as Persistent Random Motion: Theories from Experiments, Biophysical Journal 89(2) (2005) 912-931.

[120] R.N. Bracewell, R.N. Bracewell, The Fourier transform and its applications, McGraw-Hill New York1986.

[121] L. Illing, Fourier analysis, 2008.

[122] K.B. Howell, Principles of Fourier analysis, CRC Press2001.

[123] D. Morin, Fourier analysis, Harvard University: Department of Physics, 2009.

[124] M.A. Bartsch, D.L. Neuhoff, G.H. Wakefield, EECS 206 Laboratory Manual, 2003.

[125] D. Potts, G. Steidl, M. Tasche, Fast Fourier transforms for nonequispaced data: A tutorial, Modern sampling theory, Springer2001, pp. 247-270.

[126] J. Müller, M. Sixt, Cell migration: Making the waves, Current Biology 27(1) (2017) R24-R25.

[127] F. Raynaud, M.E. Ambühl, C. Gabella, A. Bornert, I.F. Sbalzarini, J.-J. Meister, A.B. Verkhovsky, Minimal model for spontaneous cell polarization and edge activity in oscillating, rotating and migrating cells, Nature Physics 12(4) (2016) 367.

[128] K. Wilson, A. Lewalle, M. Fritzsche, R. Thorogate, T. Duke, G. Charras, Mechanisms of leading edge protrusion in interstitial migration, Nature communications 4 (2013) 2896.

[129] D.T. Burnette, L. Shao, C. Ott, A.M. Pasapera, R.S. Fischer, M.A. Baird, C. Der Loughian, H. Delanoe-Ayari, M.J. Paszek, M.W. Davidson, A contractile and counterbalancing adhesion system controls the 3D shape of crawling cells, J Cell Biol 205(1) (2014) 83-96.

[130] E.L. Barnhart, J. Allard, S.S. Lou, J.A. Theriot, A. Mogilner, Adhesion-dependent wave generation in crawling cells, Current Biology 27(1) (2017) 27-38.

[131] M. Krause, A. Gautreau, Steering cell migration: lamellipodium dynamics and the regulation of directional persistence, Nature reviews Molecular cell biology 15(9) (2014) 577.

[132] F. Graner, J.A. Glazier, Simulation of biological cell sorting using a two-dimensional extended Potts model, Physical review letters 69(13) (1992) 2013.

[133] J.A. Glazier, F. Graner, Simulation of the differential adhesion driven rearrangement of biological cells, Physical Review E 47(3) (1993) 2128.

[134] M.D. Abràmoff, P.J. Magalhães, S.J. Ram, Image processing with ImageJ, Biophotonics international 11(7) (2004) 36-42.

[135] C. Metzner, C. Mark, J. Steinwachs, L. Lautscham, F. Stadler, B. Fabry, Superstatistical analysis and modelling of heterogeneous random walks, Nature communications 6 (2015) 7516.

[136] J.S. Gruver, A.A. Potdar, J. Jeon, J. Sai, B. Anderson, D. Webb, A. Richmond, V. Quaranta, P.T. Cummings, C.Y. Chung, Bimodal Analysis Reveals a General Scaling Law Governing Nondirected and Chemotactic Cell Motility, Biophysical Journal 99(2) (2010) 367-376.

[137] A.A. Potdar, J. Jeon, A.M. Weaver, V. Quaranta, P.T. Cummings, Human Mammary Epithelial Cells Exhibit a Bimodal Correlated Random Walk Pattern, PLOS ONE 5(3) (2010) e9636.

[138] K. Kruse, F. Jülicher, Oscillations in cell biology, Current Opinion in Cell Biology 17(1) (2005) 20-26.

[139] B.A. Camley, Y. Zhao, B. Li, H. Levine, W.-J. Rappel, Periodic migration in a physical model of cells on micropatterns, Physical review letters 111(15) (2013) 158102.

[140] A. Era, M. Tominaga, K. Ebine, C. Awai, C. Saito, K. Ishizaki, K.T. Yamato, T. Kohchi, A. Nakano, T. Ueda, Application of Lifeact reveals F-actin dynamics in Arabidopsis thaliana and the liverwort, Marchantia polymorpha, Plant and Cell Physiology 50(6) (2009) 1041-1048.

[141] J. Riedl, A.H. Crevenna, K. Kessenbrock, J.H. Yu, D. Neukirchen, M. Bista, F. Bradke, D. Jenne, T.A. Holak, Z. Werb, Lifeact: a versatile marker to visualize F-actin, Nature methods 5(7) (2008) 605.

[142] A. Ganguly, H. Yang, R. Sharma, K.D. Patel, F. Cabral, The role of microtubules and their dynamics in cell migration, J Biol Chem 287(52) (2012) 43359-43369.

[143] T. Mitchison, L. Cramer, Actin-based cell motility and cell locomotion, Cell 84(3) (1996) 371-379.

[144] F. Thueroff, A. Goychuk, M. Reiter, E. Frey, Bridging the gap between single cell migration and collective dynamics, bioRxiv (2019) 548677.

[145] A. Goychuk, D.B. Brückner, A.W. Holle, J.P. Spatz, C.P. Broedersz, E. Frey, Morphology and Motility of Cells on Soft Substrates, arXiv preprint arXiv:1808.00314 (2018).

[146] J.T. Daub, R.M.H. Merks, A Cell-Based Model of Extracellular-Matrix-Guided Endothelial Cell Migration During Angiogenesis, Bulletin of Mathematical Biology 75(8) (2013) 1377-1399.

[147] A.J. Kabla, Collective cell migration: leadership, invasion and segregation, Journal of The Royal Society Interface 9(77) (2012) 3268-3278.

[148] R.M.H. Merks, J.A. Glazier, A cell-centered approach to developmental biology, Physica A: Statistical Mechanics and its Applications 352(1) (2005) 113-130.

[149] J. James, E.D. Goluch, H. Hu, C. Liu, M. Mrksich, Subcellular curvature at the perimeter of micropatterned cells influences lamellipodial distribution and cell polarity, Cell motility and the cytoskeleton 65(11) (2008) 841-852.

[150] M. Mayer, J. Yang, I. Gitlin, D.H. Gracias, G.M. Whitesides, Micropatterned agarose gels for stamping arrays of proteins and gradients of proteins, Proteomics 4(8) (2004) 2366-2376.

[151] C.B. Herbert, T.L. McLernon, C.L. Hypolite, D.N. Adams, L. Pikus, C.-C. Huang, G.B. Fields, P.C. Letourneau, M.D. Distefano, W.-S. Hu, Micropatterning gradients and controlling surface densities of photoactivatable biomolecules on self-assembled monolayers of oligo (ethylene glycol) alkanethiolates, Chemistry & biology 4(10) (1997) 731-737.

[152] H. Jeon, S. Koo, W.M. Reese, P. Loskill, C.P. Grigoropoulos, K.E. Healy, Directing cell migration and organization via nanocrater-patterned cell-repellent interfaces, Nature materials 14(9) (2015) 918.

[153] H.-F. Hsu, E. Bodenschatz, C. Westendorf, A. Gholami, A. Pumir, M. Tarantola, C. Beta, Variability and Order in Cytoskeletal Dynamics of Motile Amoeboid Cells, Physical Review Letters 119(14) (2017) 148101.

[154] J. Monypenny, D. Zicha, C. Higashida, F. Oceguera-Yanez, S. Narumiya, N. Watanabe, Cdc42 and Rac family GTPases regulate mode and speed but not direction of primary fibroblast migration during platelet-derived growth factor-dependent chemotaxis, Molecular and cellular biology 29(10) (2009) 2730-2747.

[155] C.D. Nobes, A. Hall, Rho, rac, and cdc42 GTPases regulate the assembly of multimolecular focal complexes associated with actin stress fibers, lamellipodia, and filopodia, Cell 81(1) (1995) 53-62.

[156] S. Etienne-Manneville, Cdc42-the centre of polarity, Journal of cell science 117(8) (2004) 1291-1300.

[157] O. Pertz, Spatio-temporal Rho GTPase signaling–where are we now?, J Cell Sci 123(11) (2010) 1841-1850.

[158] M. Raftopoulou, A. Hall, Cell migration: Rho GTPases lead the way, Developmental biology 265(1) (2004) 23-32.

[159] K. Burridge, K. Wennerberg, Rho and Rac take center stage, Cell 116(2) (2004) 167-179.

[160] O. Pertz, L. Hodgson, R.L. Klemke, K.M. Hahn, Spatiotemporal dynamics of RhoA activity in migrating cells, Nature 440(7087) (2006) 1069.

[161] Y. Fukata, N. Oshiro, N. Kinoshita, Y. Kawano, Y. Matsuoka, V. Bennett, Y. Matsuura, K. Kaibuchi, Phosphorylation of adducin by Rho-kinase plays a crucial role in cell motility, The Journal of cell biology 145(2) (1999) 347-361.

[162] A.F. Palazzo, T.A. Cook, A.S. Alberts, G.G. Gundersen, mDia mediates Rho-regulated formation and orientation of stable microtubules, Nature cell biology 3(8) (2001) 723.

[163] A.S. Nimnual, L.J. Taylor, D. Bar-Sagi, Redox-dependent downregulation of Rho by Rac, Nature cell biology 5(3) (2003) 236.

[164] E.E. Sander, P. Jean, S. van Delft, R.A. van der Kammen, J.G. Collard, Rac downregulates Rho activity: reciprocal balance between both GTPases determines cellular morphology and migratory behavior, The Journal of cell biology 147(5) (1999) 1009-1022.

List of Publications

1. F. Zhou, S. Schaffer, C. Schreiber, F. J. Segerer, A. Goychuk, E. Frey, J. O. Rädler, Quasi-periodic migration of single cells on short microlanes, Submitted

2. F. Zhou, J. Yang, R. Xing, Y. Lin, Y. Han, C. Teng, Q. Wang, Development of large-scale size-controlled adult pancreatic progenitor cell clusters by an inkjet-printing technique, ACS applied materials & interfaces 7(21) (2015) 11624-11630.

Acknowledgement

First and foremost, I would like to express my sincere gratitude to **Professor Joachim o. Rädler**, my supervisor and the chair of Soft Condensed Matter Physics in LMU München, for giving me the opportunity to conduct research in his excellent group, and for his patience, motivation, and immense knowledge. I am grateful for every productive discussion we had and all his supports both scientifically and personally. It has been a great honor for me to be one of his Ph.D. students. I could not have imagined having a better advisor and mentor for my PhD study.

Besides my supervisor, I would like to thank **Professor Erwin Frey** for the pleasant cooperation, the contributions and suggestions about projects and problems, and last but not least the well-designed lectures, which helped shape my interest in biophysics.

My sincere thanks especially go to my current colleague **Christoph Schreiber, Sophia Schaffer,** my former colleague **Dr. Felix Segerer** and my collaborator **Andriy Goychuk** for the excellent teamwork, their efforts and time in proof-reading and correcting of my publication. I appreciate their sound knowledge of theoretical modeling and programming, as well as the fruitful discussions and their helpful suggestions.

Of course, my thanks also go to the entire chair for the relaxed and fun working atmosphere. I would like to thank **Gerlinde Schwake**, **Max Albert, Charlott Leu and Margarete Meixner** that their technical supports and administrative issues, which keep my research projects going well. Thanks also to **Dr. Philipp Paulitschke** for providing technical supports in fast scan microscope, which helps my initial research a lot. Express thanks also to my former and current colleagues **Dr. Peter Röttgermann, Dr. Anita Reiser, Alexandra Fink** and **Daniel Woschée**, for their help in cell and programming and pleasures we had together. Moreover, thanks to all

my former and current colleagues, labmates and roomates, **Dr. Sonja Westermayer**, **Dr. Farzad Sekhavati**, **Dr. Elisavet Chatzopoulou**, **Dr. Rafal Krzyszton**, **Dr. Tobias Preiß**, **Dr. Matthias Zorn**, **Dr. Alexandra Murschhauser**, **Dr. Janina Lange**, **Dr. Valentin Stierle**, **Dr. Ida Berts**, **Dr. Francesca Nicoli**, **Dr. Maricio Pilo-Pais**, **Dr. Janina Roemer**, **Dr. Amelie Heuer-Jungermann**, **Sara Kesel**, **Luisa Kneer**, **Ricarda Berger**, **Simone Ezendam**, for providing a very friendly, warm and pleasant atmosphere for any help they provided me. This is an amazing experience that I will never forget in my life.

Last and most certainly not least I wish to thank my **parents** in China and my husband **Dr. Bodong Zhang**, for their endless love and support.